CLIMATE, LAND COVER CHANGE AND THE SEASONALITY OF PHOTOSYNTHETIC ACTIVITY AND EVAPOTRANSPIRATION IN TROPICAL ECOSYSTEMS

by

Maria del Rosario Uribe Diosa

A Dissertation

Submitted to the Faculty of Purdue University

In Partial Fulfillment of the Requirements for the degree of

Doctor of Philosophy

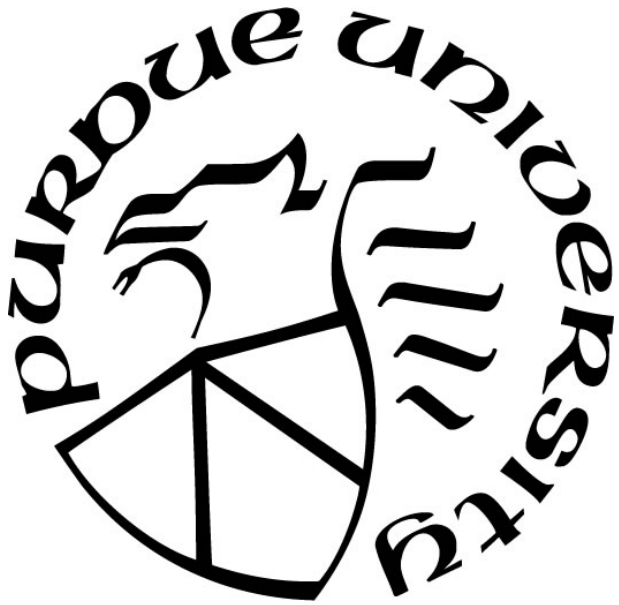

Department of Forestry and Natural Resources

West Lafayette, Indiana

August 2020

THE PURDUE UNIVERSITY GRADUATE SCHOOL
STATEMENT OF COMMITTEE APPROVAL

Dr. Jeffrey S. Dukes, Chair

Department of Forestry and Natural Resources

Dr. Carlos A. Sierra

Max Planck Institute for Biogeochemistry

Dr. Guofan Shao

Department of Forestry and Natural Resources

Dr. Lisa R. Welp

Department of Earth, Atmospheric, and Planetary Sciences

Approved by:

Dr. Robert Wagner

To anyone who thinks they can't do it

ACKNOWLEDGMENTS

I would like to thank Jeff, the largest contributor to this work. I couldn’t have done this without his academic guidance, his reassuring voice, and, most of all, his unrelenting confidence in my abilities, even when I didn't have it. I would also like to thank Carlos Sierra for his advice and mentoring in the most crucial moments of my doctorate. Thanks to Dr. Lisa Welp and Dr. Guofan Shao for their valuable advice and helping me grow as a researcher. I am also grateful to Dr. Qianlai Zhuang for his guidance during the first years of my PhD.

Thanks to the FNR and ESE faculty and staff who helped me navigate this academic world and made it easier to succeed. Thanks to the Dukes Lab, the ESE and the FNR graduate students for being there as classmates, officemates, colleagues and friends, making my days more enjoyable. Thanks to the Colombia-Purdue Partnership, specifically Juan Diego Velasquez and Carolyn Percifield, for their financial support and for being an amazing team. Thanks to the Colombian community at Purdue for making me feel the warmth of home away from home.

Last, thanks to all my Purdue friends for making this a beautiful time, it was great to have you by my side during the toughest and the happiest moments.

TABLE OF CONTENTS

LIST OF TABLES

LIST OF FIGURES

ABSTRACT

Tropical ecosystems play a key role in regulating the global climate and the carbon cycle thanks to the large amounts of water and carbon exchanged with the atmosphere. These biogeochemical fluxes are largely the result of high photosynthetic rates. Photosynthetic activity is highly dependent on climate and vegetation, and therefore can be easily modified along with changes in those two factors. A better understanding of what drives or alters photosynthetic activity in the tropics will lead to more accurate predictions of climate and subsequent effects on ecosystems. The seasonal pattern of photosynthetic activity is one of the main uncertainties that we still have about tropical ecosystems. However, this seasonality of tropical vegetation and its relationship to climate change and land cover is key to understanding how these ecosystems could be affected and have an effect on climate.

In this dissertation, I present three projects to improve our understanding about tropical ecosystems and how their photosynthetic activity is affected by climate and land cover change. The lack of field-based data has been one of the main limiting factors in our study of tropical ecosystems. Therefore, in these projects I extensively use remote sensing-derived data to analyze large scale and long term patterns. In the first study, I looked at the seasonal relationship between photosynthetic activity and climate, and how model simulations represent it. Vegetation in most of the tropics is either positively correlated with both water and light, or positively correlated with one of them and negatively with the other. Ecosystem models largely underestimate positive correlations with light and overestimate positive correlations with water. In the second study, I focus on the effect of land cover change in photosynthetic activity and transpiration in a highly deforested region in the Amazon. I find that land cover change decreases tropical forests photosynthetic activity and transpiration during the dry season. Also, land cover change increases the range of photosynthetic activity and transpiration in forests and shrublands. These effects are intensified with increasing land cover change. In the last project, I quantify the amount of change in evapotranspiration due to land cover change in the entire Amazon basin. Our remote sensing-derived estimates are well aligned with model predictions published in the past three decades. These results increase our confidence in climate models representation of evapotranspiration in the Amazon.

Findings from this dissertation highlight (1) the importance of the close relationship between climate and photosynthetic activity and (2) how land cover change is altering that relationship. We hope our results can build on our knowledge about tropical ecosystems and how they could change in the future. We also expect our analysis to be used for model benchmarking and tropical ecosystem monitoring.

CHAPTER 1. INTRODUCTION

Tropical ecosystems provide various ecosystem services of global importance, mainly as habitat for the large proportion of biodiversity they harbor and for their influence on atmospheric carbon and global climate. Warm temperatures throughout the year result in fast rates of biogeochemical processes and an ideal habitat for numerous species. Tropical forests alone contain about 25% of the terrestrial carbon, account for almost 33% of global terrestrial photosynthesis (Bonan 2008), and host about a quarter of the world's terrestrial biodiversity (Malhi et al. 2008). The tropics are also home to a high number of endemic species and serve as seasonal habitat for migrating species from higher latitudes (Barlow et al. 2018). Tropical ecosystems also have a disproportionate influence on carbon and water exchange between the biosphere and the atmosphere, and subsequently on the regional and global climates (Davidson et al. 2012; Lovejoy and Nobre 2019). However, their role as carbon sinks and climate regulators is tightly linked to anthropogenic disturbances of the climate and land cover (Bonan 2008).

Climate and land cover change represent ongoing major threats for tropical ecosystems. By 2003, 15% of the original extent of the Amazon had been deforested; this remnant area is predicted to decrease to half by 2050 in a business-as-usual scenario (Soares-Filho et al. 2006). At the same time, climate models predict average warming that ranges between 3.3 and 8 °C by the end of this century, under different greenhouse emission scenarios (Malhi et al. 2008). Also, a significant Amazonian drying has been projected by some of the models, with a 30 - 80% probability of intensification of the dry season (Malhi et al. 2008). Of greater importance is the positive feedback that arises with the destruction of the forest and the changes in climate; 120 ± 30 Pg C stored in the biomass of these forests could be released to the atmosphere and trigger further changes in radiative forcing and global warming (Malhi et al., 2008; de Gonçalves et al., 2013).

The high photosynthetic rates of vegetation in the tropics is one of the main pathways through which these ecosystems disproportionately influence climate. Photosynthetic activity, which is closely related to transpiration, largely determines the fluxes of carbon, water, and energy between the land surface and the atmosphere. In the Amazon, the largest and most studied ecosystem in the tropics, a large proportion of precipitation comes from water that has been recycled within the same region (Staal et al. 2018). The water recycled by the Amazon forests also affects precipitation in other parts of the world through teleconnections (Avissar and Werth 2005;

Lawrence and Vandecar 2015; Medvigy et al. 2013). Given the importance of, and threats faced by tropical ecosystems, there is considerable interest in understanding photosynthetic activity of these systems, how it could function under changing conditions, and how those changes could subsequently affect climate.

The seasonality of photosynthetic activity is one of the least understood aspects of tropical ecosystems (Guan et al. 2015). In contrast to temperate and boreal forests, tropical ecosystems do not have a well-fixed seasonality controlled by temperature or day length (Restrepo-Coupe et al. 2013). Photosynthetic rates in these ecosystems are closely related to variation in precipitation and radiation (Nemani et al. 2003; Seddon et al. 2016; Wagner et al. 2016). But the complex relationship between climate drivers and productivity in these ecosystems is not entirely understood (Restrepo-Coupe et al. 2013). For instance, Earth system models poorly represent seasonal trends of some tropical forests in the Amazon (Restrepo-Coupe et al. 2017; Saleska et al. 2003). The misrepresentation of seasonal photosynthetic activity suggests that carbon and water cycling in tropical ecosystems do not have realistic relationships with environmental drivers in these models.

Land cover change dramatically alters the feedbacks between the land surface and the atmosphere. Land surface properties such as albedo, surface roughness, photosynthetic activity, and transpiration are modified by changes in the land cover (Butt, Oliveira, and Costa 2011). All these mechanisms result in changes in evapotranspiration. Due to its role in water cycling and energy transfer from the land surface to the atmosphere, evapotranspiration affects precipitation and temperature (Xu et al. 2019). The impacts of land cover change on evapotranspiration and climate can range from short-term and local to long-term and global.

In the Amazon specifically, the removal of native vegetation results in substantial differences in the amount of water recycled from the land surface to the atmosphere; but, how much? The impact that these ecosystems could have on climate has been a focus of research studies since the 1970s (Spracklen and Garcia-Carreras 2015). Given the difficulty of measuring evapotranspiration and the scarcity of field-based data in the tropics, few studies have used this type of data to characterize the effects of deforestation. Most studies on the impact of land cover on climate rely on climate models (e.g., regional and global circulation models). These models also have the advantage of including complex atmospheric dynamics that allow us to understand the feedbacks between evapotranspiration, precipitation, and temperature at the local, regional, and global scales.

Modeling studies agree that continuing deforestation of the Amazon will reduce evapotranspiration and precipitation and increase temperatures (Davidson et al. 2012). However, there is uncertainty in the amount of change in evapotranspiration, precipitation, and temperature due to land cover change. The large number of studies conducted on this topic, employing a variety of different model frameworks, has resulted in a large number of estimates (Spracklen and Garcia-Carreras 2015). Studies based on remote sensing data are scarce, despite the fast development of this type of data in the past few decades. These advancements provide us the opportunity to estimate the effects of land cover change based on large-scale, long-term, and high-quality observed data.

In this dissertation, I present a broad set of studies about the feedbacks between tropical ecosystems and climate, and how they are disrupted by land cover change. In the first chapter, I analyze the relationships between climate and photosynthesis at the seasonal scale across the entire tropical region. I identify how different types of relationships are related to specific biomes and climate characteristics. I then evaluate whether land surface models accurately represent the various types of relationships. In the second chapter, I investigate the effects of changes in land cover on photosynthesis and transpiration in a highly deforested region in the Amazon. I identify how land cover change affects these variables at both annual and seasonal scales in two specific natural ecosystems, the rainforest and the Cerrado. In the last chapter, I use remote sensing-derived data to estimate how land cover change has altered evapotranspiration in the tropical forests of the Amazon basin. I compare these estimates with a full record of estimates from modeling-based studies. I also analyze spatial, seasonal, and interannual differences in deforestation-induced changes in evapotranspiration.

1.1 References

Avissar, Roni, and David Werth. 2005. "Global Hydroclimatological Teleconnections Resulting from Tropical Deforestation." *Journal of Hydrometeorology* 6(2):134–45.

Barlow, Jos, Filipe França, Toby A. Gardner, Christina C. Hicks, Gareth D. Lennox, Erika Berenguer, Leandro Castello, Evan P. Economo, Joice Ferreira, Benoit Guénard, Cecília Gontijo Leal, Victoria Isaac, Alexander C. Lees, Catherine L. Parr, Shaun K. Wilson, Paul J. Young, and Nicholas A. J. Graham. 2018. "The Future of Hyperdiverse Tropical Ecosystems." *Nature* 559(7715):517–26.

Bonan, Gordon B. 2008. "Forests and Climate Change: Forcings, Feedbacks, and the Climate Benefits of Forests." *Science* 320(5882):1444–49.

Butt, Nathalie, Paula Afonso de Oliveira, and Marcos Heil Costa. 2011. "Evidence That Deforestation Affects the Onset of the Rainy Season in Rondonia, Brazil." *Journal of Geophysical Research: Atmospheres* 116(D11).

Davidson, Eric A., Alessandro C. de Araújo, Paulo Artaxo, Jennifer K. Balch, I. Foster Brown, Mercedes M. C. Bustamante, Michael T. Coe, Ruth S. DeFries, Michael Keller, Marcos Longo, J. William Munger, Wilfrid Schroeder, Britaldo S. Soares-Filho, Carlos M. Souza, and Steven C. Wofsy. 2012. "The Amazon Basin in Transition." *Nature* 481(7381):321–28.

de Gonçalves, Luis Gustavo Gonçalves, Jordan S. Borak, Marcos Heil Costa, Scott R. Saleska, Ian Baker, Natalia Restrepo-Coupe, Michel Nobre Muza, Benjamin Poulter, Hans Verbeeck, Joshua B. Fisher, M. Altaf Arain, Phillip Arkin, Bruno P. Cestaro, Bradley Christoffersen, David Galbraith, Xiaodan Guan, Bart J. J. M. van den Hurk, Kazuhito Ichii, Hewlley M. Acioli Imbuzeiro, Atul K. Jain, Naomi Levine, Chaoqun Lu, Gonzalo Miguez-Macho, Débora R. Roberti, Alok Sahoo, Koichi Sakaguchi, Kevin Schaefer, Mingjie Shi, W. James Shuttleworth, Hanqin Tian, Zong-Liang Yang, and Xubin Zeng. 2013. "Overview of the Large-Scale Biosphere–Atmosphere Experiment in Amazonia Data Model Intercomparison Project (LBA-DMIP)." *Agricultural and Forest Meteorology* 182–183:111–27.

Guan, Kaiyu, Ming Pan, Haibin Li, Adam Wolf, Jin Wu, David Medvigy, Kelly K. Caylor, Justin Sheffield, Eric F. Wood, Yadvinder Malhi, Miaoling Liang, John S. Kimball, Scott R. Saleska, Joe Berry, Joanna Joiner, and Alexei I. Lyapustin. 2015. "Photosynthetic Seasonality of Global Tropical Forests Constrained by Hydroclimate." *Nature Geoscience* 8(4):284–89.

Lawrence, Deborah, and Karen Vandecar. 2015. "Effects of Tropical Deforestation on Climate and Agriculture." *Nature Climate Change* 5(1):27–36.

Lovejoy, Thomas E., and Carlos Nobre. 2019. "Amazon Tipping Point: Last Chance for Action." *Science Advances* 5(12):eaba2949.

Malhi, Yadvinder, J. Timmons Roberts, Richard A. Betts, Timothy J. Killeen, Wenhong Li, and Carlos A. Nobre. 2008. "Climate Change, Deforestation, and the Fate of the Amazon." *Science* 319(5860):169–72.

Medvigy, David, Robert L. Walko, Martin J. Otte, and Roni Avissar. 2013. "Simulated Changes in Northwest U.S. Climate in Response to Amazon Deforestation." *Journal of Climate* 26(22):9115–36.

Nemani, Ramakrishna R., Charles D. Keeling, Hirofumi Hashimoto, William M. Jolly, Stephen C. Piper, Compton J. Tucker, Ranga B. Myneni, and Steven W. Running. 2003. "Climate-Driven Increases in Global Terrestrial Net Primary Production from 1982 to 1999." *Science* 300(5625):1560–63.

Restrepo-Coupe, Natalia, Naomi M. Levine, Bradley O. Christoffersen, Loren P. Albert, Jin Wu, Marcos H. Costa, David Galbraith, Hewlley Imbuzeiro, Giordane Martins, Alessandro C. da Araujo, Yadvinder S. Malhi, Xubin Zeng, Paul Moorcroft, and Scott R. Saleska. 2017. "Do Dynamic Global Vegetation Models Capture the Seasonality of Carbon Fluxes in the Amazon Basin? A Data-Model Intercomparison." *Global Change Biology* 23(1):191–208.

Restrepo-Coupe, Natalia, Humberto R. da Rocha, Lucy R. Hutyra, Alessandro C. da Araujo, Laura S. Borma, Bradley Christoffersen, Osvaldo M. R. Cabral, Plinio B. de Camargo, Fernando L. Cardoso, Antonio C. Lola da Costa, David R. Fitzjarrald, Michael L. Goulden, Bart Kruijt, Jair M. F. Maia, Yadvinder S. Malhi, Antonio O. Manzi, Scott D. Miller, Antonio D. Nobre, Celso von Randow, Leonardo D. Abreu Sá, Ricardo K. Sakai, Julio Tota, Steven C. Wofsy, Fabricio B. Zanchi, and Scott R. Saleska. 2013. "What Drives the Seasonality of Photosynthesis across the Amazon Basin? A Cross-Site Analysis of Eddy Flux Tower Measurements from the Brasil Flux Network." *Agricultural and Forest Meteorology* 182–183:128–44.

Saleska, Scott R., Scott D. Miller, Daniel M. Matross, Michael L. Goulden, Steven C. Wofsy, Humberto R. da Rocha, Plinio B. de Camargo, Patrick Crill, Bruce C. Daube, Helber C. de Freitas, Lucy Hutyra, Michael Keller, Volker Kirchhoff, Mary Menton, J. William Munger, Elizabeth Hammond Pyle, Amy H. Rice, and Hudson Silva. 2003. "Carbon in Amazon Forests: Unexpected Seasonal Fluxes and Disturbance-Induced Losses." *Science* 302(5650):1554–57.

Seddon, Alistair W. R., Marc Macias-Fauria, Peter R. Long, David Benz, and Kathy J. Willis. 2016. "Sensitivity of Global Terrestrial Ecosystems to Climate Variability." *Nature* 531(7593):229–32.

Soares-Filho, Britaldo Silveira, Daniel Curtis Nepstad, Lisa M. Curran, Gustavo Coutinho Cerqueira, Ricardo Alexandrino Garcia, Claudia Azevedo Ramos, Eliane Voll, Alice McDonald, Paul Lefebvre, and Peter Schlesinger. 2006. "Modelling Conservation in the Amazon Basin." *Nature* 440(7083):520–23.

Spracklen, D. V., and L. Garcia-Carreras. 2015. "The Impact of Amazonian Deforestation on Amazon Basin Rainfall." *Geophysical Research Letters* 42(21):9546–52.

Staal, Arie, Obbe A. Tuinenburg, Joyce H. C. Bosmans, Milena Holmgren, Egbert H. van Nes, Marten Scheffer, Delphine Clara Zemp, and Stefan C. Dekker. 2018. "Forest-Rainfall Cascades Buffer against Drought across the Amazon." *Nature Climate Change* 8(6):539.

Wagner, Fabien H., Bruno Hérault, Damien Bonal, Clément Stahl, Liana O. Anderson, Timothy R. Baker, Gabriel Sebastian Becker, Hans Beeckman, Danilo Boanerges Souza, Paulo Cesar Botosso, David M. J. S. Bowman, Achim Bräuning, Benjamin Brede, Foster Irving Brown, Jesus Julio Camarero, Plínio Barbosa Camargo, Fernanda C. G. Cardoso, Fabrício Alvim Carvalho, Wendeson Castro, Rubens Koloski Chagas, Jérome Chave, Emmanuel N. Chidumayo, Deborah A. Clark, Flavia Regina Capellotto Costa, Camille Couralet, Paulo Henrique da Silva Mauricio, Helmut Dalitz, Vinicius Resende de Castro, Jaçanan Eloisa de Freitas Milani, Edilson Consuelo de Oliveira, Luciano de Souza Arruda, Jean-Louis Devineau, David M. Drew, Oliver Dünisch, Giselda Durigan, Elisha Elifuraha, Marcio Fedele, Ligia Ferreira Fedele, Afonso Figueiredo Filho, César Augusto Guimarães Finger, Augusto César Franco, João Lima Freitas Júnior, Franklin Galvão, Aster Gebrekirstos, Robert Gliniars, Paulo Maurício Lima de Alencastro Graça, Anthony D. Griffiths, James Grogan, Kaiyu Guan, Jürgen Homeier, Maria Raquel Kanieski, Lip Khoon Kho, Jennifer Koenig, Sintia Valerio Kohler, Julia Krepkowski, José Pires Lemos-Filho, Diana Lieberman, Milton Eugene Lieberman, Claudio Sergio Lisi, Tomaz Longhi Santos, José Luis López Ayala, Eduardo Eijji Maeda, Yadvinder Malhi, Vivian R. B. Maria, Marcia C. M. Marques, Renato Marques, Hector Maza Chamba, Lawrence Mbwambo, Karina Liana Lisboa Melgaço, Hooz Angela Mendivelso, Brett P. Murphy, Joseph J. O'Brien, Steven F. Oberbauer, Naoki Okada, Raphaël Pélissier, Lynda D. Prior, Fidel Alejandro Roig,

Michael Ross, Davi Rodrigo Rossatto, Vivien Rossi, Lucy Rowland, Ervan Rutishauser, Hellen Santana, Mark Schulze, Diogo Selhorst, Williamar Rodrigues Silva, Marcos Silveira, Susanne Spannl, Michael D. Swaine, José Julio Toledo, Marcos Miranda Toledo, Marisol Toledo, Takeshi Toma, Mario Tomazello Filho, Juan Ignacio Valdez Hernández, Jan Verbesselt, Simone Aparecida Vieira, Grégoire Vincent, Carolina Volkmer de Castilho, Franziska Volland, Martin Worbes, Magda Lea Bolzan Zanon, and Luiz E. O. C. Aragão. 2016. "Climate Seasonality Limits Leaf Carbon Assimilation and Wood Productivity in Tropical Forests." *Biogeosciences* 13(8):2537–62.

Xu, Donghui, Elizabeth Agee, Jingfeng Wang, and Valeriy Y. Ivanov. 2019. "Estimation of Evapotranspiration of Amazon Rainforest Using the Maximum Entropy Production Method." *Geophysical Research Letters* 46(3):1402–12.

CHAPTER 2. SEASONALITY OF TROPICAL PHOTOSYNTHESIS: A GLOBAL MAP OF DRIVERS AND COMPARISON TO MODEL OUTPUTS

2.1 Abstract

Highly productive tropical ecosystems strongly influence Earth's climate and weather patterns. Most tropical ecosystems remain warm year-round; nonetheless, their plants undergo seasonal cycles of carbon and water exchange. Previous research has shown the importance of water and light as drivers of the seasonality of vegetation activity in the tropics. Also, field-based studies have demonstrated that land surface models inaccurately simulate vegetation seasonal cycles in some specific tropical forest sites. However, field-based photosynthetic activity data are scarce in the tropics. A comprehensive understanding of the relationship of tropical photosynthetic activity and climate at the seasonal scale and how it is represented by models is lacking. In this study, we seek to identify the seasonal relationships between climate and photosynthetic activity from observations and models across the entire tropics. We characterize this seasonality using satellite-based photosynthetic activity data and link this activity to patterns of precipitation and light availability. Photosynthetic activity falls into three dominant and spatially distinct relationships with these two drivers: increases with both drivers (36% of tropical pixels), increases with rain but decreases with light (28%), and increases with light but decreases with rain (14%). These three dominant relationships track regional variation in long-term mean daily radiation, mean annual precipitation, dry season length, and the seasonal correlation between precipitation and radiation. In general, model simulations of gross primary productivity (GPP) overestimate the positive correlation of photosynthetic activity with water and underestimate the positive correlation with light. The largest discrepancies between simulations and observations are in the representation of the regions where photosynthetic activity increases with light and decreases with rain. Our clear scheme for representing the relationship between climate and photosynthetic activity can be used to benchmark tropical seasonality of GPP in land models.

2.2 Introduction

Tropical ecosystems are sometimes called the "lungs of the planet," because their high photosynthetic rates drive large fluxes of carbon and water. Tropical forests alone account for about 60% of global terrestrial photosynthesis (Mitchard, 2018) and influence precipitation patterns, even at the continental scale (Lawrence & Vandecar, 2015). Collectively, tropical ecosystems disproportionately influence Earth's climate and weather patterns (Malhi et al., 2008).

At the intra-annual or seasonal scale, climate patterns determine ecosystems' metabolism, phenological patterns, and vegetation distribution. Ecosystem metabolism, in turn, affects the climate system through photosynthesis and the associated carbon, water, and energy feedbacks to the atmosphere. But this ecosystem-atmosphere interaction is being altered by ongoing changes in the climate system. Forecasting the effects of these climatic changes on tropical ecosystems, and the subsequent consequences for biosphere-atmosphere interactions and climate at regional and global scales requires accurate estimates of current photosynthetic rates in tropical ecosystems and an understanding of their relationship with climate. While photosynthetic rates go through clear and well-understood seasonal cycles in temperate regions, seasonality of photosynthesis in the tropics is less well understood (Wu et al., 2016). Across most ecosystems in these consistently warm regions, both the patterns of seasonality and the drivers of those patterns remain largely uncharacterized (Restrepo-Coupe et al., 2017; Saleska et al., 2003).

Marked seasonal patterns in vegetation activity, although sometimes weaker or less defined in comparison to those of the temperate zones, have been observed in both field- and satellite-based measurements in the tropics. Estimates from eddy covariance towers show strong seasonal patterns in net ecosystem exchange and gross primary productivity (GPP) in most sites where data are available (Restrepo-Coupe et al., 2013; Saigusa et al., 2008). Such sites include tropical rain forests and savannas from the Amazon and Asia. Satellite-based measurements of proxies of phenology and photosynthetic activity such as leaf area index (LAI), enhanced vegetation index (EVI) and solar-induced fluorescence (SIF), often show similar seasonal patterns to those observed in the field (Bertani et al., 2017; Bradley et al., 2011a; Guan et al., 2015; Myneni et al., 2007; Xu et al., 2015). These studies demonstrate that seasonality extends across the tropics, with only a small portion of the region not showing any type of seasonality.

Land surface models, however, are unable to characterize the observed seasonal cycles, as shown for some specific sites in the Amazon (Restrepo-Coupe et al., 2017). At individual study

sites, models simulate either constant GPP or opposite seasonal patterns to the ones observed in the field (Restrepo-Coupe et al., 2017). Yet, these models are a major component of Earth System Models (ESMs) and constitute the main tool scientists currently rely on for future projections of climate, ecosystems and their interrelationship. Models that represent seasonal cycles in the tropics more accurately would be able to estimate how changes in climate seasonality (e.g., timing or length of wet and dry seasons) could affect intra-annual carbon fluxes and, subsequently, the annual carbon budgets of tropical ecosystems (Saleska et al., 2003). Accurate simulation of terrestrial water cycling, including the effects of tropical vegetation on regional to global precipitation patterns, also depends on realistic simulations of photosynthetic activity.

In order to accurately represent the seasonality of tropical photosynthetic activity in land surface models, we need to understand the climatic drivers of this seasonality. This involves recognizing how they vary from one region in the tropics to another, and the potential mechanisms and delayed responses involved in the climate-vegetation relationship. Water and light availability are the main drivers of intra-annual variation in vegetation activity in the tropics, and within the region there is wide variation in the responses to these two drivers (Nemani et al., 2003; Seddon et al., 2016). Previous studies attribute the regional differences in vegetation seasonality to water stress (Guan et al., 2015; Wagner et al., 2017). In this sense, photosynthetic activity follows precipitation cycles in drier ecosystems, such as pastures, deciduous forests or degraded forests (Bradley et al., 2011a; Huete et al., 2006). In ecosystems with higher mean annual rainfall or a shorter dry season, like evergreen forests, photosynthetic activity is either less seasonal or more closely associated with light availability (Guan et al., 2015; Nemani et al., 2003). The mechanisms leading to these different vegetation-climate relationships are still being studied and, therefore, are more challenging to represent in land surface models. Moreover, it is common for the relationship of photosynthetic activity with climate to be lagged depending on the climatic factor and vegetation types (Bradley et al., 2011a; D. Wu et al., 2015). Understanding the importance of these lagged correlations in different parts of the tropics can also guide future research and inclusion of underlying mechanisms in models.

Despite the large variation in seasonal patterns across the tropical region and the discrepancy found between GPP from field measurements and models, most satellite-based studies of tropical vegetation seasonality have focused on the Amazon basin. Moreover, model performance has only been tested at the site level, also within the Amazon. A global analysis of the drivers of

photosynthesis seasonality in the tropics and how they differ in models would unveil large-scale patterns. These discoveries could help experiments and models target weakly represented regions and ecosystems.

Here, we investigated how the seasonality of photosynthetic activity in the entire tropical region relates to the two most important regional-level climate drivers; precipitation and radiation. These two variables also provide the main forcing data used by land surface models to simulate most vegetation processes. In contrast to previous studies, rather than identifying a single climate predictor of photosynthetic activity, we sought to characterize its relationship (including direction and magnitude) with both precipitation and radiation. This approach allowed us to identify where in the tropics photosynthesis is positively or negatively associated with each of the two climate drivers, including lagged responses to these drivers. We then identified the climatic variables most commonly associated with each of the various relationships between photosynthesis and the climatic drivers. For instance, we expected photosynthesis in extremely wet regions (high mean annual precipitation (MAP) and short dry season, e.g., rainforests) to be positively correlated with light and negatively correlated with rain. In arid regions (low MAP and a long dry season, e.g., Caatinga in Brazil), we expected photosynthesis to be positively correlated with rain and negatively correlated with light. In regions that are not extremely wet or dry, and with more evenly distributed precipitation throughout the year (e.g., forests of Central America), we expected photosynthesis to be positively correlated with both water and light, but potentially with different time lags.

2.3 Methods

2.3.1 Climate data

Monthly mean precipitation and net radiation were retrieved for the period 2000-2017. Precipitation was obtained from the TRMM (TMPA/3B43) Rainfall V7 product with a spatial resolution of 0.25-degree x 0.25-degree. This product is the best estimate of an algorithm that uses multi-satellite data from two instruments, the Precipitation Radar and the TRMM Microwave Imager (Huffman et al., 2007). Incoming shortwave radiation at the surface data were obtained from the Energy Balanced and Filled (EBAF) Surface data product Edition 2.8 from the NASA Clouds and the Earth's Radiant Energy System (CERES) experiment at a 1-degree x 1-degree

spatial resolution. This product is the output of radiative transfer models that use a series of satellite-based observations of top-of-atmosphere radiation and cloud physical and radiative properties to calculate the surface data (Kato et al., 2013).

For the characterization of site-specific climate variables, we calculated mean annual precipitation, mean radiation, mean temperature, mean dry-season length, and precipitation seasonality index. All of the climate variables correspond to the average for the period 2000-2016 for each pixel. Mean annual precipitation and mean radiation were estimated using the datasets above. Mean temperature was estimated for the period of study from the Climatic Research Unit (CRU) Time-Series (TS) Version 4.02 of High-Resolution Gridded Data of Month-by-month Variation in Climate (Harris et al., 2014). The data are in a 0.5 x 0.5-degree grid and are produced based on observational data from national and external meteorological agencies. Dry-season length was obtained from the Rainy and Dry Seasons (RADS) dataset (Bombardi et al., 2019). This dataset uses global gridded daily precipitation datasets to provide several characteristics of precipitation seasonality at 0.25- x 0.25-degree spatial resolution. In RADS, seasons are calculated at the local scale based on the accumulated precipitation anomalies of each grid point. Accumulated precipitation anomalies are calculated by comparing daily precipitation against the long-term mean daily precipitation. Calculations of the accumulated anomalies start every year in the dry season, which is estimated as the first minimum harmonic of the precipitation mean annual cycle. The start and end of the wet and dry seasons correspond to inflection points in the accumulated anomalies curve for each cycle. More details of the algorithm and assumptions for these calculations are provided in Bombardi et al. (2019). The precipitation seasonality index was calculated using the Walsh and Lawler equation (Walsh & Lawler, 1981). This index uses the total annual and monthly precipitation for each year within the period of study to characterize the distribution of precipitation throughout the year. Small values indicate less seasonality or equal distribution of the precipitation throughout the year, while higher values indicate higher concentration of precipitation in fewer months.

While some areas of the tropics underwent extensive changes in land cover during the study period (Hansen et al., 2013), the models in this study used static land cover data. Because of the contrast between the coarse resolution of the data used here and the fine resolution at which land cover change occurs, we were unable to include this information in our analyses. The effects of

land cover change on seasonality of tropical GPP and its response to precipitation and radiation should be examined in future studies.

2.3.2 Satellite-based vegetation data

We used three independent datasets to estimate photosynthetic activity in this study. Two of these were satellite-based proxies: Solar Induced Fluorescence (SIF) and the Multi-Angle Implementation of Atmospheric Correction Enhanced Vegetation Index (MAIAC EVI). The third is a remote sensing-derived product based on SIF, known as GOSIF. SIF data came from the GOME2_F data products V27 (Level 3) (https://avdc.gsfc.nasa.gov/pub/data/satellite/MetOp/GOME_F/) (Joiner et al., 2013). This SIF monthly dataset is available at 0.5 x 0.5-degree resolution since 2007. The GOSIF dataset, which is based on SIF retrievals from OCO-2 in addition to a predictive model and other MODIS remote sensing and meteorological reanalysis datasets, was obtained from http://data.globalecology.unh.edu/data/GOSIF/ (Li & Xiao, 2019). GOSIF is available monthly at 0.05 x 0.05-degree resolution since 2000. MAIAC EVI was obtained from calibrated and geometrically corrected MODIS Collection 6 Level 1B satellite images (https://portal.nccs.nasa.gov/datashare/maiac/DataRelease/Global-VI-8day-0.05degree/) (A. Lyapustin et al., 2018). The monthly MAIAC EVI product is at 0.05 x 0.05-degree resolution and since 2000.

Each of the satellite-based vegetation datasets has advantages and disadvantages. SIF data from the Global Ozone Monitoring Experiment–2 on MetOp-A and -B (GOME 2) should represent photosynthetic activity well, but the temporal period available, from 2007 to 2018 is not an ideal match with available model output, and sensor degradation for GOME-2 has been a concern (Zhang et al., 2018). GOSIF data, developed from Orbiting Carbon Observatory-2 (OCO-2) measurements, should approximate the SIF data and covers a longer period, from 2000 to 2018. However, the derived data in the GOSIF product are more removed from the direct observations than SIF. MAIAC EVI has a similarly long time series as GOSIF and has been frequently used in tropical ecosystem studies; it has proved to be a better proxy of photosynthetic activity in tropical rainforests than other vegetation indices such as Normalized Difference Vegetation Index (NDVI) or MODIS EVI (Maeda et al., 2016). However, MAIAC EVI is still a vegetation index that

estimates vegetation greenness and not photosynthetic activity directly, which is more accurately estimated with SIF (Joiner et al., 2011).

Both the SIF and MAIAC EVI datasets have undergone an advanced cloud screening and filtering process, which has made them advantageous to use in the tropics compared to other remote sensing products. In SIF, the main problem of clouds for SIF retrievals is a shielding effect, as, contrary to vegetation indices, the SIF spectral signature is not affected by clouds (Joiner et al., 2014). Therefore, in the SIF dataset used here, cloud filtering is done by removing pixels with effective cloud fractions of >30%. This filter threshold has been proved to maintain spatial and temporal patterns of SIF without altering the sample size and the noise resulting from reduced coverage (Joiner et al., 2013). MAIAC EVI has a sophisticated cloud and aerosol screening correction algorithm. In this later product, pixels with atmospheric contamination are not excluded from the dataset and are not included in our study (A. I. Lyapustin et al., 2012). As part of our time series analysis, we filled data gaps of a maximum of three months using spline interpolation. Pixels with gaps longer than three months in the time series were excluded from the analysis.

2.3.3 Modeled GPP

To examine tropical seasonality exhibited in land surface models (LSMs), simulated GPP data were obtained from the TRENDY (Trends and drivers of the regional scale sources and sinks of carbon dioxide) project (Sitch et al., 2015). Most TRENDY models are LSMs commonly coupled with ESMs and used for climate projections. Here, we used TRENDY v5 S2 simulations from CLM4.5 (Oleson et al., 2013), JULES (Best et al., 2011), and LPJ-GUESS (Smith et al., 2001). In TRENDY, each model is run globally with different spatial scales and land cover types, but with the same forcing data. Land cover data for the simulations is fixed and provided by each modeling group. In addition to the LSM-simulated GPP, two global GPP products, Fluxcom (Jung & Team, 2016; Tramontana et al., 2016) and VPM (Zhang et al., 2017), were also analyzed. These datasets are derived using field observations, satellite-based measurements, and reanalysis meteorological data, in combination with interpolation or machine learning techniques. The final products are global-scale gridded GPP estimates with long temporal coverage and high spatial resolution (see Table S1 for details).

2.3.4 Data analysis

We used time series analysis to identify relationships between climate variables (i.e., precipitation and radiation) and various estimates of photosynthetic activity (i.e., SIF, GOSIF, MAIAC EVI, and simulated GPP) across the entire tropics. We used cross-correlation function (CCF) analysis (Box et al., 2015), to examine time series of monthly data for each pixel in the tropics (20°N - 20°S) from 2000 to 2015 (except SIF and GOSIF, which were analyzed for 2007-2017 and 2000-2017, respectively). Although the SIF dataset covered different years than the other datasets, the 11 years of SIF data provide a robust basis for our seasonal analyses, and the SIF analyses can be broadly validated with the longer and independent GOSIF dataset. We excluded from all analyses all pixels with a mean EVI of less than 0.1. Those low EVI pixels, which correspond to barren lands or extremely low vegetation cover, were removed to avoid noise in the photosynthetic activity data and the subsequent calculations. Prior to the analysis, each pair of climate and photosynthetic activity variables was resampled to a common spatial resolution in order to enable time series analysis at the pixel level.

We used CCF analysis to calculate direct (i.e., same month) and lagged correlations between each climate variable (i.e., independent variable) and each photosynthetic activity variable (i.e., response variable). We quantified lagged correlations between one and four months because a variety of physiological and ecological mechanisms can potentially delay responses of photosynthetic activity to climate (D. Wu et al., 2015). Our lagged correlations analysis allowed us to determine the strongest immediate or lagged correlation between precipitation or radiation and photosynthetic activity.

In CCF analysis, temporal dependencies or high autocorrelation in the independent variable (in this case our climate variables) can hide true relationships or suggest false ones. "Prewhitening" can remove autocorrelations by extracting the "white noise" from the independent variable and applying the same transformation to the response variable, in this case, photosynthetic activity (Cryer & Chan, 2008). We used prewhitening to counteract autocorrelation, allowing us to analyze the actual linear relationship between the two time series. The data were pre-whitened by first finding an autoregressive integrated moving average (ARIMA) model for the climate variable time series, and then fitting the photosynthetic activity time series to the ARIMA model. ARIMA models are built using information contained in the time series and are commonly used in forecasting, but in the case of this study, and prewhitening in general, they are used to filter the

original series. The CCF was finally performed on the climate series model residuals and the filtered photosynthetic activity time series (Box et al., 2015; Probst et al., 2012). An example of the CCF analysis is available at https://github.com/rosariouribed/ccf_tropics.

Given that precipitation and radiation are two highly correlated variables, we were interested in an analysis that considered the relationship of photosynthetic activity with the two variables individually and in combination. We determined the sign of the maximum direct or lagged correlation coefficient with each variable and then classified the type of relationship based on the signs and strengths of the two coefficients. For instance, photosynthetic activity could be correlated positively with precipitation and negatively with radiation or have a non-significant relationship with precipitation and positive with radiation, and so on (Fig. 2.1, upper-right reference panel). We created a map for each of the photosynthetic activity datasets showing the type of relationship with climate for each pixel. We assessed the agreement between the results from satellite and model data using the Kappa coefficient (κ) for map agreement (Cohen, 1960). The Kappa coefficient compares the agreement between two maps against a hypothetical scenario of randomly assigned values. Coefficients range from -1 to 1, where 0 indicates that the evaluated map is as good as if random values were selected, negative values suggest the map is worse than random values, and positive values suggest the evaluated map matches the reference map better than random values. Values closer to 1 indicate a better agreement between the maps. We also calculated the overall difference (D) as a second measurement of agreement of our results. Overall difference has been suggested to provide a more reliable comparison between maps than the Kappa coefficient (Pontius & Santacruz, 2014). Calculations of D take into account how well maps agree on (1) the number of pixels classified in each category (i.e., quantity difference) and (2) the location of the pixels in each category, given the number of pixels in each of the categories (i.e., allocation difference) (Pontius & Santacruz, 2014). Larger D values indicate greater disagreement between the maps, either because of under- or overestimation of pixels in the different categories, or because of inaccurate spatial allocation of the pixels in each of the categories. Comparisons between maps were also performed at the biome level in order to identify models' biome-specific shortcomings.

We then used the classification of type of relationship and additional climate properties of each pixel to identify climate properties most closely associated with a specific type of relationship.

Only the most common types of relationships (i.e., more than 10% of the pixels) were included in the comparison.

The additional climate properties included mean annual precipitation, mean radiation, mean temperature, dry season length, precipitation seasonality index, and the correlation between monthly precipitation and radiation. We used Kruskal-Wallis nonparametric tests (Kruskal & Wallis, 1952) to identify significant differences in the climate properties among the type of relationships. If the Kruskal-Wallis result was significant ($\propto$=0.05) for a particular variable, we followed up with a pairwise comparison among all types of relationships through the Dunn test with Bonferroni correction (Dunn, 1964). This nonparametric post hoc test can be used for independent groups with non-normal distributions and different sizes. All analyses were performed in R 3.4.0 (R Core Team, 2017), including the forecast v8.2 (Hyndman, 2017), TSA v1.01 (Chan & Ripley, 2012), FSA v0.8.22 (Ogle et al., 2018) and diffeR (Pontius Jr. & Santacruz, 2019) packages.

2.4 Results

2.4.1 Relationship of photosynthetic activity with precipitation and radiation in satellite data

Based on the direction of the correlations between photosynthetic activity and the two climate drivers, most sites in the tropics can be classified into three categories: photosynthetic activity that is (1) positively correlated with both precipitation and radiation, (2) positively correlated with precipitation but negatively correlated with radiation, and (3) positively correlated with radiation but negatively with precipitation (i.e., regions 1, 2 and 3 in Fig. 2.1 upper-left reference panel). From this point, we will refer to these three types of relationships as cosynchronous, rain-following and light-following, respectively. For MAIAC EVI and SIF, these three type of relationships together account for 78-88% of the pixels in the tropics, where the cosynchronous pixels correspond to 36-38%, the rain-following are 28-40% and the light-following are 10-14% of the pixels for the two datasets, respectively (Fig. 2.1). Even though both datasets agree on the dominance of these three types of relationships, there are some differences between the two datasets in the proportion of pixels that show each of these three dominant types (Fig. 2.1). In the SIF dataset, more pixels are cosynchronous and light-following and fewer are

rain-following than in the MAIAC EVI product. The spatial distribution of the three types of relationships is moderately consistent between the two datasets, with a kappa coefficient of agreement of 0.5 and overall difference of 35.12% (Table 1, Fig. 2.2). The results from GOSIF agree closely with those from SIF and EVI ($\kappa = 0.52$ and 0.65, D= 33.42 and 22.58%, respectively), providing stronger confidence in our results (Appendix A, Fig. A1).

Based on the SIF results, cosynchronous pixels (i.e., positive correlations with both precipitation and light) are located across all biomes, but make up the largest fraction (45-86%) of savannas and shrublands, dry broadleaf forests, flooded savannas, montane shrublands, and conifer forest (Appendix A, Fig. A2). The rain-following relationship (28% across all biomes) is most common in the savannas and shrublands, dry forests, flooded savannas, and xeric shrublands. Light-following seasonality is mostly clustered in the rainforests, specifically those of the Amazon basin and southeast Asia.

Other type of relationships are not common (<22% in total), including negative correlations with both drivers (<3% of pixels) and weak correlations with one (<6% of pixels) or both (<3% of pixels) drivers. For the SIF dataset, these other types of correlations occur mostly in the rainforest in South America, central Africa and southeast Asia. A more detailed look at areas with the weakest relationships shows a prevalence of pixels with very low intra-annual variability in photosynthetic activity. These less distinct types of relationships could also be explained by a higher diversity of vegetation cover or land cover change during the study period.

The seasonal peak of photosynthesis most commonly occurred within two months of the seasonal peak of precipitation, while lags with radiation had a much wider range of variation, from 0 to 4 months (Fig. 2.3, Appendix A Fig. A3). These lags also varied among the types of relationships. For the cosynchronous relationship, lags of correlations with precipitation ranged between 0-2 months and with radiation between 3-4 months. For the rain-following relationship, lags with both precipitation and radiation occurred between 0-2 months. For the light-following relationship, the lags of correlations with precipitation were in a wide range of 0-4 months and correlations with radiation, although also quite variable, were most commonly lagged by 0 to 3 months. Geographically, the small number of longer time lags with precipitation occur in the tropical rainforests of South America (Appendix A, Fig. A3), which is mostly a light-following region. The wide variation of time lags with radiation is also evident in its large spatial variation (Appendix A, Fig. A3). A large proportion of the longer time lags with radiation coincide with

cosynchronous regions in the higher tropical latitudes of Africa and Australia. Examples of the seasonal pattern of precipitation, radiation and photosynthetic activity from SIF in pixels from the three main types of relationships are displayed in the Supplementary Materials (Appendix A, Fig. A4).

2.4.2 Climate properties of the different types of relationships of photosynthetic seasonality with precipitation and radiation

Each of the three dominant climate-seasonality relationships was associated with distinct climatic properties (Fig. 2.4a-e). Areas with a cosynchronous relationship tended to have relatively low annual rainfall (Median = 1217 and Interquantile Range = 26 mm), high mean daily radiation ($\tilde{x}$ = 227.9 and IQR = 1.12 W m-2), a long dry season ($\tilde{x}$ = 221.9 and IQR = 1.4 days), relatively low mean temperature ($\tilde{x}$ = 25.7 and IQR = 0.1 °C), and high rainfall seasonality ($\tilde{x}$ = 0.8 and IQR = 0.01). Rain-following pixels had low mean annual precipitation ($\tilde{x}$ = 1214 and IQR = 24 mm), high mean daily radiation ($\tilde{x}$ = 227.9 and IQR = 0.9 W m-2), an intermediate-length dry season ($\tilde{x}$ = 203.1 and IQR = 1.6 days), higher mean temperature ($\tilde{x}$ = 26.1 and IQR = 0.1 °C), and intermediate rainfall seasonality ($\tilde{x}$ = 0.8 and IQR = 0.01). Light- following pixels had high mean annual precipitation ($\tilde{x}$ = 2466 and IQR = 40 mm), low mean daily radiation ($\tilde{x}$ = 201.5 and IQR = 0.7 W m-2), a short dry season ($\tilde{x}$ = 189.9 and IQR = 1.1 days), high mean temperature ($\tilde{x}$ = 26.4 and IQR = 0.1 °C), and low precipitation seasonality ($\tilde{x}$ = 0.5 and IQR = 0.01). The climates of areas with the light- following relationship stood out as distinct from those in other areas across four of the five variables – only temperature, by not differing from regions with the rain-following relationship, bucked this trend. Cosynchronous and rain-following pixels had similar mean annual precipitation and mean daily radiation, but cosynchronous pixels had a longer dry season, lower mean temperature, and larger precipitation seasonality index.

In areas with a cosynchronous relationship, light and precipitation typically were abundant during the same or similar times of year (Fig. 2.4f). Thus, in these areas, we hypothesize that photosynthesis would be greatest during the times of year that were both wet and bright. In contrast, in areas with the other two dominant types of relationships, the rainiest times of year were the darkest, and the driest seasons were brightest. In these areas, we expect that GPP responds most positively to the climate factor that is most limiting. Thus, areas that have lower mean annual precipitation and a longer dry season would be water-limited and show a positive correlation with

rainfall, and consequently a negative correlation with radiation. In areas with higher mean annual precipitation and a shorter dry season, GPP would be limited by light; photosynthesis would be greatest during the brightest times of year and slower during the wetter (and darker) times of year.

2.4.3 Relationship of photosynthetic activity with water and light in ecosystem models

In land surface models, GPP showed the same three dominant type of relationships with climate that we found in the satellite data. However, the proportion of vegetation with each type of relationship and their spatial distribution differed from those in observations (Figs. 2.1 and 2.2). In the simulated data, the rain- following relationship was more widespread than any other (51-53%), and always more common than in the satellite-based datasets. In contrast, the proportion of cosynchronous pixels was typically lower than that shown by satellite data (20-39%), similar to the less-frequent light-following relationship (6-11%). Kappa coefficients and overall differences between the models' results and the MAIAC EVI and SIF datasets (Table 1) ranged from 0.28 to 0.54 and 35.05 to 50.23%, respectively, with LPJ-GUESS showing the most similarity to both satellite-based datasets. Overall, the models produced more similar GPP predictions to one another than to the satellite-based observations (Table 1).

Other vegetation products analyzed in this study also tended to show different patterns from those in models and observations (Figs. 2.1 and 2.2). Fluxcom GPP had a high percentage of pixels with cosynchronous and rain-following relationships (48% and 37%), while light- following relationships were less common than in the satellite data (8%). VPM GPP showed a lot more diversity in the types of relationships, with the greatest proportion of the tropics having cosynchronous and light- following relationships (39% and 31%), and slightly less area covered by rain-following pixels (25%). The Kappa coefficients and overall differences indicate that VPM output agreed more closely with both satellite-based datasets and with the models than Fluxcom (Table 1). Similar to the satellite observations, the model most similar to these two GPP products was LPJ-GUESS.

In our biome-level comparisons (Table S2), the best agreement between SIF and most models was found in montane grasslands and shrublands (κ = 0.46-0.57, D = 18-25%), flooded grasslands and savannas (κ = 0.38-0.44, D = 28.6-34.2%), and grasslands and savannas (κ = 0.33-0.46, D = 30.7-41.8%), in that order. In contrast, low agreement was found in mangroves (κ = -0.17-0.28, D = 52.2-72.7%), rainforest (κ = 0.19-0.34, D = 45.4-62.7%) and deserts and xeric

shrublands (κ = 0.12-0.33, D = 31.5-41.5%). In dry forests, Fluxcom and VPM showed closer agreement with SIF than the land surface models did.

2.5 Discussion

As our analyses show, the seasonality of photosynthetic activity in the tropics is tightly linked to water and light availability throughout the year. The implications for the tropics of ongoing changes in climate, especially in precipitation patterns, and in land cover, will depend on how these changes interact with and affect the seasonal cycles of the vegetation. Accurate predictions of future carbon and water exchange will require models that realistically simulate these relationships. Here, we provide a novel classification that compiles information of the separate relationship with the precipitation and radiation across the entire tropics. Our classification is not only descriptive of the type of relationship of photosynthetic activity with climate across the tropics, but it also provides a clear scheme for model comparison. We also identify where and for which climate variables lagged correlations occur and need to be accounted for in ecosystem models.

Our analysis distinguishes between three dominant types of relationships linking the seasonality of photosynthetic activity to precipitation and radiation (Fig. 2.5). Using our classification, we are able to identify regions where seasonality is positively or negatively correlated with the two climate drivers. The distribution of the three most common relationships is associated with the distributions of local climate properties such as mean annual precipitation, mean daily radiation, precipitation seasonality and the relationship between precipitation and radiation (Fig. 2.4). Cosynchronous relationships are found in regions with a low mean annual precipitation, high mean daily radiation, long dry season, and high precipitation seasonality. These regions correspond to water-limited biomes located in higher latitudes where precipitation and radiation are not negatively correlated, meaning water and light are abundant at approximately the same time. Rain-following relationships are found in regions with similar precipitation and radiation characteristics and are also common in similar biomes. However, this relationship is more common at lower latitudes where precipitation and radiation are negatively correlated. Vegetation from cosynchronous and rain-following regions is likely water-stressed, and therefore responds positively to water availability. What differentiates the regions with these two types of relationships is the timing of radiation with respect to precipitation. In the cosynchronous

relationship, vegetation is adapted to take advantage of seasonal availability (up to 4 months) of both water and light. In the rain-following relationship, vegetation is adapted to periods of increased rainfall that do not coincide with abundant light. The mechanisms by which plant species have adapted to the timing of the two drivers (or been selected by them) could determine vegetation responses to any future changes in the seasonal timing of precipitation and radiation. Recognizing the specific correlation of photosynthetic activity in these regions with the availability of water and light may lead to studies that identify relevant adaptive traits and selective processes, and to better-informed predictions.

The third most common type of relationship, the light-following relationship, is found in regions with high mean annual precipitation, low mean daily radiation, short dry season, low precipitation seasonality, and a negative correlation between precipitation and radiation. This relationship and climate characteristics are very specific to the rainforests of South America where previous field (Restrepo-Coupe et al., 2013) and satellite (Bertani et al., 2017; Bradley et al., 2011b; Wagner et al., 2017) findings show light-driven seasonal photosynthetic activity. Similarly, the spatial distributions of the rain- and light- following relationships found here are comparable to the wet- and dry-season greening regions for tropical rainforests, with those forests in the central Amazon and southeast Asia greening in the dry season, when radiation peaks (Doughty et al., 2019; Guan et al., 2015).

The common climate properties found within each of the different types of relationships show that biomes that share similar climate characteristics can have the same type of seasonality and relationship to climate, despite potential differences in microclimate or soil properties (Meir & Pennington, 2011). At the same time, a single biome can have different relationships with climate depending on location, even at large spatial scales. Our climate characterization highlights the importance of water limitation (i.e., mean annual precipitation, dry season length, and precipitation seasonality) and the precipitation-radiation intra-annual correlation. Together, these two variables define large-scale patterns of photosynthetic activity at the seasonal level. The strong relationship between site-specific climate and the climatic drivers of photosynthetic seasonality is especially important considering the uncertainty in projections of future climate, and particularly precipitation patterns, for different sub-regions in the tropics (Hilker et al., 2014).

The predominance of lagged correlations with precipitation and radiation observed here is consistent with the analyses of Bradley et al. (2011) and Wu et al. (2015). These time lags suggest

that responses of vegetation to rain and light can be strongly influenced by intermediate or indirect processes. Important processes that can lead to delayed responses of photosynthetic activity to climate include vegetation growth in the case of savannas, and leaf phenology in the case of forests and shrublands. Vegetation growth and leaf development may continue after the seasonal peaks in delivery of water or light, such that the ecosystem reaches maximum biomass of leaves, or of the most photosynthetically-efficient leaves, later in the season. This continued growth could cause delayed peaks in photosynthetic activity relative to resource delivery. We found the most common long lags to be with radiation in the cosynchronous relationship, and with precipitation in the light-following relationships. In cosynchronous regions, correlations with precipitation were strongest for short time lags, while correlations with radiation tended to be strongest after longer lags. In these regions, radiation peaks typically occur 1-4 months before those of precipitation. The longer radiation lags mostly occur in the higher tropical latitudes. We speculate that this delayed correlation is the result of plant growth and leaf development continuing throughout the summer season (i.e., continuing after peak radiation), with increased precipitation later in the season leading to a spike in photosynthetic activity.

In light-following regions, precipitation and photosynthetic activity are negatively correlated at relatively long lags. The light-following relationship is common in tropical forests, where trees have been shown to increase photosynthetic activity throughout the dry season due to the vegetation's capacity to obtain water from deep soil layers when shallow soils are dry (Nepstad et al., 1994; Restrepo-Coupe et al., 2013). Thus, soil water storage and adaptive leaf development and demography likely regulate the relationship between precipitation and photosynthetic activity in these regions. Both mechanisms have previously been demonstrated to mediate the relationship between climate and photosynthetic activity in tropical forests (Guan et al., 2015; Restrepo-Coupe et al., 2013; Wu et al., 2016, 2017), and likely play a strong role in our results. For instance, some of these forests' photosynthetic activity peaks happen in the late dry season, months after precipitation declined; similarly, they reach low photosynthetic activity levels in the late wet season months after precipitation has peaked. However, site-specific differences in variables such as soil texture and plant traits also likely contribute to the observed geographical variation in these time lags. Our results suggest that it is important for models to consider mechanisms such as these, which can affect the relationships of tropical ecosystems' photosynthetic activity with precipitation

and light. Our results show the extent of the area of different types of relationships and the associated time lags with each driver.

In general, land surface models accurately represent most of the regional variation in the type of relationship of photosynthesis with precipitation and radiation, with some specific deficiencies. However, models tend to overestimate the extent of positive relationships with precipitation and underestimate the extent of positive relationships with radiation. These two issues result in models overestimating the number of rain-following pixels and underestimating the number of cosynchronous and light-following pixels. Cosynchronous relationships are missed by models in some scattered regions and biomes across the tropics, with the largest misrepresented area located in the dry forests of Southeast Asia. The seasonality of these forests and the underlying mechanisms driving their strong positive lagged correlation with light should be further explored. Leaf phenology potentially plays a role in this lagged correlation, but less research has focused on the seasonality of photosynthetic activity of forests of this region.

The largest differences between SIF and models are in rainforest regions. Model misrepresentation of the seasonality of photosynthetic activity was previously demonstrated using GPP data from eddy flux towers in the Amazon (Restrepo-Coupe et al., 2017). Our results show the extent of this misrepresentation across the entire Amazon and other smaller rainforest areas in Asia. The misrepresentation of rainforests, one of the largest biomes in the tropics, and their characteristic light-following relationship is of major concern. As mentioned above, incorporating increased rooting depth, leaf demography, or other processes could improve the representation of seasonality in simulations (Poulter et al., 2009; Wu et al., 2017; Serbin et al., 2017). The VPM GPP dataset was able to reproduce the light-following relationship, something that neither the models nor Fluxcom GPP did. VPM's capacity to represent this type of relationship might be associated with the light-based model it uses to estimate GPP, which is not used by the other datasets analyzed in this study. This light-use efficiency (LUE) GPP type of model not only gives high importance to radiation but also takes into account the fraction of PAR absorbed by chlorophyll, which directly depends on EVI and helps to improve the representation of the seasonal variation of photosynthetic capacity (Zhang et al., 2017). Among the three models and the two global GPP datasets studied, LPJ-GUESS and VPM showed the closest agreement with our satellite-based results.

Land cover change has undoubtedly influenced the types of relationships observed in SIF and MAIAC EVI. The model output analyzed here uses a static land cover type and could, therefore, misrepresent some of the observed dynamics between climate and SIF and MAIAC EVI. Therefore, we recommend a careful reading of our comparison in regions with high levels of land cover change.

Despite all the physiological, microclimatic and ecological variation in the tropics, at large spatial and temporal scales, observed relationships of photosynthetic activity with precipitation and radiation emerged in clear, distinct patterns. The large-scale nature of this study, at relatively low resolution, necessarily ignores important ecological factors and confounding variables associated with both climate and photosynthetic activity. Nutrient availability, microclimate, topography, soil texture, plant community dynamics, and anthropogenic disturbances are all important factors that influence photosynthetic activity and are not considered here. Yet, the broad spatial patterns identified here can guide research on the predominant mechanistic processes driving photosynthetic activity. The model and GPP products evaluation presented here revealed the types of climate-vegetation relationships that are least accurately simulated by models. We expect that our classification of the types of relationships will simplify model comparison and benchmarking for tropical ecosystems. Our characterization of the time lags shows the existence and extent of important delayed relationships of photosynthetic activity with each of the climate drivers in specific vegetation types and regions in the tropics. These results should guide modeling and experimental studies about the potential processes that determine seasonality of photosynthetic activity in the tropics. We believe this improved understanding could lead to more realistic predictions of how tropical vegetation will respond to ongoing climate change and feedback to the climate system.

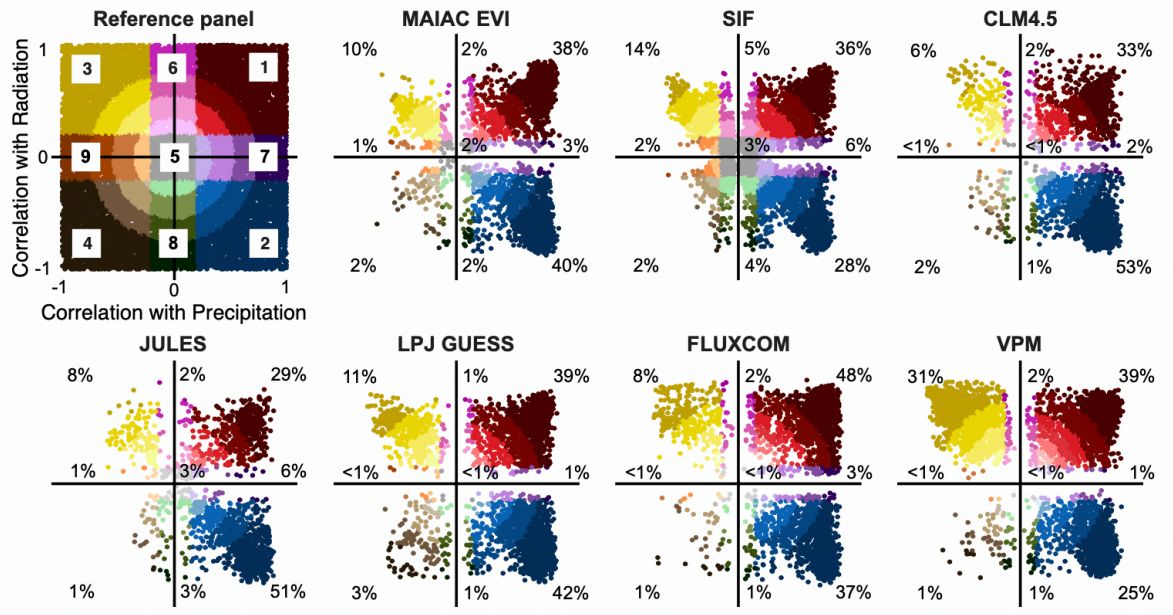

Fig. 2.1. Scatterplots showing the maximum correlation coefficient from the CCF analysis for vegetation productivity from each of the datasets with precipitation (x axis) and radiation (y axis). (Top-left/Reference panel): the nine colors and numbers correspond to each of the types of relationships; the rings indicate the strength of the correlation with both drivers (distance from the origin). Regions 1-4 (red, blue, yellow, and brown) indicate significant correlations with both drivers. Region 5 (gray color) indicates non-significant relationships with any driver. Regions 6-9 (pink, purple, green, and orange indicate non-significant correlations with one of the drivers. (Other panels): the numbers indicate the percentage of pixels with the type of relationship where the number is located.

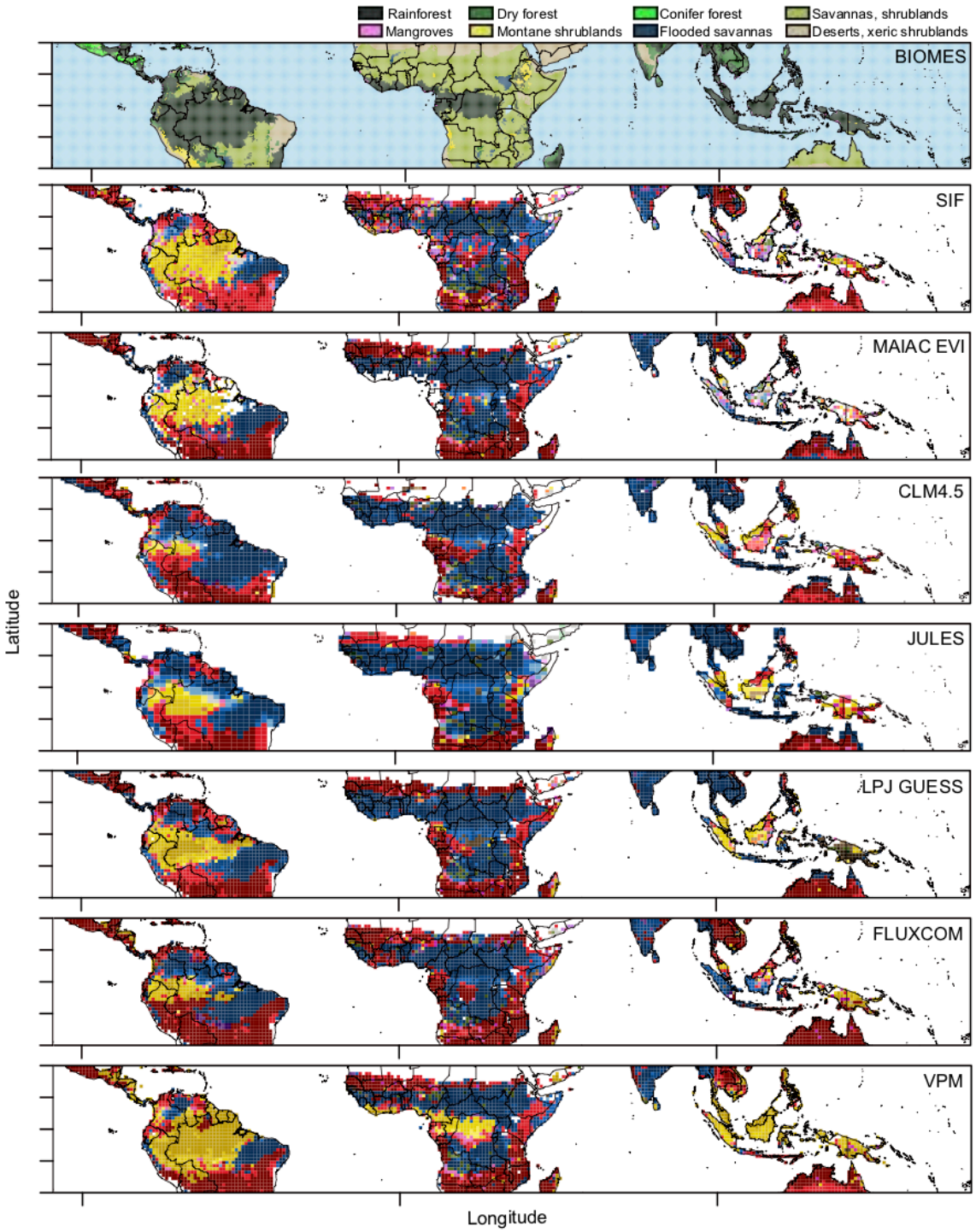

Fig. 2.2. Maps of biomes and results from the CCF analysis. (Top panel): biomes of the tropics (WWF). (Other panels): Maps showing the spatial distribution of the maximum correlation coefficient from the CCF analysis for vegetation productivity from each of the datasets with precipitation and radiation. Colors in the map correspond to the colors and numbers in the reference panel Fig. 2.1, which contain information about the type of combined relationship and strength of the correlations. White pixels correspond to water bodies or pixels with scarce data for CCF analysis.

Table 2.1. Kappa coefficients (κ) and overall difference (D) between the maps resulting from the CCF analysis (Fig. 2.2). Larger κ values indicate closer agreement between the results of two datasets. Larger D values indicate larger differences between the results of two datasets.

	MAIAC EVI	CLM4.5	JULES	LPJ-GUESS	FLUXCOM	VPM
SIF	κ = 0.5	0.28	0.3	0.39	0.4	0.48
	D = 35.12	50.23	49.31	43.16	41.15	37.26
MAIAC EVI		0.45	0.45	0.55	0.5	0.55
		35.05	35.31	29.02	31.96	31.24
CLM4.5			0.52	0.54	0.44	0.31
			28.2	29.03	34.81	49.2
JULES				0.55	0.4	0.32
				28.42	38.6	48.18
LPJ-GUESS					0.43	0.47
					36.42	36.6
FLUXCOM						0.43
						39.01

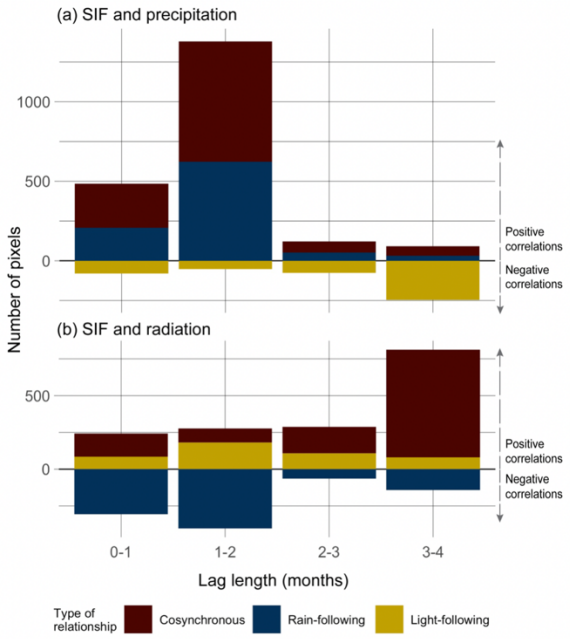

Fig. 2.3. Frequency (number of pixels) of the length of lags in the strongest correlations between SIF and (a) precipitation and (b) radiation for the three most common types of relationships (n=2533). Colors correspond to the colors of the types of relationships shown in the reference panel in Fig. 2.1. In order to differentiate the direction of the correlation, the count of pixels with positive correlation coefficients between the climate driver and SIF is shown upward and the count with negative correlation coefficients is shown downward. Note the difference in scales between (a) and (b).

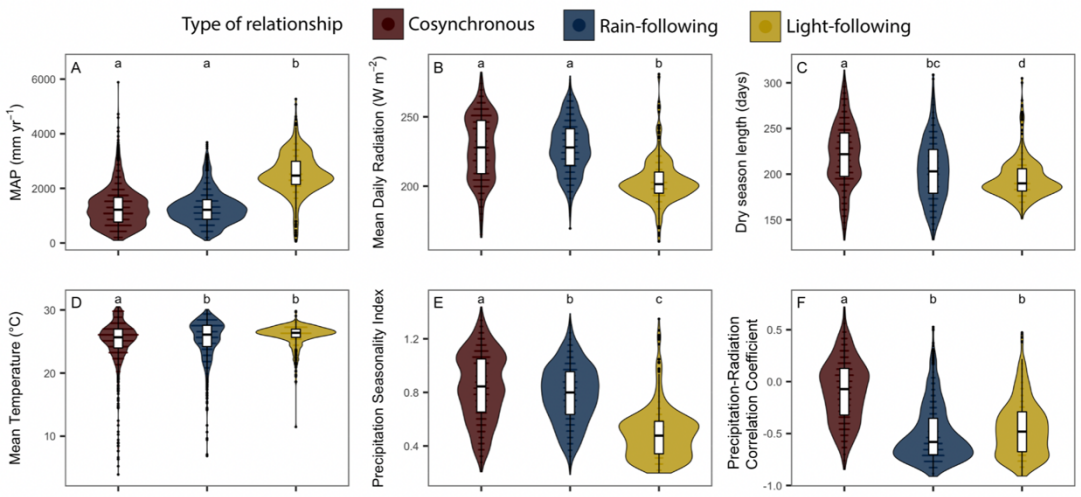

Fig. 2.4. Climate characteristics of the three most common types of relationships inferred from SIF. The shape of the violin plots and the horizontal lines inside of them represent number of pixels; wider shapes and longer horizontal lines are more pixels at that level of that specific variable. The boxplot shows the median and the quartiles. Significant differences between pairs of groups are represented through letters; groups with same letters are not significantly different. Colors and numbers of the types of relationships (legend) correspond to the colors and numbers in the reference panel in Fig. 2.1.

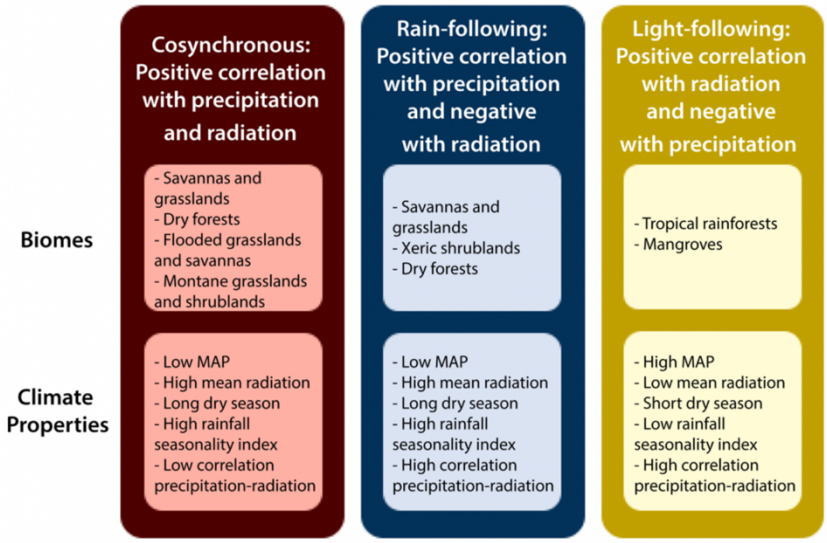

Fig. 2.5. Summary of the most important types of relationships identified in this study. Includes climate properties and the biomes where each of them is more common.

2.6 References

Bertani, G., Wagner, F. H., Anderson, L. O., & Aragão, L. E. O. C. (2017). Chlorophyll Fluorescence Data Reveals Climate-Related Photosynthesis Seasonality in Amazonian Forests. Remote Sensing, 9(12), 1275. https://doi.org/10.3390/rs9121275

Best, M. J., Pryor, M., Clark, D. B., Rooney, G. G., Essery, R. L. H., Ménard, C. B., Edwards, J. M., Hendry, M. A., Porson, A., Gedney, N., Mercado, L. M., Sitch, S., Blyth, E., Boucher, O., Cox, P. M., Grimmond, C. S. B., & Harding, R. J. (2011). The Joint UK Land Environment Simulator (JULES), model description – Part 1: Energy and water fluxes. Geoscientific Model Development, 4(3), 677–699. https://doi.org/10.5194/gmd-4-677-2011

Bombardi, R. J., Kinter, J. L., & Frauenfeld, O. W. (2019). A Global Gridded Dataset of the Characteristics of the Rainy and Dry Seasons. Bulletin of the American Meteorological Society. https://doi.org/10.1175/BAMS-D-18-0177.1

Box, G. E. P., Jenkins, G. M., Reinsel, G. C., Ljung, G. M., & Ljung, G. M. (2015). Time Series Analysis: Forecasting and Control. John Wiley & Sons, Incorporated. http://ebookcentral.proquest.com/lib/purdue/detail.action?docID=2064681

Bradley, A. V., Gerard, F. F., Barbier, N., Weedon, G. P., Anderson, L. O., Huntingford, C., Aragão, L. E. O. C., Zelazowski, P., & Arai, E. (2011a). Relationships between phenology, radiation and precipitation in the Amazon region. Global Change Biology, 17(6), 2245–2260. https://doi.org/10.1111/j.1365-2486.2011.02405.x

Bradley, A. V., Gerard, F. F., Barbier, N., Weedon, G. P., Anderson, L. O., Huntingford, C., Aragão, L. E. O. C., Zelazowski, P., & Arai, E. (2011b). Relationships between phenology, radiation and precipitation in the Amazon region. Global Change Biology, 17(6), 2245–2260. https://doi.org/10.1111/j.1365-2486.2011.02405.x

Chan, K.-S., & Ripley, B. (2012). TSA: Time Series Analysis. R package version 1.01. https://CRAN.R-project.org/package=TSA

Cohen, J. (1960). A Coefficient of Agreement for Nominal Scales. Educational and Psychological Measurement, 20(1), 37–46. https://doi.org/10.1177/001316446002000104

Cryer, J. D., & Chan, K.-S. (2008). Time Series Analysis: With Applications in R (2nd ed.). Springer-Verlag. https://doi.org/10.1007/978-0-387-75959-3

Doughty, R., Köhler, P., Frankenberg, C., Magney, T. S., Xiao, X., Qin, Y., Wu, X., & Moore, B. (2019). TROPOMI reveals dry-season increase of solar-induced chlorophyll fluorescence in the Amazon forest. Proceedings of the National Academy of Sciences, 116(44), 22393–22398. https://doi.org/10.1073/pnas.1908157116

Dunn, O. J. (1964). Multiple Comparisons Using Rank Sums. Technometrics, 6(3), 241–252. JSTOR. https://doi.org/10.2307/1266041

Guan, K., Pan, M., Li, H., Wolf, A., Wu, J., Medvigy, D., Caylor, K. K., Sheffield, J., Wood, E. F., Malhi, Y., Liang, M., Kimball, J. S., Saleska, S. R., Berry, J., Joiner, J., & Lyapustin, A. I. (2015). Photosynthetic seasonality of global tropical forests constrained by hydroclimate. Nature Geoscience, 8(4), 284–289. https://doi.org/10.1038/ngeo2382

Hansen, M. C., Potapov, P. V., Moore, R., Hancher, M., Turubanova, S. A., Tyukavina, A., Thau, D., Stehman, S. V., Goetz, S. J., Loveland, T. R., Kommareddy, A., Egorov, A., Chini, L., Justice, C. O., & Townshend, J. R. G. (2013). High-Resolution Global Maps of 21st-Century Forest Cover Change. Science, 342(6160), 850–853. https://doi.org/10.1126/science.1244693

Harris, I., Jones, P. D., Osborn, T. J., & Lister, D. H. (2014). Updated high-resolution grids of monthly climatic observations – the CRU TS3.10 Dataset. International Journal of Climatology, 34(3), 623–642. https://doi.org/10.1002/joc.3711

Hilker, T., Lyapustin, A. I., Tucker, C. J., Hall, F. G., Myneni, R. B., Wang, Y., Bi, J., Mendes de Moura, Y., & Sellers, P. J. (2014). Vegetation dynamics and rainfall sensitivity of the Amazon. Proceedings of the National Academy of Sciences, 111(45), 16041–16046. https://doi.org/10.1073/pnas.1404870111

Huete, A. R., Didan, K., Shimabukuro, Y. E., Ratana, P., Saleska, S. R., Hutyra, L. R., Yang, W., Nemani, R. R., & Myneni, R. (2006). Amazon rainforests green-up with sunlight in dry season. Geophysical Research Letters, 33(6). https://doi.org/10.1029/2005GL025583

Huffman, G. J., Bolvin, D. T., Nelkin, E. J., Wolff, D. B., Adler, R. F., Gu, G., Hong, Y., Bowman, K. P., & Stocker, E. F. (2007). The TRMM Multisatellite Precipitation Analysis (TMPA): Quasi-Global, Multiyear, Combined-Sensor Precipitation Estimates at Fine Scales. Journal of Hydrometeorology, 8(1), 38–55. https://doi.org/10.1175/JHM560.1

Hyndman, R. (2017). _forecast: Forecasting functions for time series and linear models_. R package version 8.2. http://pkg.robjhyndman.com/forecast

Joiner, J., Guanter, L., Lindstrot, R., Voigt, M., Vasilkov, A. P., Middleton, E. M., Huemmrich, K. F., Yoshida, Y., & Frankenberg, C. (2013). Global monitoring of terrestrial chlorophyll fluorescence from moderate-spectral-resolution near-infrared satellite measurements: Methodology, simulations, and application to GOME-2. Atmospheric Measurement Techniques, 6(10), 2803–2823. https://doi.org/10.5194/amt-6-2803-2013

Joiner, J., Yoshida, Y., Vasilkov, A. P., Schaefer, K., Jung, M., Guanter, L., Zhang, Y., Garrity, S., Middleton, E. M., Huemmrich, K. F., Gu, L., & Belelli Marchesini, L. (2014). The seasonal cycle of satellite chlorophyll fluorescence observations and its relationship to vegetation phenology and ecosystem atmosphere carbon exchange. Remote Sensing of Environment, 152, 375–391. https://doi.org/10.1016/j.rse.2014.06.022

Joiner, J., Yoshida, Y., Vasilkov, A. P., Yoshida, Y., Corp, L. A., & Middleton, E. M. (2011). First observations of global and seasonal terrestrial chlorophyll fluorescence from space. Biogeosciences, 8(3), 637–651. https://doi.org/10.5194/bg-8-637-2011

Jung, M., & Team, F. (2016). FLUXCOM (RS+METEO) Global Land Carbon Fluxes using CRUNCEP climate data [Data set]. https://doi.org/10.17871/fluxcom_rs_meteo_cruncepv6_1980_2013_v1

Kato, S., Loeb, N. G., Rose, F. G., Doelling, D. R., Rutan, D. A., Caldwell, T. E., Yu, L., & Weller, R. A. (2013). Surface Irradiances Consistent with CERES-Derived Top-of-Atmosphere Shortwave and Longwave Irradiances. Journal of Climate, 26(9), 2719–2740. https://doi.org/10.1175/JCLI-D-12-00436.1

Kruskal, W. H., & Wallis, W. A. (1952). Use of Ranks in One-Criterion Variance Analysis. Journal of the American Statistical Association, 47(260), 583–621. JSTOR. https://doi.org/10.2307/2280779

Lawrence, D., & Vandecar, K. (2015). Effects of tropical deforestation on climate and agriculture. Nature Climate Change, 5(1), 27–36. https://doi.org/10.1038/nclimate2430

Li, X., & Xiao, J. (2019). A Global, 0.05-Degree Product of Solar-Induced Chlorophyll Fluorescence Derived from OCO-2, MODIS, and Reanalysis Data. Remote Sensing, 11(5), 517. https://doi.org/10.3390/rs11050517

Lyapustin, A. I., Wang, Y., Laszlo, I., Hilker, T., G.Hall, F., Sellers, P. J., Tucker, C. J., & Korkin, S. V. (2012). Multi-angle implementation of atmospheric correction for MODIS (MAIAC): 3. Atmospheric correction. Remote Sensing of Environment, 127, 385–393. https://doi.org/10.1016/j.rse.2012.09.002

Lyapustin, A., Wang, Y., Korkin, S., & Huang, D. (2018). MODIS Collection 6 MAIAC algorithm. Atmospheric Measurement Techniques, 11(10), 5741–5765. https://doi.org/10.5194/amt-11-5741-2018

Maeda, E. E., Moura, Y. M., Wagner, F., Hilker, T., Lyapustin, A. I., Wang, Y., Chave, J., Mõttus, M., Aragão, L. E. O. C., & Shimabukuro, Y. (2016). Consistency of vegetation index seasonality across the Amazon rainforest. International Journal of Applied Earth Observation and Geoinformation, 52, 42–53. https://doi.org/10.1016/j.jag.2016.05.005

Malhi, Y., Roberts, J. T., Betts, R. A., Killeen, T. J., Li, W., & Nobre, C. A. (2008). Climate Change, Deforestation, and the Fate of the Amazon. Science, 319(5860), 169–172. https://doi.org/10.1126/science.1146961

Meir, P., & Pennington, R. T. (2011). Climatic Change and Seasonally Dry Tropical Forests. In R. Dirzo, H. S. Young, H. A. Mooney, & G. Ceballos (Eds.), Seasonally Dry Tropical Forests: Ecology and Conservation (pp. 279–299). Island Press/Center for Resource Economics. https://doi.org/10.5822/978-1-61091-021-7_16

Mitchard, E. T. A. (2018). The tropical forest carbon cycle and climate change. Nature, 559(7715), 527. https://doi.org/10.1038/s41586-018-0300-2

Myneni, R. B., Yang, W., Nemani, R. R., Huete, A. R., Dickinson, R. E., Knyazikhin, Y., Didan, K., Fu, R., Juárez, R. I. N., Saatchi, S. S., Hashimoto, H., Ichii, K., Shabanov, N. V., Tan, B., Ratana, P., Privette, J. L., Morisette, J. T., Vermote, E. F., Roy, D. P., … Salomonson, V. V. (2007). Large seasonal swings in leaf area of Amazon rainforests. Proceedings of the National Academy of Sciences, 104(12), 4820–4823. https://doi.org/10.1073/pnas.0611338104

Nemani, R. R., Keeling, C. D., Hashimoto, H., Jolly, W. M., Piper, S. C., Tucker, C. J., Myneni, R. B., & Running, S. W. (2003). Climate-Driven Increases in Global Terrestrial Net Primary Production from 1982 to 1999. Science, 300(5625), 1560–1563. https://doi.org/10.1126/science.1082750

Nepstad, D. C., de Carvalho, C. R., Davidson, E. A., Jipp, P. H., Lefebvre, P. A., Negreiros, G. H., da Silva, E. D., Stone, T. A., Trumbore, S. E., & Vieira, S. (1994). The role of deep roots in the hydrological and carbon cycles of Amazonian forests and pastures. Nature, 372(6507), 666–669. http://search.proquest.com/docview/16600521?rfr_id=info%3Axri%2Fsid%3Aprimo

Ogle, D. H., Wheeler, P., & Dinno, A. (2018). FSA: Fisheries Stock Analysis. R package version 0.8.22. https://github.com/droglenc/FSA

Oleson, K., Lawrence, M., Bonan, B., Drewniak, B., Huang, M., Koven, D., Levis, S., Li, F., Riley, J., Subin, M., Swenson, S., Thornton, E., Bozbiyik, A., Fisher, R., Heald, L., Kluzek, E., Lamarque, J.-F., Lawrence, J., Leung, R., … Yang, Z.-L. (2013). Technical description of version 4.5 of the Community Land Model (CLM). https://doi.org/10.5065/D6RR1W7M

Pontius Jr., R. G., & Santacruz, A. (2019). DiffeR: Metrics of Difference for Comparing Pairs of Maps or Pairs of Variables (R package version 0.0-6) [Computer software]. https://CRAN.R-project.org/package=diffeR

Pontius, R. G., & Santacruz, A. (2014). Quantity, exchange, and shift components of difference in a square contingency table. International Journal of Remote Sensing, 35(21), 7543–7554. https://doi.org/10.1080/2150704X.2014.969814

Poulter, B., Heyder, U., & Cramer, W. (2009). Modeling the Sensitivity of the Seasonal Cycle of GPP to Dynamic LAI and Soil Depths in Tropical Rainforests. Ecosystems, 12(4), 517–533. https://doi.org/10.1007/s10021-009-9238-4

Probst, W. N., Stelzenmüller, V., & Fock, H. O. (2012). Using cross-correlations to assess the relationship between time-lagged pressure and state indicators: An exemplary analysis of North Sea fish population indicators. ICES Journal of Marine Science, 69(4), 670–681. https://doi.org/10.1093/icesjms/fss015

R Core Team. (2017). R: A language and environment for statistical computing. R Foundation for Statistical Computing, Vienna, Austria. https://www.R-project.org/

Restrepo-Coupe, N., da Rocha, H. R., Hutyra, L. R., da Araujo, A. C., Borma, L. S., Christoffersen, B., Cabral, O. M. R., de Camargo, P. B., Cardoso, F. L., da Costa, A. C. L., Fitzjarrald, D. R., Goulden, M. L., Kruijt, B., Maia, J. M. F., Malhi, Y. S., Manzi, A. O., Miller, S. D., Nobre, A. D., von Randow, C., … Saleska, S. R. (2013). What drives the seasonality of photosynthesis across the Amazon basin? A cross-site analysis of eddy flux tower

measurements from the Brasil flux network. Agricultural and Forest Meteorology, 182–183, 128–144. https://doi.org/10.1016/j.agrformet.2013.04.031

Restrepo-Coupe, N., Levine, N. M., Christoffersen, B. O., Albert, L. P., Wu, J., Costa, M. H., Galbraith, D., Imbuzeiro, H., Martins, G., Araujo, A. C. da, Malhi, Y. S., Zeng, X., Moorcroft, P., & Saleska, S. R. (2017). Do dynamic global vegetation models capture the seasonality of carbon fluxes in the Amazon basin? A data-model intercomparison. Global Change Biology, 23(1), 191–208. https://doi.org/10.1111/gcb.13442

Saigusa, N., Yamamoto, S., Hirata, R., Ohtani, Y., Ide, R., Asanuma, J., Gamo, M., Hirano, T., Kondo, H., Kosugi, Y., Li, S.-G., Nakai, Y., Takagi, K., Tani, M., & Wang, H. (2008). Temporal and spatial variations in the seasonal patterns of CO2 flux in boreal, temperate, and tropical forests in East Asia. Agricultural and Forest Meteorology, 148(5), 700–713. https://doi.org/10.1016/j.agrformet.2007.12.006

Saleska, S. R., Miller, S. D., Matross, D. M., Goulden, M. L., Wofsy, S. C., da Rocha, H. R., de Camargo, P. B., Crill, P., Daube, B. C., de Freitas, H. C., Hutyra, L., Keller, M., Kirchhoff, V., Menton, M., Munger, J. W., Pyle, E. H., Rice, A. H., & Silva, H. (2003). Carbon in Amazon Forests: Unexpected Seasonal Fluxes and Disturbance-Induced Losses. Science, 302(5650), 1554–1557. JSTOR. http://www.jstor.org/stable/3835784

Seddon, A. W. R., Macias-Fauria, M., Long, P. R., Benz, D., & Willis, K. J. (2016). Sensitivity of global terrestrial ecosystems to climate variability. Nature, 531(7593), 229–232. https://doi.org/10.1038/nature16986

Sitch, S., Friedlingstein, P., Gruber, N., Jones, S. D., Murray-Tortarolo, G., Ahlström, A., Doney, S. C., Graven, H., Heinze, C., Huntingford, C., Levis, S., Levy, P. E., Lomas, M., Poulter, B., Viovy, N., Zaehle, S., Zeng, N., Arneth, A., Bonan, G., … Myneni, R. (2015). Recent trends and drivers of regional sources and sinks of carbon dioxide. Biogeosciences, 12(3), 653–679. https://doi.org/10.5194/bg-12-653-2015

Smith, B., Prentice, I. C., & Sykes, M. T. (2001). Representation of Vegetation Dynamics in the Modelling of Terrestrial Ecosystems: Comparing Two Contrasting Approaches within European Climate Space. Global Ecology and Biogeography, 10(6), 621–637. JSTOR. http://www.jstor.org/stable/3182691

Tramontana, G., Jung, M., Schwalm, C. R., Ichii, K., Camps-Valls, G., Ráduly, B., Reichstein, M., Arain, M. A., Cescatti, A., Kiely, G., Merbold, L., Serrano-Ortiz, P., Sickert, S., Wolf, S., & Papale, D. (2016). Predicting carbon dioxide and energy fluxes across global FLUXNET sites with regression algorithms. Biogeosciences, 13(14), 4291–4313. https://doi.org/10.5194/bg-13-4291-2016

Wagner, F. H., Hérault, B., Rossi, V., Hilker, T., Maeda, E. E., Sanchez, A., Lyapustin, A. I., Galvão, L. S., Wang, Y., & Aragão, L. E. O. C. (2017). Climate drivers of the Amazon forest greening. PLOS ONE, 12(7), e0180932. https://doi.org/10.1371/journal.pone.0180932

Walsh, R. P. D., & Lawler, D. M. (1981). Rainfall Seasonality: Description, Spatial Patterns and Change Through Time. Weather, 36(7), 201–208. https://doi.org/10.1002/j.1477-8696.1981.tb05400.x

Wu, D., Zhao, X., Liang, S., Zhou, T., Huang, K., Tang, B., & Zhao, W. (2015). Time-lag effects of global vegetation responses to climate change. Global Change Biology, 21(9), 3520–3531. https://doi.org/10.1111/gcb.12945

Wu, J., Albert, L. P., Lopes, A. P., Restrepo-Coupe, N., Hayek, M., Wiedemann, K. T., Guan, K., Stark, S. C., Christoffersen, B., Prohaska, N., Tavares, J. V., Marostica, S., Kobayashi, H., Ferreira, M. L., Campos, K. S., Silva, R. da, Brando, P. M., Dye, D. G., Huxman, T. E., … Saleska, S. R. (2016). Leaf development and demography explain photosynthetic seasonality in Amazon evergreen forests. Science, 351(6276), 972–976. https://doi.org/10.1126/science.aad5068

Wu, J., Serbin, S. P., Xu, X., Albert, L. P., Chen, M., Meng, R., Saleska, S. R., & Rogers, A. (2017). The phenology of leaf quality and its within-canopy variation is essential for accurate modeling of photosynthesis in tropical evergreen forests. Global Change Biology, 23(11), 4814–4827. https://doi.org/10.1111/gcb.13725

Xu, L., Saatchi, S. S., Yang, Y., Myneni, R. B., Frankenberg, C., Chowdhury, D., & Bi, J. (2015). Satellite observation of tropical forest seasonality: Spatial patterns of carbon exchange in Amazonia. Environmental Research Letters, 10(8), 084005. https://doi.org/10.1088/1748-9326/10/8/084005

Zhang, Y., Joiner, J., Gentine, P., & Zhou, S. (2018). Reduced solar-induced chlorophyll fluorescence from GOME-2 during Amazon drought caused by dataset artifacts. Global Change Biology, 24(6), 2229–2230. https://doi.org/10.1111/gcb.14134

Zhang, Y., Xiao, X., Wu, X., Zhou, S., Zhang, G., Qin, Y., & Dong, J. (2017). A global moderate resolution dataset of gross primary production of vegetation for 2000–2016. Scientific Data, 4, 170165. https://doi.org/10.1038/sdata.2017.165.

CHAPTER 3. LAND COVER CHANGE ALTERS SEASONAL PHOTOSYNTHETIC ACTIVITY AND TRANSPIRATION OF AMAZON FORESTS AND SHRUBLANDS

3.1 Abstract

The relationship between tropical ecosystems and the atmosphere influences the local, regional, and global climate. This relationship is largely based on photosynthetic activity and transpiration of vegetation. When the natural vegetation is replaced, both of these processes are altered, with consequences for climate. Land cover change in the Amazon started decades ago and is expected to continue. Because of the close relationship of vegetation with climate, it is key to understand and monitor the effects of land cover change on photosynthetic activity and transpiration. However, long-term data are scarce in the tropics, hindering our ability to study these effects in the field. Here, we use remote sensing data to analyze the impact of land cover change on photosynthetic activity and transpiration at the seasonal scale in the southern Amazon. This region, which includes tropical forest and the Cerrado ecosystems, has seen high rates of land cover change. We find that this land cover change has reduced photosynthetic activity and transpiration in forest-dominated regions, specifically during the dry season. The decrease in photosynthetic activity is also observed in a switch from dry season greening in forest regions to dry season browning. In contrast, land cover change increases photosynthetic activity in shrubland-dominated pixels during the wet season, and has no effect during the dry season. In both ecosystems, land cover change results in a higher annual range of photosynthetic activity, typically because of either higher maximum or lower minimum photosynthetic rates. The observed effects are often intensified with increasing land cover change. We expect this study to contribute to our current knowledge and model representation of the effects of land cover change on photosynthetic activity and transpiration.

3.2 Introduction

Tropical ecosystems provide several ecosystem services to the rest of the planet. In addition to storing large amounts of carbon in live biomass and sheltering biodiversity, they influence the regional and global climate (Nobre et al., 2016). The high rates of photosynthetic activity that

characterize these ecosystems lead to large and fast exchanges of water, energy, and carbon with the atmosphere. This strong interaction with the atmosphere influences climate in different ways. For instance, about 32% of the Amazon rainfall is produced locally, and 75% of the rainfall is returned to the atmosphere (Lovejoy & Nobre, 2019; Staal et al., 2018). In addition to affecting local rainfall, these forests also influence continental precipitation (Lawrence & Vandecar, 2015), regional surface temperature (Alkama & Cescatti, 2016), and atmospheric carbon concentrations (Hubau et al., 2020).

Natural ecosystems of the Amazon basin and the ecosystem services they provide to the rest of the planet are threatened by high rates of anthropogenic land cover change (LCC; Nobre et al., 2016). Current estimates indicate that about 17% of the tropical forests of the Amazon basin have been deforested (Lovejoy & Nobre, 2019). Model projections estimate that, in a business-as-usual scenario, as much as 47% of the Brazilian Amazon could be deforested by 2050 (Spracklen and Garcia-Carreras 2015).

Removing and replacing native vegetation changes carbon and water cycling, among many other socio-economic and environmental effects (Chambers & Artaxo, 2017; Marengo et al., 2018; Spracklen & Garcia-Carreras, 2015). The changes in carbon and water exchanges with the atmosphere are, in large part, the result of differences in photosynthetic rates and water-use efficiency between the original and the replacing vegetation (Butt et al., 2011). In the Amazon, tropical forests increase photosynthetic activity and transpiration during the dry season (Saleska et al., 2003; Zemp et al., 2017). Deep roots and hydraulic redistribution enable large, old trees to access water in the deeper layers of the soil (Nepstad et al., 1994; Rafael S. Oliveira et al., 2005). Without these large trees, other vegetation types in similar climatic conditions could not access deep water, which would limit photosynthetic activity and growth during the dry season (R. S. Oliveira et al., 2005). Changes in land cover that alter the relationship between photosynthetic activity and climate would modify the relationship between the land surface and the atmosphere (Nepstad et al., 1994). More specifically, a shift in the seasonality of photosynthetic activity could shift the seasonality of precipitation (Chambers & Artaxo, 2017). Furthermore, changes in precipitation seasonality affect vegetation distribution, phenology, and photosynthetic activity. This feedback loop could, eventually, lead to a tipping point for ecosystems in this region (Marengo et al., 2018).

In the Amazon region, there have been challenges in monitoring the changing relationship between land cover and regional climate as land cover continues to change. Historically, large scale changes in precipitation, temperature, and evapotranspiration due to LCC in the Amazon have been studied using global circulation models (GCM) (Chambers & Artaxo, 2017; D'Almeida et al., 2007). Fewer studies have used field- and remote sensing-derived data to investigate these changes (Vergopolan and Fisher 2016). In addition to problems with the lack of observational studies, land surface models coupled to GCMs inaccurately represent seasonality of photosynthetic activity of tropical forests of the Amazon (Restrepo-Coupe et al., 2017, Chapter 1). Modern remote sensing datasets provide a useful tool for investigating changes in photosynthetic activity and transpiration in the Amazon.

Understanding how LULCC affects seasonality of photosynthetic activity and transpiration is necessary if we are to predict the effects of LULCC on water and carbon cycling. In this study, we estimate the current effects of LULCC on photosynthetic activity and transpiration by evaluating differences in remote sensing-derived data products between areas with low and high LULCC. We answer the following questions: What is the effect of LULCC in photosynthetic activity and transpiration in two ecosystems in the Amazon? Are these effects different between the wet and the dry season? And, does the magnitude of these effects change as LULCC increases within an area? We hypothesized that photosynthetic activity and transpiration decrease with LULCC, specifically during the dry season, in both ecosystems. We expected these dry season reductions to decrease annual averages and to increase the range of variation of photosynthetic activity and transpiration.

3.3 Methods

To test the effects of LULCC we compared photosynthetic activity and transpiration in areas with high and low land cover change in a region located in the southeastern Amazon. We used linear mixed-effects models to identify differences in average, minimum, maximum and variation in photosynthetic activity and transpiration. We ran separate tests for the dry and wet seasons, and for forest- and Cerrado-dominated pixels.

3.3.1 Area of study and data collection

Our analysis is based on a 3.7 million km2 region in the southwestern part of the Amazon basin, where the "Arc of Deforestation" is located (Fig. 3.1). This region has undergone extensive LCC and includes the two most common types of natural vegetation in the Amazon (i.e., tropical rainforest and Cerrado) (Silva et al., 2016). Thus, this area of study allowed us to compare regions with high and low LCC for both forest and the Cerrado ecosystems.

Land cover data were obtained from the European Space Agency Climate Change Initiative Land Cover Time Series v2.0.7. This is an annual product of land cover available for the period 1992-2015 at a 300 m spatial resolution (ESA, 2017). Land cover was estimated using unsupervised classification and machine learning algorithms for change detection and delineation of remote sensing land products (MERIS, AVHRR, SPOT-VGT, and PROBA-V). The dataset has 22 land cover types, including natural (e.g., tree, shrubland, and grassland) and anthropogenic (e.g., cropland and urban) land covers. Fourteen of the 22 land cover types are found in the area of study. We excluded urban areas and water bodies from our analyses. The Cerrado ecosystem is classified as a shrubland in this dataset, therefore, we will refer to the Cerrado ecosystem as shrublands from this point on.

We used remote sensing-derived monthly data of photosynthetic activity and transpiration between 2007 and 2016. Photosynthesis was analyzed using measurements of Solar Induced Fluorescence (SIF), a remote sensing measurement of the energy emitted by leaves as fluorescence, which is highly correlated with plant photosynthesis (Joiner et al., 2011). We used the GOME2_F product V27 (Level 3) from the Global Ozone Monitoring Experiment-2 on MetOp-A and MetOp-B (https://avdc.gsfc.nasa.gov/pub/data/satellite/MetOp/GOME_F/) (Joiner et al., 2013). This monthly dataset is available at a 0.5-degree x 0.5-degree spatial resolution since 2007. Transpiration (TR) data were obtained from the Global Land Evaporation Amsterdam Model (GLEAM). In GLEAM, the different components of actual evapotranspiration are derived using potential evaporation and a multiplicative evaporative stress factor (Martens et al., 2017). Potential evaporation is calculated with the Priestley and Taylor equation, which is based on air temperature and radiation. The stress factor in vegetated areas is based on remote-sensing data of Vegetation Optical Depth (VOD) and root-zone soil moisture content. VOD accounts for phenological constraints and soil moisture for water availability for vegetation transpiration (Martens et al.,

2017). The GLEAM transpiration dataset is available at 0.25- x 0.25-degree resolution between 1980 and 2018.

We used the Rainy and Dry Seasons (RADS) dataset (Bombardi et al., 2019) to define the start and end of the dry and wet seasons for each year between 2007-2016. RADS uses the TRMM global gridded daily precipitation dataset to provide several characteristics of precipitation seasonality at 0.25 x 0.25-degree resolution. Seasons are defined based on accumulated precipitation anomalies (S), which correspond to the difference between daily precipitation and the annual daily average precipitation. The calculation of the S starts at a date t_0 within the dry season every year (i.e., full cycle). In each pixel, t_0 is estimated as the minimum of the first harmonic in the mean annual cycle of precipitation. The start and end of the wet season are calculated by finding inflection points in S for each site and each year. Starting in t_0, in the dry season, the S curve first declines. When the rainy season starts, S increases progressively and causes an inflection point in the curve. The S curve is smoothed to eliminate false inflection points. More details about the algorithms and assumptions used in these calculations can be found in Bombardi et al. (2017, 2019). We provide a description of the wet and dry seasons in the area of study in the Supplementary Materials (Supplementary Text).

Mean elevation data were obtained from the SRTM30 Digital Elevation Model (DEM) dataset (Saatchi, 2013). This dataset is derived using Shuttle Radar Topography Mission (SRTM) and the U.S. Geological Survey's GTOPO30 data. The data original resolution is 30 arc seconds (~ 1 km). The transpiration, RADS, and elevation datasets were all resampled with bilinear interpolation to match the 0.5-degree resolution of the SIF dataset.

3.3.2 Pixel-pair selection and data analysis

To test the difference in photosynthetic activity and transpiration between regions with high and low LCC, we extracted pixels with high rates of LCC between 1992 and 2015. Given that the resolution of our SIF and transpiration data was coarser than the land cover data, we calculated the percentage of smaller pixels (300m x 300m) within a larger pixel (0.5º x 0.5º) with a change of land cover type from 1992 to 2015. For the pair selection, we first selected all the pixels in the region with high LCC using a threshold of more than 20% smaller pixels with LCC in a larger pixel (Appendix B, Fig. B2). We then found a reference pixel for each of the high LCC pixels selected. The reference pixel is a pixel with the same dominant land cover type but low LCC (i.e.,

less than 5% smaller pixels with LCC in a larger pixel). A maximum distance of one degree (~ 100 km) was allowed between each pair of high and low LCC pixels; if no pixel with low LCC within such proximity was found, the high LCC pixel was discarded. A detailed graphic explanation of the LCC calculations and the pixels selected for the 20% threshold are shown in the supplementary information (Appendix B, Fig. B1-B2, respectively).

We built linear mixed-effects models (LMMs) to test if there were significant differences in SIF and TR between all pairs of pixels (low and high LCC). Given that SIF data are only available since 2007, we performed our SIF and transpiration comparative analysis for the period 2007-2016. We calculated each pixel's mean (Eq. 1a-b), mean minimum (Eq. 2a-b), mean maximum (Eq. 3a-b), and average range (Eq. 4a-b) SIF and TR. Each mean value was calculated as an annual (Eqs. 1a, 2a, 3a, 4a) or seasonal average (Eqs. 1b, 2b, 3b, 4b), separately for the wet and the dry seasons. We calculated one additional metric to measure the mean change in SIF and transpiration from the start to the end of each season (Eq. 5). The start and end dates of each season were obtained from RADS.

$$\overline{x_Y} = \frac{1}{n_Y}\sum_{j=1}^{n_Y} x_j \quad \text{Eq. 1a;} \qquad \overline{x_{SS}} = \frac{1}{n_{SS}}\sum_{p=1}^{n_{SS}} x_p \quad \text{Eq. 1b}$$

$$\overline{x_{Ymin}} = \frac{1}{n_Y}\sum_{j=1}^{n_Y} x_{min,j} \quad \text{Eq. 2a;} \qquad \overline{x_{SSmin}} = \frac{1}{n_{SS}}\sum_{p=1}^{n_{SS}} x_{min,p} \quad \text{Eq. 2b}$$

$$\overline{x_{Ymax}} = \frac{1}{n_Y}\sum_{j=1}^{n_Y} x_{max,j} \quad \text{Eq. 3a;} \qquad \overline{x_{SSmax}} = \frac{1}{n_{SS}}\sum_{p=1}^{n_{SS}} x_{max,p} \quad \text{Eq. 3b}$$

$$\overline{x_{Yrange}} = \frac{1}{n_Y}\sum_{j=1}^{n_Y}(x_{max,j} - x_{min,j}) \quad \text{Eq. 4a}$$

$$\overline{x_{SSrange}} = \frac{1}{n_{SS}}\sum_{p=1}^{n_{SS}}(x_{max,p} - x_{min,p}) \quad \text{Eq. 4b}$$

$$\overline{\Delta x_{SS}} = \frac{1}{n_{SS}}\sum_{p=1}^{n_{SS}}(x_{eos,p} - x_{sos,p}) \quad \text{Eq. 5}$$

Where x represents either SIF or TR; SS represents either wet or dry season; n_Y, and n_{SS} represent the number of years and seasons; x_j, and x_p denote annual and seasonal observations; x_{min} and x_{max} indicate the minimum and maximum values of a year or season; and x_{eos} and x_{sos} denote end and start of season values (Appendix B, Fig. B3).

In our LMMs, the different SIF and TR metrics are the response variables, LCC level (i.e., high and low) is the categorical explanatory variable, elevation is a covariate and pixel pair is a random effect. To account for the possibility of spatial autocorrelation, we also fit models that included spatial autocorrelation functions. The final model for each metric was selected based on the Akaike information criterion (AIC) value, after meeting the regression assumptions. LMMs

provide estimates for the difference between low and high LCC pixels (β_1; Appendix B, Fig. B4) and their statistical significance (p-value). We also fit LMMs separately for the two most important ecosystems in the area of study, forests (β_{1f}) and shrublands (β_{1s}). LMM analyses were performed using the R package *nlme* (Pinheiro et al., 2020).

To understand how variables were affected by increasing extents of LCC, we performed the same pixel selection and statistical analyses using a range of different LCC thresholds. We varied the threshold for high-LCC pixels, using thresholds of >10%, >30% and >40% of smaller pixels with LCC within a larger pixel (Appendix B, Fig. B1). For each definition of "high-LCC" pixels, we identified a reference pixel (i.e., less than 5% smaller pixels with LCC in a larger pixel) using the same criteria used in the main analyses above. Finally, we calculated the same metrics and fit the LMM for each LCC threshold category. We compared the estimated differences and statistical significance of high vs. low LCC across the different high LCC thresholds. The number of pairs selected under each threshold is provided in Table S1.

We investigated whether any differences in photosynthesis and transpiration between high- and low-LCC regions could be caused by different precipitation patterns, rather than LCC. To test differences in precipitation, we compared the annual precipitation and the dry and wet season lengths and intensities. We used the same methods used to compare SIF and transpiration and the same pixel samples. Paired low- and high-LCC pixels did not differ in mean annual precipitation, or in the durations or total precipitation of the dry and wet seasons (Table S2), suggesting that any differences in photosynthetic activity and transpiration result from differences in land cover (i.e., vegetation), rather than climate.

3.4 Results

The effects of land cover change on photosynthetic activity and transpiration depended on the season and ecosystem type (Fig. 3.3). In forests, LCC decreased SIF and TR in the dry season. In shrublands, LCC increased SIF in the wet season. The average range of SIF increased with LCC in forests in the dry season and in shrublands in both seasons. The average range of TR increased with LCC only in forested pixels during the dry season. Most effects of LCC intensified in regions where a greater fraction of the landscape was converted, despite smaller sample sizes.

3.4.1 Land cover change and precipitation in the area of study

The most common land cover types in 1992 were forests and shrublands, which covered about 63% and 17% of the region, correspondingly (Fig. 3.2). By that same year, about 14% of the region was already converted to herbaceous cropland, woody cropland, or some mosaic between natural vegetation and cropland. By 2015, forests had decreased to 55%, a loss of about 12% of the forest extent from 1992. Shrublands, surprisingly, were only reduced to 16% of land cover in 2015, a reduction of about 3%, of their 1992 area. This small reduction could be explained by the high conversion rates of shrublands to anthropogenic cover before 1992. Agricultural expansion through the Cerrado biome started in the 1920s, and some estimates indicate that by 2002, about 40-55% of the Cerrado biome (i.e., shrublands in the Brazilian Amazon) had already been converted to pastures or agricultural lands (Klink & Machado, 2005; Sano et al., 2008). In our region of study, anthropogenic land cover types increased from 14% in 1992 to 21% in 2015. The main anthropogenic land cover types in the region were herbaceous and woody croplands. In 1992, each of these two covers represented 6% of the region. By 2015, they expanded to 7 and 11%, with a greater increase in woody than herbaceous croplands. By 2007, the year when SIF and transpiration measurements used here started, most LCC had already happened. In 2007, forest, shrubland, and anthropogenic covers were 56%, 16%, and 21% of the region.

3.4.2 Photosynthetic activity and land cover change

Across the entire region, LCC affected photosynthetic activity differently in the wet and dry seasons. Throughout the wet season, LCC increased photosynthesis; 65% of pixels with high LCC had higher means, and 59% had higher minimum and maximum SIF than their paired low LCC pixels (Fig. 3.4e-g). In contrast, in the dry season, LCC consistently reduced photosynthesis; 78%, 71%, and 62% high LCC pixels had a lower mean, minimum, and maximum SIF, respectively (Fig. 3.4i-k). SIF average range was significantly larger in the high LCC pixels in the dry season (61% of pairs of pixels) (Fig. 3.4l).

The opposing effects of LCC during the wet and dry seasons drove mean annual SIF values in different directions. LCC significantly decreased mean annual minimum SIF (62% of pixels), while increasing mean annual maximum SIF (60% of pixels) (Fig. 3.4b-c). Together, these changes led to increases in the annual range of SIF in 73% of pixels (Fig. 3.4d).

Broadleaf evergreen forests were the most common dominant land cover type in 1992 and the one with the highest LCC between 1992 and 2015. Therefore, our pooled results were often dominated by those pixels. In forest-dominated pixels, LCC resulted in lower mean and minimum annual SIF (73% and 68% of pixels, respectively) (Fig. 3.4a-b). In the dry season, LCC reduced mean and minimum SIF (88% and 78% of pixels, respectively) (Fig. 3.4i-k). Contrary to the annual and dry season decrease in SIF, LCC increased mean and minimum SIF in the wet season (68% of the pixels) (Fig. 3.4e-h). The average annual and dry season range of SIF increased with LCC in 65% and 60% of the pixels, respectively.

Shrublands, the second most common land cover in 1992, often showed opposite trends to forests. In shrubland-dominated pixels, LCC increased mean and maximum annual SIF in 93% and 86% of pixels (Fig. 3.4a,c). These increases were driven by wet season responses; during this time, LCC increased mean and maximum SIF (86% of pixels) (Fig. 3.4e,g). In the dry season, neither the mean, minimum, or maximum SIF were significantly different under high LCC. However, LCC increased the mean range of SIF at the annual scale (86% of pixels) and in both seasons (86% of pixels in the wet and 79% in the dry season).

3.4.3 Transpiration and land cover change

Across both vegetation types, LCC reduced transpiration in the dry season; 75%, 74%, and 68% of high LCC pixels had lower mean, minimum and maximum TR, respectively (Fig. 3.5i-k). In the wet season, LCC did not significantly affect mean, minimum, maximum, or range of TR (Fig. 3.5e-h). Therefore, the lower annual TR seems to be driven by the reduction in TR in the dry season; 79%, 62%, and 70% high-LCC pixels had lower mean, minimum and maximum annual transpiration, respectively (Fig. 3.5a-c). The average range of TR increased with LCC within the dry season (66% and 51% of pixels, respectively) (Fig. 3.5l).

The reductions in transpiration due to LCC across the two vegetation types were primarily caused by the differences in pixels that were originally dominated by forests (Fig. 3.5). In forest-dominated pixels, LCC reduced transpiration; 86%, 71%, and 76% of high LCC pixels had lower mean, minimum, and maximum annual TR, respectively (Fig. 3.5a-c). The annual reductions were a result of decreased TR in the dry season; 86%, 84%, and 76% of high LCC pixels had lower mean, minimum, and maximum TR, respectively (Fig. 3.5i-k). In shrublands, the change was

opposite to that of forests, with LCC increasing transpiration values on average. However, this increase in transpiration in high-LCC shrubland-dominated pixels was not significant.

3.4.4 Different LCC thresholds and changes in SIF and transpiration

The estimated differences between high- and low-LCC pixels tend to increase in magnitude as the threshold percentage of LCC to be considered high-LCC (i.e., >10%, >20%, >30% or >40%) increases (Fig. 3.6). Even though the sample size decreased because there were fewer pixels with the highest percentages of LCC, several differences continued to be significant. Differences tended to increase with the LCC threshold for (1) annual, wet, and dry season SIF, and (2) annual and dry season TR metrics for the pooled land cover types and forests. Mean and minimum SIF became increasingly lower in the dry season and at the annual scale, and higher in the wet season, although to a lesser extent (Fig. 3.6a). With increasing LCC differences, the effect of LCC on maximum SIF became larger in the wet season and at the annual scale, and smaller in the dry season (Fig. 3.6a). Land cover change increasingly reduced mean and minimum TR in the dry season and at the annual scale (Fig. 3.6b). In the wet season, the mean, minimum, and maximum TR differences were only significantly reduced at the >10% LCC threshold (Fig. 3.6b). The mean ranges of SIF and TR in the dry season and at the annual scale also increased with higher LCC thresholds up to >30%; at the >40% threshold, the effects either tapered or decreased in magnitude (Fig. 3.6a,b).

The SIF and TR dry season decreases observed in high-LCC forested pixels strongly and progressively increased in magnitude with higher LCC thresholds (Fig. 3.6c-d). In the wet season, both SIF and TR in forested pixels increased from LCC thresholds of >10 to >20%, but the increases either tapered (in SIF) or decreased in magnitude (in TR) for thresholds above >30%. In the wet season, LCC-driven increases in SIF and TR got larger as thresholds increased from >10 to >20%, and tapered or slightly decreased at the >30 and >40% thresholds. The annual and dry season range of SIF and TR increased along with LCC thresholds up to >30%; at the >40% threshold, the effects of LCC either tapered or decreased in magnitude (Fig. 6c,d).

The LCC threshold analysis for shrubland pixels was only feasible for two thresholds due to a lack of pixels with LCC higher than 30% to perform our comparisons (Fig. 3.6e-f). For the analyzed thresholds, most changes became larger as LCC differences increased from >10% to >20% (Fig. 3.6c,f). This pattern was observed for annual, wet, and dry season SIF mean, maximum, and range. TR differences between high and low LCC pixels dominated by shrublands were only

significant for some metrics, and only at the >10% LCC threshold. These metrics were dry season mean transpiration, annual and dry season minimum, and decreases in the annual, wet, and dry season range. Other metrics, such as maximum TR across all seasons, and most metrics in the wet season, were not significantly different at any LCC threshold.

3.4.5 Dry season "greening" and land cover change

We evaluated the effect of LCC on changes in photosynthetic activity from the beginning to the end of the dry season. Photosynthesis and transpiration increased throughout the dry season in forest-dominated pixels with low LCC (Fig. 3.7b,e). Land cover change strongly dampened this pattern; in forested pixels with high LCC, the change in SIF and TR during the dry season significantly decreased (Fig. 3.7b,e). Throughout the wet season, SIF and TR decreased in pixels with low LCC. With high LCC, the change in SIF and TR throughout the wet season increased and is closer to zero (Fig. 3.7b,e).

In contrast to forests, shrubland photosynthesis and transpiration increased across the wet season and decreased during the dry season in pixels with low LCC (Fig. 3.7c,f). Also contrasting with forest, LCC in shrubland amplified the seasonal changes in these properties; SIF increased even more in the wet season and decreased more in the dry season with high LCC (Fig. 3.7c,f). Most of these changes in SIF and TR throughout the seasons with LCC intensified with increasing LCC thresholds (Fig. 3.8).

3.5 Discussion

Water, carbon and energy feedbacks from tropical ecosystems to the atmosphere strongly influence the local, regional, and global climates. Land cover change has the potential to significantly alter those feedbacks, particularly the rate and timing at which water, energy, and carbon are returned to the atmosphere. In this study, we identified the effects of LULCC on photosynthetic activity and transpiration using remote sensing-derived data. We also analyzed the distinct and consistent effects between ecosystems and between the dry and wet seasons.

In forest-dominated pixels, LCC reduced annual photosynthetic activity and transpiration, mainly by slowing these processes during the dry season. We also observed the reduction in photosynthetic activity with LCC in the switch from dry season "greening" to dry season

"browning" in forests. During the wet season, LCC increased mean photosynthetic activity, without significantly affecting transpiration. However, this wet season increase in photosynthetic activity did not compensate for the decrease during the dry season so the annual average values decreased with LULCC. Photosynthetic activity patterns of common anthropogenic vegetation types in the Amazon, such as pastures for cattle or croplands without irrigation (Seymour & Harris, 2019), are consistent with our observations. During the wet season, crops and grasses reach their productivity peaks, with SIF values and transpiration rates resembling those from forested areas. In the dry season, these non-irrigated croplands and pastures are either cleared (e.g., annual crops) or have a natural decrease in productivity (e.g., perennial plants) (Doughty et al., 2019). Our results agree with previous findings of dry season greening in the Amazon tropical forests and dry season water limitation in vegetation types with shallower roots (Nepstad et al., 1994; R. S. Oliveira et al., 2005; Rafael S. Oliveira et al., 2005).

Differences in dry season photosynthetic activity and transpiration between forests and anthropogenic vegetation are essential for the balance of the water cycle in this region (Marengo et al., 2018; Zemp et al., 2017). Positive feedbacks involving decreased water flow from the land surface to the atmosphere and vice versa can lead the ecosystem to a tipping point (Marengo et al., 2018; Zemp et al., 2017). Even if it takes a longer time to reach this point at a large spatial scale, local and regional agriculture likely will be affected in the near future (Coe et al., 2017; Lawrence & Vandecar, 2015). Analyses similar to the one presented here could help monitor changes in the water cycling feedback and vegetation responses to such changes. The increased availability of remote sensing data allows for large-scale evaluation of changes in photosynthetic activity and transpiration patterns at the annual and seasonal scale. This information can be used to evaluate the influence of agricultural management in the region (Voldoire & Royer, 2004); for instance, by tracking larger-scale changes in SIF and transpiration under different (1) degrees of land cover change, (2) spatial patterns of land cover change, (3) agricultural land cover types, or (4) farming practices.

The effect of LCC on shrubland-dominated pixels showed very different trends in both photosynthetic activity and transpiration. Photosynthetic activity was similar in the dry season under high and low LCC, but significantly increased under high LCC in the wet season. Unlike forests, shrublands and croplands are both expected to be water-stressed and to decrease their photosynthetic activity during the dry season. The increased photosynthetic activity with LCC

during the wet season could be explained by productivity optimization in human-managed vegetation during the growing season. In the wet season, high LCC pixels' SIF even approached that of forests. Although LCC increased photosynthetic activity in the wet season, it had little effect on transpiration. This contrast could be explained by different water use efficiency of shrublands, croplands, and pastures. However, it could also be a result of the parameters used in the algorithms for transpiration estimates. We recommend (1) studying differences in water use efficiency of shrublands and common croplands in this area, and (2) closely examining the parameters used in the transpiration algorithms for these vegetation types. This would lead to more accurate estimates of the impact of shrubland cover change on the water cycle.

Land cover change increased mean annual and seasonal ranges of photosynthetic activity and transpiration in both forest- and shrubland-dominated pixels. Human-managed vegetation is expected to cause this type of pattern, particularly with non-irrigated and annual crops. Most of these practices promote plant growth and increased photosynthetic activity during the growing season (i.e., months of increased water availability) and a complete decline in photosynthetic activity for the rest of the year. Neither forests nor shrublands have such extreme changes in photosynthetic activity. The increasing ranges of photosynthetic activity and transpiration caused by LCC are likely to affect the local and regional climate seasonality (Leite-Filho et al., 2019; Wright et al., 2017).

The differences found in photosynthetic activity and transpiration between the high and low LCC regions intensify with increasing LCC. Although agroecosystems and other converted systems typically remain a small fraction of the landscape (i.e., within a pixel), even in "high-LCC" regions, these pixels often showed differences large enough to be considered significant. The increases in the magnitude of the effects of LCC in photosynthetic activity and transpiration are consistent with GCM projections. Our analyses may be used to validate and benchmark past and future simulations that explore multiple deforestation scenarios.

Our results indicate that LCC affected both photosynthetic activity and transpiration, in both wet and dry seasons. However, we did not find the mean annual precipitation, duration or total precipitation in the dry and wet seasons to be significantly different between low and high LCC regions. We, therefore, attribute the differences in photosynthetic activity and transpiration to differences in vegetation ecophysiology. The lack of changes in precipitation rates accompanied by decreases in the amount of water transpired back to the atmosphere indicate a different fate for

a fraction of the precipitated water. This finding supports previous modeling and observational LCC studies that show an increase in water runoff and river discharge (Coe et al., 2009; Dos Santos et al., 2018; Guimberteau et al., 2017; Swann et al., 2015). Most of those studies relate changes in runoff and river discharge with decreased evapotranspiration and small changes in precipitation.

We used remote sensing-derived data of photosynthetic activity and transpiration to quantify differences in high- and low-LCC regions at annual and seasonal scales. LCC decreased photosynthetic activity and transpiration in the dry season in forest-dominated pixels. Additionally, LCC increased the range of photosynthetic activity and transpiration in forest- and shrubland-dominated pixels. Most changes found in photosynthetic activity and transpiration intensify with higher LCC. Measuring and assessing changes in remotely-sensed photosynthetic activity and transpiration resulting from LCC can be used to (1) characterize human-induced changes to water and carbon fluxes and their impacts on natural ecosystems, (2) evaluate the effects of different agricultural practices in the region, and (3) benchmark photosynthetic and transpiration flux simulations in land surface and climate models. Finally, the combined analysis of changes in photosynthetic activity and transpiration should also help us understand the relationship between these two processes in the different vegetation types in this region. We hope our results highlight the value of rapidly developing remote sensing-derived data for public policy and for future studies in ecophysiology, climate modeling, and LCC impact in the Amazon.

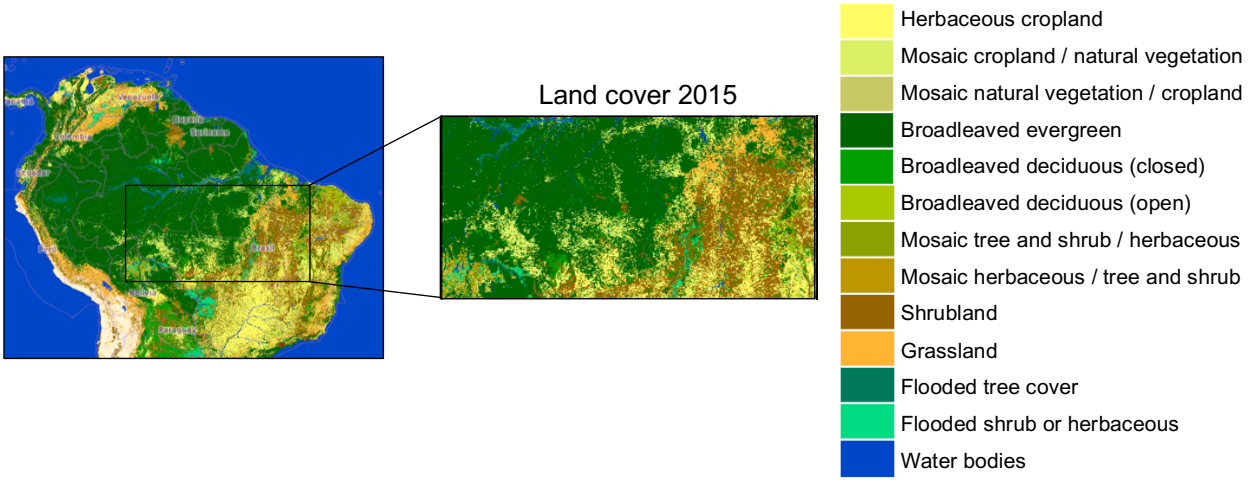

Fig. 3.1. Location of the area of study and land cover types in 2015.

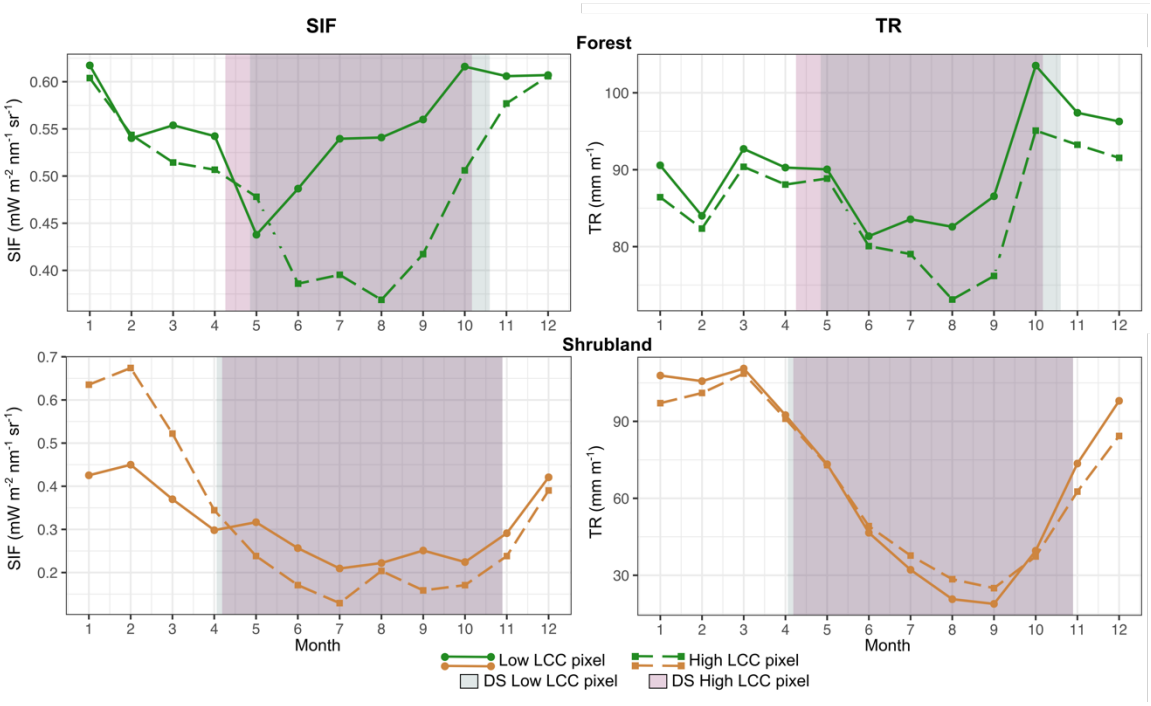

Fig. 3.2. Representative seasonal profiles of mean monthly SIF and transpiration (TR) in low- and high-LCC pixels for forest- and shrubland-dominated sites. Shaded areas represent the dry season in the low- (gray) and high-LCC (pink) pixels, as calculated from the RADS dataset (see Methods).

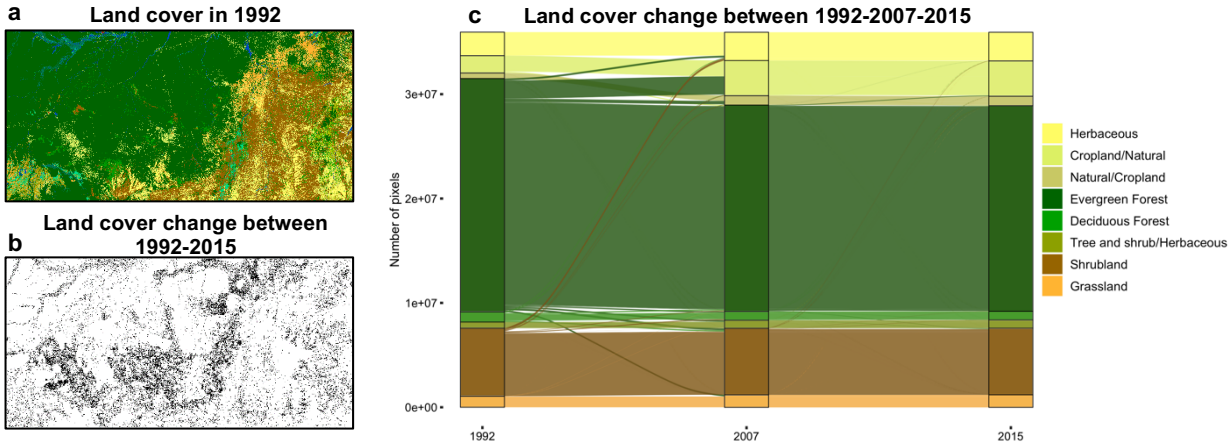

Fig. 3.3. Land cover and land cover change in the area of study. (a) Land cover types in 1992, (b) pixels that changed land cover type from 1992 to 2015, and (c) land cover change from 1992 to 2007 and 2015 (only land cover types greater than 2% are displayed). The color legend is the same for (a) and (c). In (b), pixels in white had the same land cover type in 1992 and 2015, and pixels in black had different land cover types in 1992 and 2015.

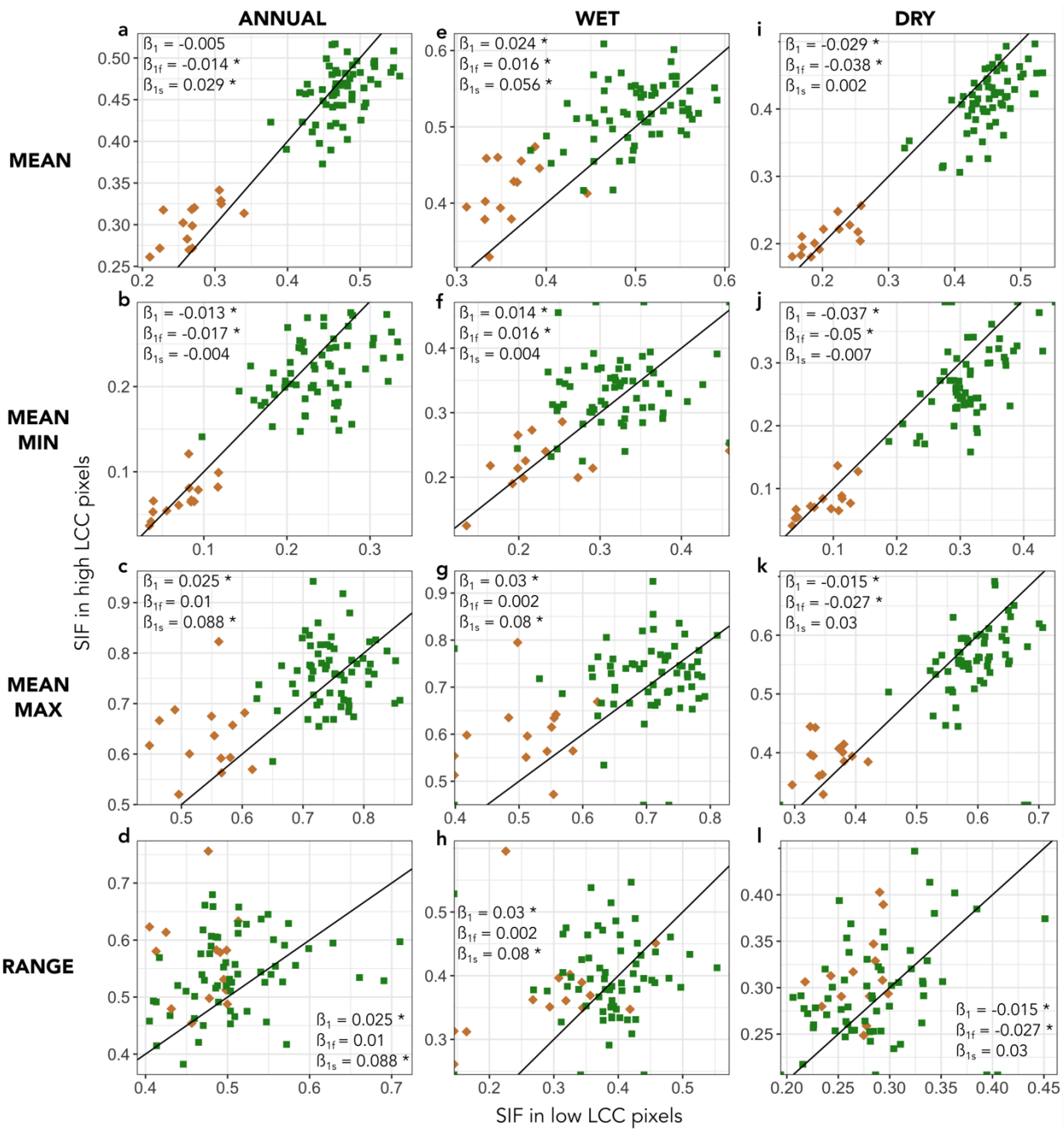

Fig. 3.4. SIF (mW m^{-2} nm^{-1} sr^{-1}) of low (x-axis) vs. high (y-axis) LCC pixels for each metric (rows) and at the annual and seasonal scale (columns). Colors correspond to forest- (green) and shrubland- (gold) dominated pixels. LMM estimates for the difference of SIF in low and high LCC are represented by $ß_1$, $ß_{1f}$ and $ß_{1s}$ for all pixels, forest- and shrubland-dominated pixels, correspondingly. Asterisks (*) indicate statistically significant effects of LCC ($p < 0.05$).

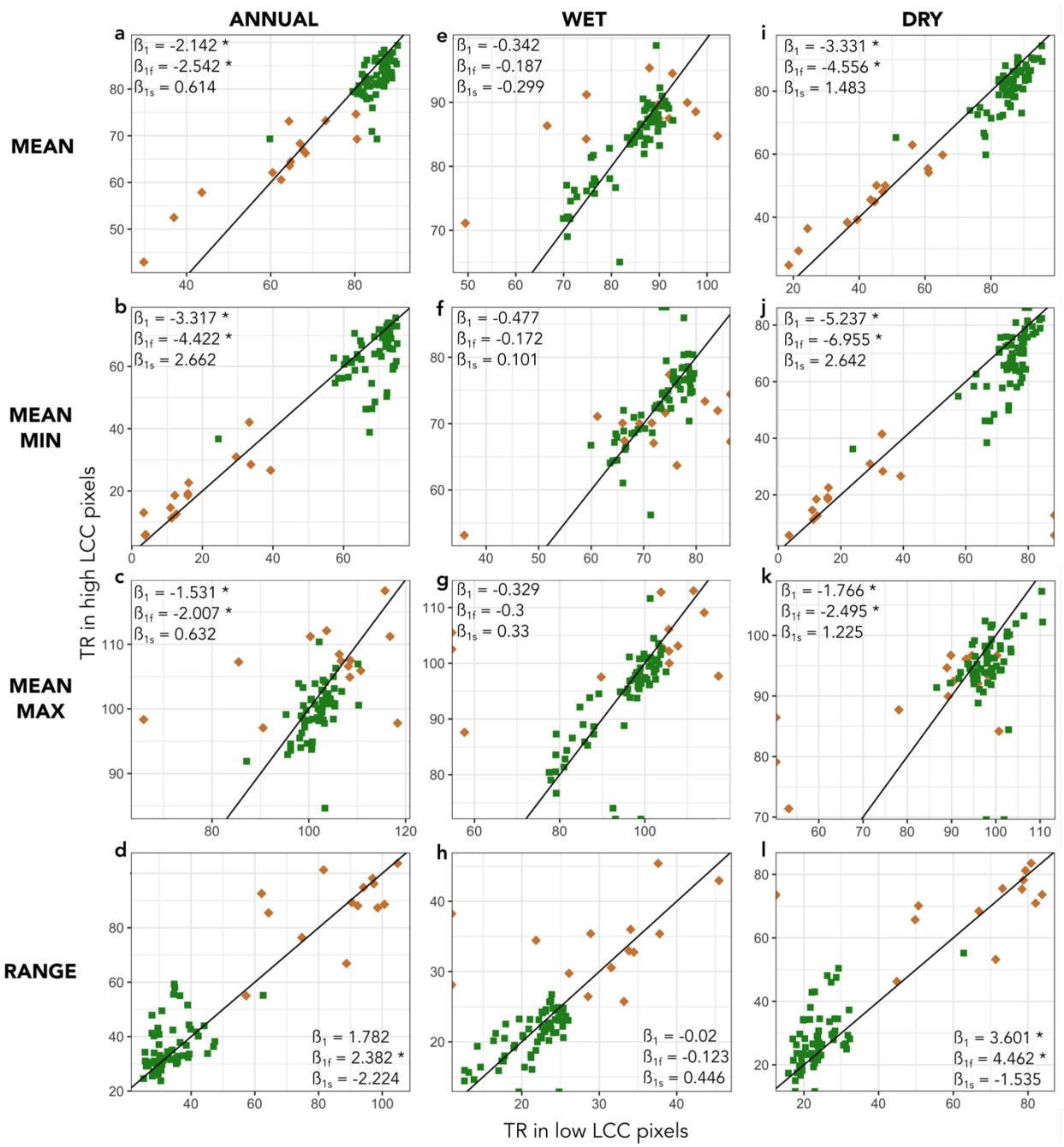

Fig. 3.5. Transpiration (mm m^{-1}) of low (x-axis) vs. high (y-axis) LCC pixels for each metric (rows) and at the annual and seasonal scale (columns). Colors correspond to forest- (green) and shrubland- (gold) dominated pixels. LMM estimates for the difference of SIF in low and high LCC are represented by $ß_1$, $ß_{1f}$ and $ß_{1s}$ for all pixels, forest- and shrubland-dominated pixels, correspondingly. Asterisks (*) indicate statistically significant effects of LCC ($p < 0.05$).

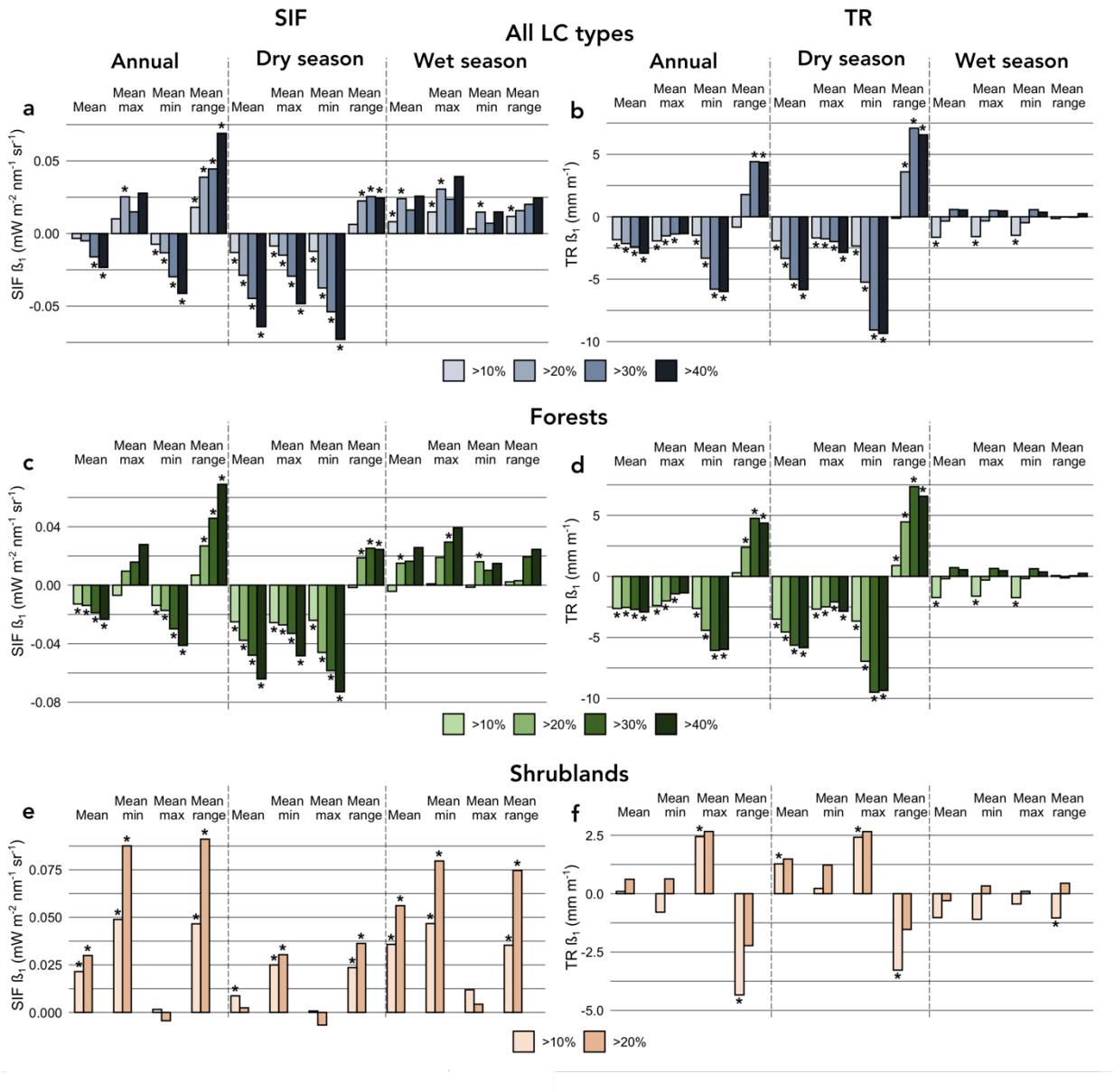

Fig. 3.6. Estimates of the effect of LCC ($ß_1$) on SIF (left-column) and transpiration (right-column) when different thresholds for high LCC are selected (i.e., >10%, >20%, >30%, and >40%). Top row: all LC types (blue); middle row: forest-dominated pixels (green); bottom row: shrubland-dominated pixels (gold). Asterisks (*) indicate a statistically significant effect of LCC ($p < 0.05$).

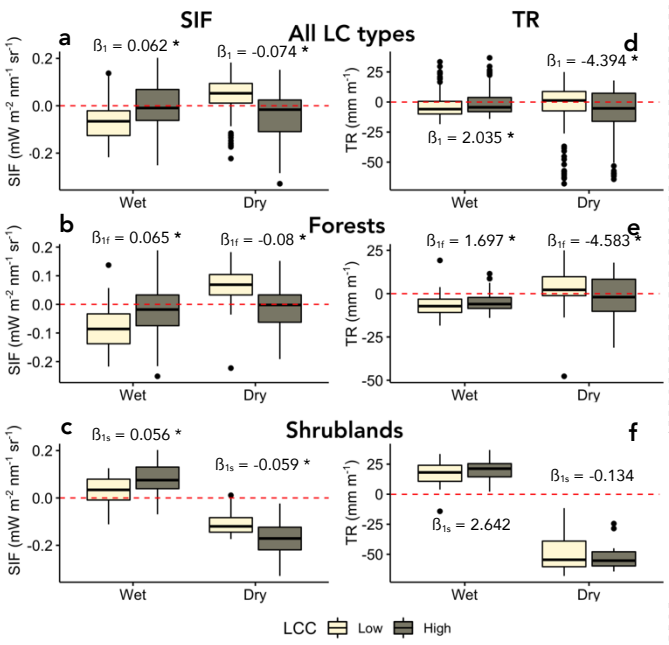

Fig. 3.7. Wet and dry season changes in SIF and transpiration in low vs. high LCC pixels. Each boxplot shows the minimum, first quartile, median, third quartile, and maximum data points. Outliers are shown as black dots outside the boxplot. $ß_1$, $ß_{1f}$ and $ß_{1s}$ values indicate the LMM estimate for the difference of SIF and transpiration in low and high LCC, for all pixels, forests and shrublands, correspondingly. Asterisks (*) indicate statistically significant effects of LCC ($p < 0.05$).

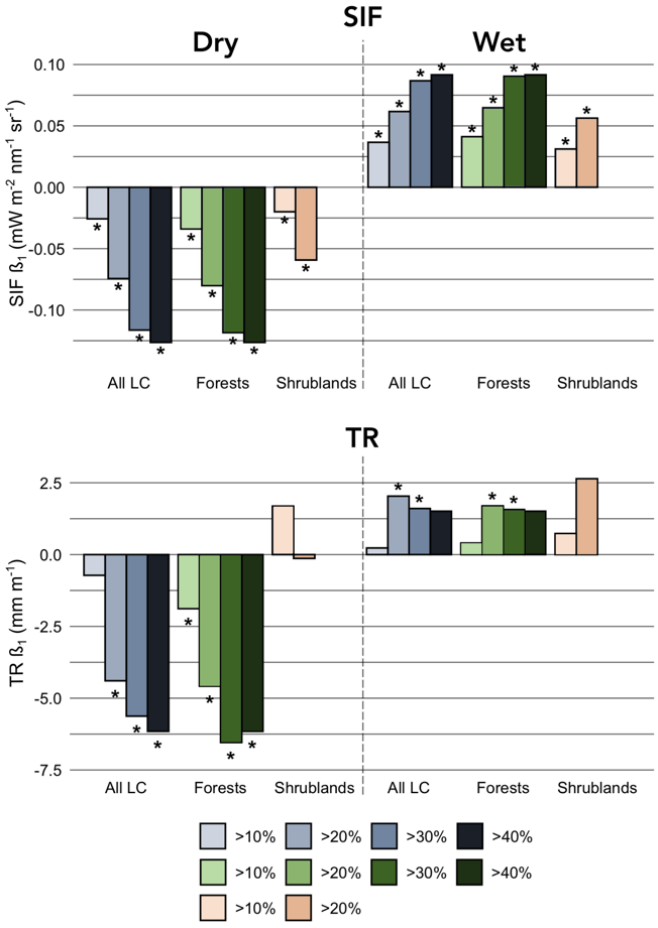

Fig. 3.8. Estimates of the effect of LCC on SIF and transpiration in the wet and dry season when different thresholds for high land cover change are selected. Asterisks (*) indicate statistically significant effects of LCC ($p < 0.05$).

3.6 References

Alkama, R., & Cescatti, A. (2016). Biophysical climate impacts of recent changes in global forest cover. Science, 351(6273), 600–604. https://doi.org/10.1126/science.aac8083

Bombardi, R. J., Kinter, J. L., & Frauenfeld, O. W. (2019). A Global Gridded Dataset of the Characteristics of the Rainy and Dry Seasons. Bulletin of the American Meteorological Society. https://doi.org/10.1175/BAMS-D-18-0177.1

Bombardi, R. J., Pegion, K. V., Kinter, J. L., Cash, B. A., & Adams, J. M. (2017). Sub-seasonal Predictability of the Onset and Demise of the Rainy Season over Monsoonal Regions. Frontiers in Earth Science, 5. https://doi.org/10.3389/feart.2017.00014

Butt, N., Oliveira, P. A. de, & Costa, M. H. (2011). Evidence that deforestation affects the onset of the rainy season in Rondonia, Brazil. Journal of Geophysical Research: Atmospheres, 116(D11). https://doi.org/10.1029/2010JD015174

Chambers, J. Q., & Artaxo, P. (2017). Deforestation size influences rainfall. Nature Climate Change, 7(3), 175–176. https://doi.org/10.1038/nclimate3238

Coe, M. T., Brando, P. M., Deegan, L. A., Macedo, M. N., Neill, C., & Silvério, D. V. (2017). The Forests of the Amazon and Cerrado Moderate Regional Climate and Are the Key to the Future. Tropical Conservation Science, 10, 1940082917720671. https://doi.org/10.1177/1940082917720671

Coe, M. T., Costa, M. H., & Soares-Filho, B. S. (2009). The influence of historical and potential future deforestation on the stream flow of the Amazon River – Land surface processes and atmospheric feedbacks. Journal of Hydrology, 369(1), 165–174. https://doi.org/10.1016/j.jhydrol.2009.02.043

D'Almeida, C., Vörösmarty, C. J., Hurtt, G. C., Marengo, J. A., Dingman, S. L., & Keim, B. D. (2007). The effects of deforestation on the hydrological cycle in Amazonia: A review on scale and resolution. International Journal of Climatology, 27(5), 633–647. https://doi.org/10.1002/joc.1475

Dos Santos, V., Laurent, F., Abe, C., & Messner, F. (2018). Hydrologic Response to Land Use Change in a Large Basin in Eastern Amazon. Water, 10(4), 429. https://doi.org/10.3390/w10040429

Doughty, R., Köhler, P., Frankenberg, C., Magney, T. S., Xiao, X., Qin, Y., Wu, X., & Moore, B. (2019). TROPOMI reveals dry-season increase of solar-induced chlorophyll fluorescence in the Amazon forest. Proceedings of the National Academy of Sciences, 116(44), 22393–22398. https://doi.org/10.1073/pnas.1908157116

ESA. (2017). Land Cover CCI Product User Guide Version 2 [Tech. Rep.]. ESA. maps.elie.ucl.ac.be/CCI/viewer/download/ESACCI-LC-Ph2-PUGv2_2.0.pdf

Guimberteau, M., Ciais, P., Ducharne, A., Boisier, J. P., Aguiar, A. P. D., Biemans, H., Deurwaerder, H. de, Galbraith, D., Kruijt, B., Langerwisch, F., Poveda, G., Rammig, A., Rodriguez, D. A., Tejada, G., Thonicke, K., Randow, C. von, Randow, R. C. S. von, Zhang, K., & Verbeeck, H. (2017). Impacts of future deforestation and climate change on the hydrology of the Amazon Basin: A multi-model analysis with a new set of land-cover

change scenarios. Hydrology and Earth System Sciences, 21(3), 1455–1475. https://doi.org/10.5194/hess-21-1455-2017

Hubau, W., Lewis, S. L., Phillips, O. L., Affum-Baffoe, K., Beeckman, H., Cuní-Sanchez, A., Daniels, A. K., Ewango, C. E. N., Fauset, S., Mukinzi, J. M., Sheil, D., Sonké, B., Sullivan, M. J. P., Sunderland, T. C. H., Taedoumg, H., Thomas, S. C., White, L. J. T., Abernethy, K. A., Adu-Bredu, S., … Zemagho, L. (2020). Asynchronous carbon sink saturation in African and Amazonian tropical forests. Nature, 579(7797), 80–87. https://doi.org/10.1038/s41586-020-2035-0

Joiner, J., Yoshida, Y., Vasilkov, A. P., Yoshida, Y., Corp, L. A., & Middleton, E. M. (2011). First observations of global and seasonal terrestrial chlorophyll fluorescence from space. Biogeosciences, 8(3), 637–651. https://doi.org/10.5194/bg-8-637-2011

Klink, C. A., & Machado, R. B. (2005). Conservation of the Brazilian Cerrado. Conservation Biology, 19(3), 707–713. JSTOR. https://www.jstor.org/stable/3591058

Lawrence, D., & Vandecar, K. (2015). Effects of tropical deforestation on climate and agriculture. Nature Climate Change, 5(1), 27–36. https://doi.org/10.1038/nclimate2430

Leite-Filho, A. T., Pontes, V. Y. de S., & Costa, M. H. (2019). Effects of Deforestation on the Onset of the Rainy Season and the Duration of Dry Spells in Southern Amazonia. Journal of Geophysical Research: Atmospheres, 124(10), 5268–5281. https://doi.org/10.1029/2018JD029537

Lovejoy, T. E., & Nobre, C. (2019). Amazon tipping point: Last chance for action. Science Advances, 5(12), eaba2949. https://doi.org/10.1126/sciadv.aba2949

Marengo, J. A., Souza, C. M. J., Thonicke, K., Burton, C., Halladay, K., Betts, R. A., Alves, L. M., & Soares, W. R. (2018). Changes in Climate and Land Use Over the Amazon Region: Current and Future Variability and Trends. Frontiers in Earth Science, 6. https://doi.org/10.3389/feart.2018.00228

Martens, B., Miralles, D. G., Lievens, H., Schalie, R. van der, Jeu, R. A. M. de, Fernández-Prieto, D., Beck, H. E., Dorigo, W. A., & Verhoest, N. E. C. (2017). GLEAM v3: Satellite-based land evaporation and root-zone soil moisture. Geoscientific Model Development, 10(5), 1903–1925. https://doi.org/10.5194/gmd-10-1903-2017

Nepstad, D. C., de Carvalho, C. R., Davidson, E. A., Jipp, P. H., Lefebvre, P. A., Negreiros, G. H., da Silva, E. D., Stone, T. A., Trumbore, S. E., & Vieira, S. (1994). The role of deep roots in the hydrological and carbon cycles of Amazonian forests and pastures. Nature, 372(6507), 666–669. http://search.proquest.com/docview/16600521?rfr_id=info%3Axri%2Fsid%3Aprimo

Nobre, C. A., Sampaio, G., Borma, L. S., Castilla-Rubio, J. C., Silva, J. S., & Cardoso, M. (2016). Land-use and climate change risks in the Amazon and the need of a novel sustainable development paradigm. Proceedings of the National Academy of Sciences, 113(39), 10759–10768. https://doi.org/10.1073/pnas.1605516113

Oliveira, R. S., Bezerra, L., Davidson, E. A., Pinto, F., Klink, C. A., Nepstad, D. C., & Moreira, A. (2005). Deep root function in soil water dynamics in cerrado savannas of central Brazil. Functional Ecology, 19(4), 574–581. https://doi.org/10.1111/j.1365-2435.2005.01003.x

Oliveira, Rafael S., Dawson, T. E., Burgess, S. S. O., & Nepstad, D. C. (2005). Hydraulic redistribution in three Amazonian trees. Oecologia, 145(3), 354–363. https://doi.org/10.1007/s00442-005-0108-2

Pinheiro, J., Bates, D., DebRoy, S., & Sarkar, D. (2020). *_nlme: Linear and Nonlinear Mixed Effects Models_. R package* (Version 3.1-144) [Computer software]. R Core Team. https://CRAN.R-project.org/package=nlme

Restrepo-Coupe, N., Levine, N. M., Christoffersen, B. O., Albert, L. P., Wu, J., Costa, M. H., Galbraith, D., Imbuzeiro, H., Martins, G., Araujo, A. C. da, Malhi, Y. S., Zeng, X., Moorcroft, P., & Saleska, S. R. (2017). Do dynamic global vegetation models capture the seasonality of carbon fluxes in the Amazon basin? A data-model intercomparison. Global Change Biology, 23(1), 191–208. https://doi.org/10.1111/gcb.13442

Saatchi, S. (2013). LBA-ECO LC-15 SRTM30 Digital Elevation Model Data, Amazon Basin: 2000. ORNL Distributed Active Archive Center. https://doi.org/10.3334/ORNLDAAC/1181

Saleska, S. R., Miller, S. D., Matross, D. M., Goulden, M. L., Wofsy, S. C., da Rocha, H. R., de Camargo, P. B., Crill, P., Daube, B. C., de Freitas, H. C., Hutyra, L., Keller, M., Kirchhoff, V., Menton, M., Munger, J. W., Pyle, E. H., Rice, A. H., & Silva, H. (2003). Carbon in Amazon Forests: Unexpected Seasonal Fluxes and Disturbance-Induced Losses. Science, 302(5650), 1554–1557. JSTOR. http://www.jstor.org/stable/3835784

Sano, E. E., Rosa, R., Brito, J. L. S., & Ferreira, L. G. (2008). Mapeamento semidetalhado do uso da terra do Bioma Cerrado. Pesquisa Agropecuária Brasileira, 43(1), 153–156. https://doi.org/10.1590/S0100-204X2008000100020

Seymour, F., & Harris, N. L. (2019). Reducing tropical deforestation. Science, 365(6455), 756–757. https://doi.org/10.1126/science.aax8546

Silva, M. E. S., Pereira, G., & da Rocha, R. P. (2016). Local and remote climatic impacts due to land use degradation in the Amazon "Arc of Deforestation." Theoretical and Applied Climatology, 125(3), 609–623. https://doi.org/10.1007/s00704-015-1516-9

Spracklen, D. V., & Garcia-Carreras, L. (2015). The impact of Amazonian deforestation on Amazon basin rainfall. Geophysical Research Letters, 42(21), 9546–9552. https://doi.org/10.1002/2015GL066063

Staal, A., Tuinenburg, O. A., Bosmans, J. H. C., Holmgren, M., Nes, E. H. van, Scheffer, M., Zemp, D. C., & Dekker, S. C. (2018). Forest-rainfall cascades buffer against drought across the Amazon. Nature Climate Change, 8(6), 539. https://doi.org/10.1038/s41558-018-0177-y

Swann, A. L. S., Longo, M., Knox, R. G., Lee, E., & Moorcroft, P. R. (2015). Future deforestation in the Amazon and consequences for South American climate. Agricultural and Forest Meteorology, 214–215, 12–24. https://doi.org/10.1016/j.agrformet.2015.07.006

Vergopolan, Noemi, and Joshua B. Fisher. 2016. “The Impact of Deforestation on the Hydrological Cycle in Amazonia as Observed from Remote Sensing.” *International Journal of Remote Sensing* 37(22):5412–30.

Voldoire, A., & Royer, J. F. (2004). Tropical deforestation and climate variability. Climate Dynamics, 22(8), 857–874. https://doi.org/10.1007/s00382-004-0423-z

Wright, J. S., Fu, R., Worden, J. R., Chakraborty, S., Clinton, N. E., Risi, C., Sun, Y., & Yin, L. (2017). Rainforest-initiated wet season onset over the southern Amazon. Proceedings of the National Academy of Sciences, 114(32), 8481–8486. https://doi.org/10.1073/pnas.1621516114

Zemp, D. C., Schleussner, C.-F., Barbosa, H. M. J., & Rammig, A. (2017). Deforestation effects on Amazon forest resilience. Geophysical Research Letters, 44(12), 6182–6190. https://doi.org/10.1002/2017GL072955.

CHAPTER 4. REDUCTIONS IN AMAZON BASIN EVAPOTRANSPIRATION AFTER DEFORESTATION: ESTIMATES FROM REMOTE SENSING AND MODELS

4.1 Abstract

In the Amazon region, extensive deforestation has the potential to change the relationship between the land and atmosphere, and ultimately, climate. Many regional and global climate models suggest that deforestation will reduce evapotranspiration (ET) and affect climate. However, ET data based on remote sensing and physical models have not yet been used to estimate the net effect of deforestation. The increasing availability of relevant satellite data provides a new opportunity to estimate changes in ET from deforestation during the past couple of decades. Here, we estimate the change in ET due to deforestation in the Amazon basin using two remote sensing-derived datasets for the period 2000-2018. We compare our estimates with those from previous modeling studies. Our results indicate a basin-wide decrease in ET of 0.11 mm d^{-1} (2.81%) and 0.06 mm d^{-1} (1.58%) from the GLEAM and MODIS datasets, respectively, due to deforestation of 9.3% of the region. These estimates are in close agreement with previous modeling estimates, which collectively predict ET will decrease by 0.007 mm d^{-1} or 0.21% for each 1% increase in deforestation. Together, our remote sensing-derived estimates and our synthesis of model predictions provide a best estimate for how past and future deforestation affect ET in the Amazon, with implications for the regional climate. Our spatial and seasonal analyses also highlight the importance of specific changes in ET in the southern part of the basin as well as during the dry season.

4.2 Introduction

The vast tropical forests of the Amazon basin have a strong relationship with the atmosphere that influences the regional and global climates. The region's warm temperatures and abundant rainfall have shaped the dense and highly productive forests. At the same time, the forests help regulate local temperatures, regional and global precipitation, and atmospheric carbon (Lawrence and Vandecar 2015; Prevedello et al. 2019). Estimates suggest that about a third of the regional rainfall originates within the Amazon basin and 20% has been transpired at least once by

the Amazon forests (Staal et al. 2018). Precipitation patterns in other parts of South America and in distant extratropical regions are also influenced by water recycling in the Amazon through teleconnections (Lawrence and Vandecar 2015). Forest cover in the tropics has also been associated with lower mean and maximum temperatures, and lower diurnal temperature variations (Alkama and Cescatti 2016; Cohn et al. 2019; Prevedello et al. 2019). However, the natural feedbacks of energy, carbon and water between tropical forests and the atmosphere are threatened by human-induced land cover change (Davidson et al. 2012; Lovejoy and Nobre 2019).

Recent estimates indicate that 17% of the Amazon has already been deforested and this area is expected to keep increasing (Lovejoy and Nobre 2019). The highest deforestation rates are located in the Brazilian Amazon, in the southern and eastern parts of the basin, and in the lower Andes in the western border of the basin (Malhi et al. 2008). Cattle ranching, agriculture (e.g., for soy and palm oil), and selective logging are the main drivers of land clearing (Davidson et al. 2012). By 2050, models predict that almost half of the forests of the Amazon basin will be converted to other land cover types (Spracklen and Garcia-Carreras 2015). These deforestation predictions range from 28% under a governance scenario to 47% under a business-as-usual scenario (Soares-Filho et al. 2006). The effects of deforestation in the Amazon can range from local to global scales (Cohn et al. 2019; Lawrence and Vandecar 2015; Swann et al. 2015). Therefore, it is important to evaluate the magnitude of the effects of deforestation on climate at different temporal and spatial scales.

Evapotranspiration (ET) is the most important link between changes in land cover and changes in climate (Fisher et al. 2017). ET is related to several mechanisms through which land cover change affects water and energy fluxes from the land surface to the atmosphere (Bonan 2008; Cai et al. 2019). Replacing the natural land cover modifies ET rates and partitioning through changes in (1) albedo and the amount of energy available for evaporation; (2) roughness length and aerodynamic resistance to transpiration; (3) the amount of precipitation intercepted by vegetation; (4) leaf area index, stomatal resistance, and photosynthetic and transpiration rates; (5) soil water storage capacity and plant water stress; and (6) water infiltration and runoff (Butt, Oliveira, and Costa 2011; Cai et al. 2019; Voldoire and Royer 2004). A better understanding of the changes in ET would help to improve our information about changes in the cycling of water and energy in the Amazon.

Multiple efforts have been made to estimate the effects of deforestation in ET and climate in the Amazon (D'Almeida et al. 2007; Guimberteau et al. 2017). ET cannot be directly measured from remote sensing, and field data from the Amazon are scarce. Therefore, most ET studies are based on regional and global circulation models and land surface models. Simulating the feedbacks between the atmosphere and the land surface with process-based models allows testing of different land cover scenarios and their effects on different aspects of climate. However, in the last two decades, a few global ET datasets have been developed based on meteorological and remote sensing data (Miralles et al. 2016; Paca et al. 2019). These datasets use algorithms that describe the biogeophysical processes of ET and are driven by remote sensing measurements of vegetation, soil water content, and climate (Miralles et al. 2016).

As a result of a few decades of modeling efforts, many estimates of the changes in ET that result from land cover change are now available. However, the almost two decades' worth of remote sensing-derived ET data have rarely been used to estimate the effects of deforestation (Vergopolan and Fisher 2016). Here, we first estimate the change in ET caused by deforestation in the Amazon basin using remote sensing-derived data. Second, we analyze estimates from previous modeling studies and compare them with our remote sensing-based estimates. We specifically answer the questions: How much does ET change as a result of deforestation in the Amazon basin according to remote sensing-derived datasets? Are there spatial and temporal trends in the effect of deforestation on ET? And, do our remote sensing-derived estimated changes in ET agree with models' predictions? We hypothesized that deforestation has caused a decrease in ET, in accordance with previous modeling studies. We expected a larger effect of deforestation in ET in the southern Amazon, where deforestation has occurred at higher rates. Because of crops and pastures lower resistance to drought, we also expected higher reduction of ET due to deforestation during months and years with low precipitation.

4.3 Methods

4.3.1 Data

Land cover data were obtained from the European Space Agency Climate Change Initiative Land Cover Time Series v2.0.7. This product provides annual land cover data for the period 1992-2018 at a 300-meter spatial resolution (ESA 2017). Land cover types are obtained using

unsupervised classification and machine learning algorithms for change detection and delineation of remote sensing land products (MERIS, AVHRR, SPOT-VGT and PROBA-V). The dataset has 22 land cover types including natural (e.g., tree, grassland and shrubland) and anthropogenic (e.g., cropland and urban) land covers. We used the definition of Amazon basin from Mayorga et al. (2012), where land topography from ETOPO5 was used to trace watershed limits of the Amazon river tributaries (Mayorga et al. 2005). We then identified the tropical forest biome within the basin using the biome distribution from Olson et al. (2001) to delimit our area of study (Fig. 4.1).

Evapotranspiration data were obtained from two remote sensing-derived datasets, namely, the Global Land Evaporation Amsterdam Model (GLEAM v3.3a) and the MODIS/Terra Net Evapotranspiration Gap-Filled product (MOD16A2GF V006) (Martens et al. 2017; Miralles et al. 2011; S. Running et al. 2019). Both datasets are global products with a strong physical modeling component largely driven by remote sensing and climate reanalysis data. GLEAM data are available as monthly averages for the period 1980-2018 at a spatial resolution of 0.25- x 0.25-degree resolution. MODIS data are available as 8-day composites for the period 2000-2018 at a 500- x 500-meter resolution. Our analyses were performed with monthly averages for the period 2000-2018 at a 0.25- x 0.25-degree resolution to match the temporal and spatial resolution of both datasets.

GLEAM evapotranspiration is derived by estimating potential evaporation, rainfall interception and a stress factor (Martens et al. 2017). Potential evaporation is calculated with the Priestley-Taylor (PT) equation, which is based on air temperature, net radiation and vegetation cover type. Rainfall interception is estimated using the Gash analytical model based on precipitation and vegetation properties. The stress factor, which accounts for water availability and phenological constraints, is estimated from microwave remote-sensing data of vegetation optical depth (VOD) and estimates of root-zone soil moisture. Lower VOD or soil moisture result in higher evaporative stress. An advantage of using GLEAM ET in tropical forests is its exclusive use of microwave remote sensing observations (Martens et al. 2017). Unlike visible and infrared radiation, microwaves are relatively unaffected by clouds, which can severely limit data collection in the wet season in the tropics. Furthermore, GLEAM uses a detailed interception model that is ideal for forested regions where canopy interception and evaporation represent a large fraction of ET.

Similar to GLEAM, MODIS ET is also calculated with a combination of algorithms, climate reanalysis data and satellite imagery. However, both ET datasets differ in the algorithms

and satellite datasets used. MODIS ET is based on the Penman-Monteith (PM) equation, in which ET is also a function of vapor pressure deficit and aerodynamic and canopy resistances in addition to the climate limitations included in the PT equation (S. W. Running et al. 2019). The PM equation is used to separately calculate vegetation transpiration, canopy evaporation, and soil evaporation. Input data for these calculations include reanalysis meteorological data (e.g., air temperature, PAR, specific humidity), and MODIS vegetation data (e.g., Leaf Area Index (LAI), Fraction of Photosynthetically Active Radiation (FPAR)), albedo, and land cover. For instance, FPAR is used as a proxy of vegetation cover fraction to estimate the radiation partitioning between canopy and soil surface within a pixel; LAI is used in the wet canopy evaporation and stomatal conductance calculations. An advantage of MODIS ET is that it is parameterized for 11 vegetation types, including evergreen broadleaf forests, grasslands and croplands.

4.3.2 Estimate of changes in ET due to deforestation

In order to estimate the change in ET due to deforestation, we compared monthly remote sensing-derived ET with ET from a simulated non-land cover change scenario. This simulated scenario, from this point called the no-LCC scenario, was built by predicting ET in areas of high land cover change as if there had not been land cover change. First, we identified areas with low and high land cover change in the Amazon basin. The fraction of land cover change was determined by calculating the proportion of 300-m pixels with anthropogenic land cover types (i.e., pasture, croplands, and mosaics of natural and anthropogenic vegetation) within each 0.25-degree evapotranspiration pixel (Fig. 4.1). We then masked out high land cover change areas (>1% pixels with land cover change) and used ET data from low land cover change areas to estimate ET for the masked areas of high land cover change. The interpolation of the ET data from low land cover change pixels to the high land cover change areas was performed with universal kriging. This technique has been extensively used and has proven to be a robust interpolation method in the environmental sciences (Li and Heap 2014). Using kriging, we estimated potential values of ET in the no-LCC scenario using observed ET from nearby undisturbed forests. We specifically avoided using additional climate data for our predictions (e.g., precipitation or temperature) since they could be associated with climate-land cover-ET feedbacks.

Kriging is an interpolation technique to predict unknown values of a variable of interest in new locations based on measured values in other locations (Singh and Verma 2019). The

predictions result from using the spatial autocorrelation in the data. The kriging process is divided in two main steps, the spatial model fitting and the predictions. Given a set of locations $(s_1, \dots, s_n)$ and the corresponding known values of our variable of interest $(Z(s_1), \dots, Z(s_n))$, we fit a spatial model that describes the correlation among the available data. Model fitting is done by calculating the sample variogram, which corresponds to the semi-variance $\gamma(h)$ of the measured data points separated by different distances h (Eq. 1, Plant 2012).

$$\gamma(h) = \frac{1}{2|N(h)|}\sum_{i=1}^{N(h)}(Z(s_i + h) - Z(s_i))^2 \quad \text{(Eq. 1)}$$

We fit a model that describes the semi-variance of the sample and use that model to predict values for the new locations. In our case, predictions were performed through universal kriging (Eq. 2). In this kriging method, new values are the sum of a regional mean estimated as a function of location $\mu(s)$, and the random, spatially-correlated error $\varepsilon(s)$ calculated with the fitted model (Singh and Verma 2019).

$$Z(s) = \mu(s) + \varepsilon(s) \quad \text{(Eq. 2)}$$

We used K-fold cross validation to evaluate the accuracy of our interpolation. The validation process consists of (1) removing 1/k of the measured data points; (2) performing the predictions at the location of the removed data points; and (3) comparing the predictions with the actual values. Multiple iterations of the same process are repeated with different groups of data points removed in each iteration, until all the points in the dataset have been removed at least once. After completing all the iterations, diagnostic statistics such as mean error (bias) and root mean square error (RMSE) are calculated. The cross-validation results are shown in Table S1. We used the R packages *gstat* (Gräler, Pebesma, and Heuvelink 2016; Pebesma 2004) and *automap* (Hiemstra et al. 2009) for the kriging and cross-validation analyses.

To estimate the effect of land cover change on ET (ΔET), we calculated the difference between the observed and the no-LCC scenario ET from each dataset. We calculated absolute (mm d^{-1}) and relative (%) differences between the ET estimates from the two scenarios across the entire Amazon basin. We followed up with spatial and temporal analyses of ET changes caused by deforestation. We evaluate seasonal and interannual variation in our basin-wide estimates, and separately for the northern and southern halves of the basin. The boundary between the two regions corresponds exactly to the median latitude of the basin (dotted line in Fig. 4.1).

4.3.3 Synthesis of estimates of change in ET due to deforestation from modeling studies

We collected and synthesized publications that estimate the effects of deforestation on ET in the Amazon basin. Using Google Scholar and Web of Science in February, 2020, we searched scientific articles in peer reviewed journals using the terms "evapotranspiration + deforestation + Amazon". The initial results included 11,000 studies in Google Scholar and 110 studies in Web of Science. We examined titles and abstracts of the papers in the search results to identify studies that were relevant to this study. We examined all titles and abstracts in the Web of Science Results. In Google Scholar, results were ranked by relevance and titles and abstracts were searched starting with the most relevant results. This search continued until more than 30 consecutive articles' titles and abstracts were found not to be relevant for this study. From the studies initially identified as related to the topic, we selected those with available data for estimates of changes in ET. If a relevant study was referenced in one of our selected publications but was not part of our initial search results, the new study was added to the collection. The final collection includes 40 studies with different amounts of data availability.

Using the identified studies, we compared the estimated changes in ET under different deforestation scenarios. We fit a regression model to evaluate the agreement and trend in the estimates across specified levels of deforestation. The linear regression was forced through the intercept, with no change in ET with no change in deforestation. We used the *stats* R package to perform the regressions (R Core Team 2019). We compared our results from the satellite-based data analyses with the synthesis of estimates from the modeling studies. We compare our estimated values with the mean projected ET change inferred from modeling studies. We also compare our ET estimates with data from previous modeling studies that related changes in ET to changes in precipitation, temperature, and sensible heat flux across the Amazon basin.

4.4 Results

4.4.1 Estimated changes in ET in the Amazon basin due to deforestation from remote sensing-derived data

The GLEAM datasets suggest that deforestation reduced mean ET in the Amazon basin by 0.11 mm d^{-1}, or 2.81%, during the period 2000-2018; ET dropped from 3.84 (±0.35) mm d^{-1} in our simulation of intact forest to an actual mean ET of 3.74 ±0.34 mm d^{-1} (Fig. 4.2a,c,e). The MODIS datasets suggest a smaller effect of deforestation; a reduction of 0.06 mm d^{-1}, or 1.58%. The

MODIS analyses suggest that an intact, fully forested Amazon would have averaged ET of 3.63 (±0.42) mm d^{-1}, as compared to an estimate of actual ET of 3.57 ±0.36 mm d^{-1} (Fig. 4.2b,d,f).

The two datasets show different spatial variation in ET within the region (Fig. 4.2a-b). In GLEAM, ET is higher in the northern and central part of the basin and lower in some regions in the western, southern and southeastern parts of the basin. In MODIS, the highest ET values are in some parts of the northeastern and southeastern regions. The areas where ET differs between observations and the no-LCC scenario coincide with the spatial pattern of deforestation (Fig. 4.1); most of these areas are located along the western border, or are in patches in the southern and northern parts of the Amazon.

The effect of deforestation on ET was distinctly higher in the southern part of the basin than the in northern part. In the southern region, deforestation decreased ET by 0.18 mm d^{-1} or 5.5% in the GLEAM dataset. In the no-LCC scenario, average GLEAM ET was 3.55 (±0.62) mm d^{-1}, and decreased to 3.37 (±0.6) mm d^{-1} in the deforested scenario. In this same region, the decrease in MODIS ET was 0.12 mm d^{-1} or 3.25%. In the no-LCC scenario, MODIS ET was 3.57 (±0.4) mm d^{-1}, decreasing to 3.46 (±0.32) mm d^{-1} with observed deforestation. In the northern part, the decrease in GLEAM ET from deforestation was only 0.06 mm d^{-1} or 1.4%. In this dataset, the average no-LCC scenario ET was 4.03 (±0.24) mm d^{-1} and dropped to 3.97 (±0.23) mm d^{-1} with deforestation. In MODIS, the decrease in ET was 0.03 mm d^{-1} or 0.7%, where the no-LCC scenario mean ET was 3.66 (±0.5) mm d^{-1} and dropped to 3.63 (±0.49) mm d^{-1}. The full time series of observed and no-LCC ET and the difference between the two are shown in the supplementary materials (Appendix C, Fig. C1).

In addition to spatial variation, there was also seasonal variation in the observed and no-LCC scenario ET, as well as in the effect of deforestation on ET. In both remote sensing datasets, the seasonal variations were stronger in the southern than in the northern part of the basin.

In the northern Amazon (Fig. 4.3-left column), mean monthly ET values fluctuated over a range of 0.63 mm d^{-1} (3.58-4.21 mm d^{-1}) in GLEAM and 1.22 mm d^{-1} (3.15-4.37 mm d^{-1}) in MODIS (Fig. 4.3a,c). The seasonal variation of GLEAM showed one peak in ET in the wet season and a second one by the end of the dry season (Fig. 4.3a). In MODIS, there was a single peak by the end of the dry season (Fig. 4.3c). ET in the no-LCC scenario from GLEAM was only slightly but constantly higher than observed ET for this region, with a mean monthly difference of between

0.05 and 0.07 mm d^{-1} (Fig. 4.3b and Fig. 4.4). For MODIS, the difference remained close to zero for most of the year, with a peak of 0.07 mm d^{-1} during the dry season (Fig. 4.3d and Fig. 4.4).

In the southern Amazon (Fig. 4.3-right column), GLEAM ET variation was over two times higher than in the northern part, with an annual range of 1.6 mm d^{-1} (2.43- 4.03 mm d^{-1}) (Fig. 4.3f). The seasonal pattern of GLEAM ET followed that of precipitation, decreasing in the dry season and increasing in the wet season. In the MODIS dataset, the annual range of ET in the southern part was smaller; only 0.46 mm d^{-1} (3.17 to 3.63 mm d^{-1}), and the seasonal pattern did not follow precipitation (Fig. 4.3h). The mean monthly variation in the effect of deforestation ranged between 0.08 and 0.27 mm d^{-1} in GLEAM and -0.03 and 0.4 mm d^{-1} in MODIS (Fig. 4.3g,i). In GLEAM, the effect of deforestation on ET peaked both in the middle of the wet season and late in the dry season, while in MODIS there was one single large peak in the late dry season (Fig. 4.3g,i and Fig. 4.4).

Year-to-year variation in ET was relatively small. In the northern region, mean annual ET had a range of 0.21 mm d^{-1} (3.84 to 4.05 mm d^{-1}) and 0.47 mm d^{-1} (3.33 to 3.8 mm d^{-1}) in GLEAM and MODIS, respectively (Fig. 4.5a,c), across the 18-year dataset. In the southern region, mean annual ET range was 0.21 mm d^{-1} (3.26 to 3.47 mm d^{-1}) in GLEAM and 0.51 mm d^{-1} (3.13 to 3.64 mm d^{-1}) in MODIS (Fig. 4.5f,h). The small year-to-year variation was observed across extremely dry (e.g., 2004-2005, 2009-2010, 2015-2016) and wet years (e.g., 2007-2008, 2010-2011, 2011-2012), when GLEAM and MODIS ET were not consistently higher or lower than other years.

In both GLEAM and MODIS, the difference between ET in the no-LCC and deforested scenarios remained relatively constant across years in both the northern and southern regions. In the northern region, these differences remained between 0.05 to 0.06 mm d^{-1} in GLEAM and 0.02 to 0.03 mm d^{-1} in MODIS (Fig. 4.5b,d). In the southern region, these differences were larger, ranging from 0.19 to 0.26 mm d^{-1} in GLEAM and 0.06 to 0.16 mm d^{-1} in MODIS (Fig. 4.5g,i).

4.4.2 Synthesis of estimates of changes in ET in the Amazon basin from deforestation: modeling and remote sensing studies

Modeling studies consistently predict decreased ET as a result of deforestation in the Amazon basin and our ET estimates closely follow this pattern. Across all of the studies, when the deforestation extent used in the simulations is taken into account, mean ET is estimated to decrease by -0.007 mm d^{-1} or -0.2% for each 1% increase in deforestation (Fig. 4.6). Our estimated ET

change from remote sensing data is well within the range of modeling estimates. GLEAM and MODIS ET showed an average change of -0.06 and -0.11 mm d^{-1} or -1.6 and 2.8%, while the linear regression for the change in models' estimates of ET predicts a -0.069 mm d^{-1} or 2% decrease in ET at our 9.3% deforestation.

Differences in ET obtained from the control simulations in the different studies illustrate the variation across the model structures and the simulation setups (input data, deforestation scenarios, etc). The mean annual ET in control scenarios is 3.73 mm d^{-1}, with estimates as low as 2.28 mm d^{-1} and as high as 5.74 mm d^{-1}. In the deforestation scenarios, the mean annual ET is 3.09 mm d^{-1} and ranges from 1.64 to 5.21 mm d^{-1}. The studies analyzed here differ in several ways, including (1) spatial and temporal coverage and resolution of the simulations; (2) model structure, input data and parameter estimation; and (3) deforestation and climate scenarios (Appendix C, Table C2 and Fig. C2).

Model development, data quality and availability, and computational advances are expected to influence the simulation results. Mean ET change was -0.84 mm d^{-1} (-19.1%) and -0.26 mm d^{-1} (-12.9%) in studies before and after the year 2000, respectively. The higher estimated changes of older studies are partly caused by a prevalent use of total deforestation of the Amazon forests. Across our collection of studies, one of the biggest advances has been the simulation of more realistic deforestation scenarios. However, even if we focus on studies considering 100% deforestation in the Amazon, older studies have larger absolute values (-0.87 mm d^{-1}) than newer studies (-0.54 mm d^{-1}) and similar relative values (-19.8% and -21.8%, respectively).

Predictions of the change of precipitation with changes in ET are not as consistent as they are for the effects of deforestation on ET. Simulations range from positive to negative changes in precipitation, and are particularly scattered at low absolute changes in ET (Fig. 4.7a,b). Precipitation differences range between -5.45 and 1.08 mm d^{-1} and between -56 and 15.3%. The linear model fit from models data suggests a decrease of 0.9 mm d^{-1} and 0.7% in precipitation for each unit (mm d^{-1} or %) change in ET (Fig. 4.7a-b). According to the predicted relationship between changes in ET and P from modeling studies, our GLEAM and MODIS ET change estimates would suggest -0.09 mm d^{-1} (-1.87%) and -0.06 mm d^{-1} (-1.05%) changes in P, respectively. These estimates, however, ignore the complex atmospheric dynamics that have led to divergent precipitation change estimates due to deforestation (Khanna et al. 2017; Ramos da Silva, Werth, and Avissar 2008). As addressed in previous modeling studies, changes in

precipitation are highly influenced by the effect of deforestation mesoscale thermodynamics and moisture convergence, which are highly variable.

Modeling studies also indicate an increase in temperature due to deforestation. This relationship indicates an increase of 1.64 degrees Celsius per each 1 mm d^{-1} of decrease in ET (Fig. 4.7c). Our estimates of mean ET change from GLEAM and MODIS thus would imply temperature increases of 0.17 and 0.1 degrees Celsius, respectively. Changes in temperature with ET are associated with changes in sensible heat flux (H). According to modeling studies, H increases 8.02 W m^{-2} (1%) with each 1 mm d^{-1} (1%) decrease in ET (Fig. 4.7d). This trend would represent an increase of 0.84 W m^{-2} (2.8%) and 0.49 W m^{-2} (1.6%) based on our mean ET change estimates from GLEAM and MODIS, respectively.

4.5 Discussion

ET is a key connection between land cover and climate. This relationship is particularly important in the Amazon basin, where large amounts of water and energy are exchanged with the atmosphere. In accordance with our hypothesis, using remote sensing-derived datasets, we estimated a decrease in ET due to deforestation between 2000 and 2018. These estimates are in close agreement with a long record of estimates from modeling studies. Additionally, we found the effects of deforestation on ET to be larger and with higher seasonal variation in the southern than in the northern part of the basin. These effects usually peaked in the late dry season, but, contrary to our expectations, showed low interannual variation.

The agreement in ET change is observed despite the large variation in the methodological differences used to estimate it among the collection of studies. Even though climate models and remote sensing-derived datasets share some structural principles about ET, there is also a wide variation in parameter estimates, input data, and other model assumptions. The consistency of the previous estimates through time, even under continuous model improvement, and the close fit of our estimate into those predictions, increases the confidence in the predicted changes in ET. The differences among estimates help to quantify uncertainty and to provide a wider view of potential paths for future changes in ET with continued deforestation.

Our estimates revealed the stronger influence of deforestation on ET in the southern part of the basin. The differences between southern and northern Amazonia have also been observed in recent modeling studies with more realistic scenarios of deforestation (Alves et al. 2017; Zemp

et al. 2017). The higher differences observed in the southern part of the basin are the result of higher deforestation rates, at least in part. In simulations of total deforestation in the entire region, the ET decrease after deforestation is also higher in the southern than in the northern Amazon (Voldoire and Royer 2004). Those studies attribute the regional difference to the year-round high precipitation rates in the northern Amazon. Constant water availability reduces vegetation water stress, including in croplands and pastures, resulting in ET rates from these anthropogenic land cover types that are more similar to those of forests. An important region of large changes in ET in our study stretches along the western border of the basin. This region, close to the Andean mountains, showed large differences in ET between our non-deforested scenario and observations. The differences in this region could be partly due to the transition zone where it is located (i.e., lowlands to higher elevations), and the impact this has on the spatial autocorrelation technique used in this study. Given the differences between areas at higher elevation and lowland forests, the interpolation predictions might overestimate ET in these regions. On the other hand, there were also contrasting results in the effect of deforestation on ET from both datasets in some parts of this same region; GLEAM and MODIS predict lower and higher ET with deforestation, respectively. These discrepancies could be attributed to the potential lack of appropriate parameters in the ET algorithms for mountainous tropical vegetation, where ET has been less studied (Ochoa-Sánchez et al. 2019).

Over the entire basin, the changes in ET due to deforestation increased during the dry season. We hypothesize that this seasonal effect of deforestation on ET is related to differences in water stress between forest and other vegetation during the dry season. Previous research has shown the ability of Amazon forests to maintain and even increase photosynthetic activity during the dry season (Guan et al. 2015; Saleska et al. 2003). Large roots allow trees to reach water stored in the deeper soil layers. Other vegetation types with shorter roots, such as grasses and crops, are not able to access deep soil layers and are therefore water-limited during the dry season (Nepstad et al. 1994). These ET differences in the dry season have been reported by some of the modeling studies analyzed here (Dirmeyer and Shukla 1994; Kleidon and Heimann 2000; Lean and Rowntree 1993; Zemp et al. 2017). However, current land surface models are not able to capture the increase in photosynthetic activity during the dry season (Restrepo-Coupe et al. 2017). This could represent an important strength of GLEAM and MODIS ET, which capture this seasonal pattern. We believe that (1) using remote sensing observations for data assimilation and model

benchmarking, and (2) exploring the mechanisms incorporated in the ET calculations in GLEAM, MODIS, and other modeling studies that accurately capture the dry-season response would allow us to identify the components leading to these improved ET simulations. Accurate simulation of dry season ET is highly relevant for prediction of wet season onset in the Amazon (Khanna et al. 2017; Leite-Filho, Costa, and Fu 2020; Nobre, Sellers, and Shukla 1991; Wright et al. 2017).

Effects of deforestation on annual ET remained essentially constant, even across years of extreme drought or floods. Deforestation also did not seem to alter interannual variation of ET in general. These results are in agreement with some modeling studies where deforestation experiments have shown independent effects from ENSO events (Polcher and Laval 1994). Other studies have suggested that deforestation effects are greatest during extremely dry years (Ramos da Silva et al. 2008; Voldoire and Royer 2004). In these studies, ET differences between the control and the deforestation scenario are the result of soil water stress. The effect of Amazonian droughts and the resilience of Amazon forests to prolonged droughts is still an active field of study (Koren et al. 2018).

Our deforestation estimates are very conservative. While current estimates of deforestation are around 17% for the Amazon basin (Lovejoy and Nobre 2019), our deforestation estimates are under 10%. To place the deforestation estimates we used in our ET calculations in a larger context, we separately calculated deforestation extent from the Tree Cover data of Hansen et al. (2013) from 2000-2018 in our area of study. In these calculations, the deforestation percentage by 2018 was about 12.8%, which is 2.8% higher than our estimates from ESA Land Cover. The deforestation difference between the Tree Cover dataset and ours arises in part from our masking out areas close to the river in an attempt to remove pixels with substantial coverage of open water from the analyses. Our estimates from both ESA and Tree Cover data are still lower than other reported deforestation estimates. We believe this mismatch in estimates is likely due to differences among studies in the definitions of the Amazon's boundaries.

Our GLEAM and MODIS ET estimates are within the range of previous site-level measurements and basin-wide modeled ET estimates: from 2.1 to 4.49 mm d^{-1} (Costa et al. 2010; Maeda et al. 2017; Paca et al. 2019; Xu et al. 2019). However, there are strong spatial and temporal differences between the two datasets. The difference in the algorithms and remote sensing input data in the two datasets has previously led to spatial and temporal differences in ET estimates (Miralles et al. 2016). In our case, mean ET estimates are generally lower in MODIS than in

GLEAM in the central and northwestern part of the Amazon basin. Previous studies have indicated the tendency of the MODIS ET product to underestimate ET in tropical forests (Miralles et al. 2016), which could partially explain our results. However, we also observed low MODIS ET specifically during the wetter months both in the northern and southern Amazon. Another shortcoming of MODIS is its reliance on satellite imagery that is highly susceptible to cloudiness, which is a known issue in the tropics and could explain differences in seasonal trends. Overall, we found GLEAM to show expected amounts of ET and its spatial and seasonal variation in the Amazon basin were closer to those estimated in previous studies.

The remote-sensing derived ET data in this study support previous predictions from modeling about the trajectory of basin-wide ET change under continuing deforestation. Evaluating the magnitude of the effect of change in ET on climate and the region's ecosystems will require further work. Therefore, we hope that this more precise estimate of changes in ET with deforestation can help future studies looking at changes in climate and the water budget of the Amazon. We also acknowledge that although there is broad agreement across models about how deforestation influences ET, there is a strong possibility of encountering a tipping point in the relationship as deforestation proceeds (Lovejoy and Nobre 2019; Zemp et al. 2017). While predicting a tipping point is a complex task, we believe that the fast development of dynamic vegetation models coupled to Earth System Models has the potential to provide valuable insight into this problem.

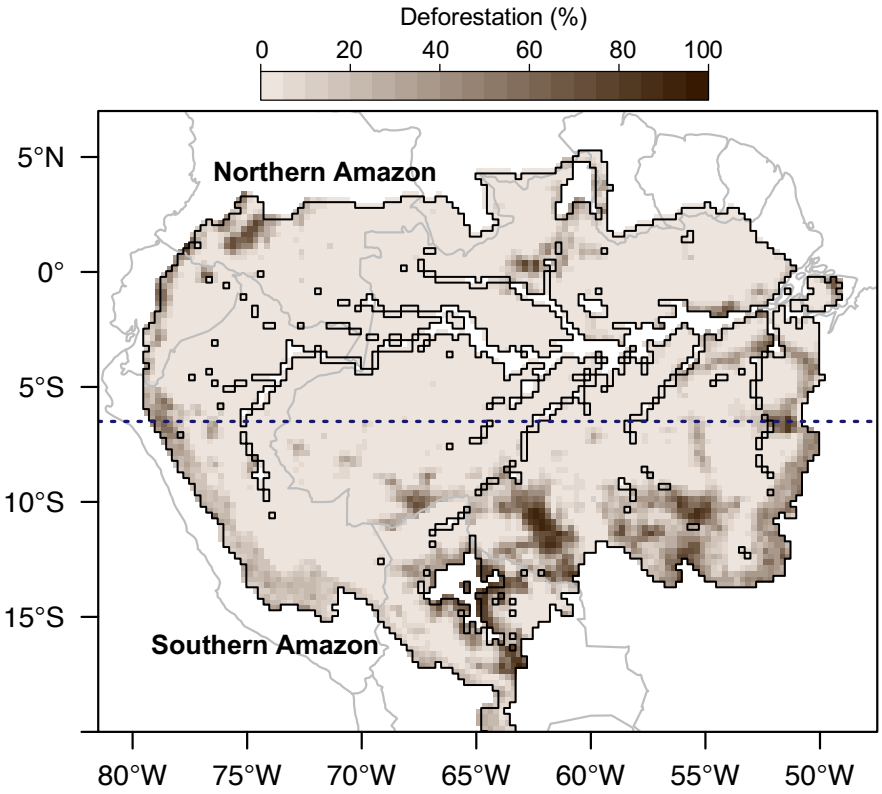

Fig. 4.1. Average deforestation (%) in the Amazon basin from ESA-CCI 2000-2018. The black line shows the boundaries of the area of study (i.e., tropical forests of the Amazon basin). We excluded from our analyses pixels that were not tropical forest (e.g., savannas and shrublands) and those with water cover >5%. The horizontal dotted line delimits the northern and southern regions of the basin used in our analyses

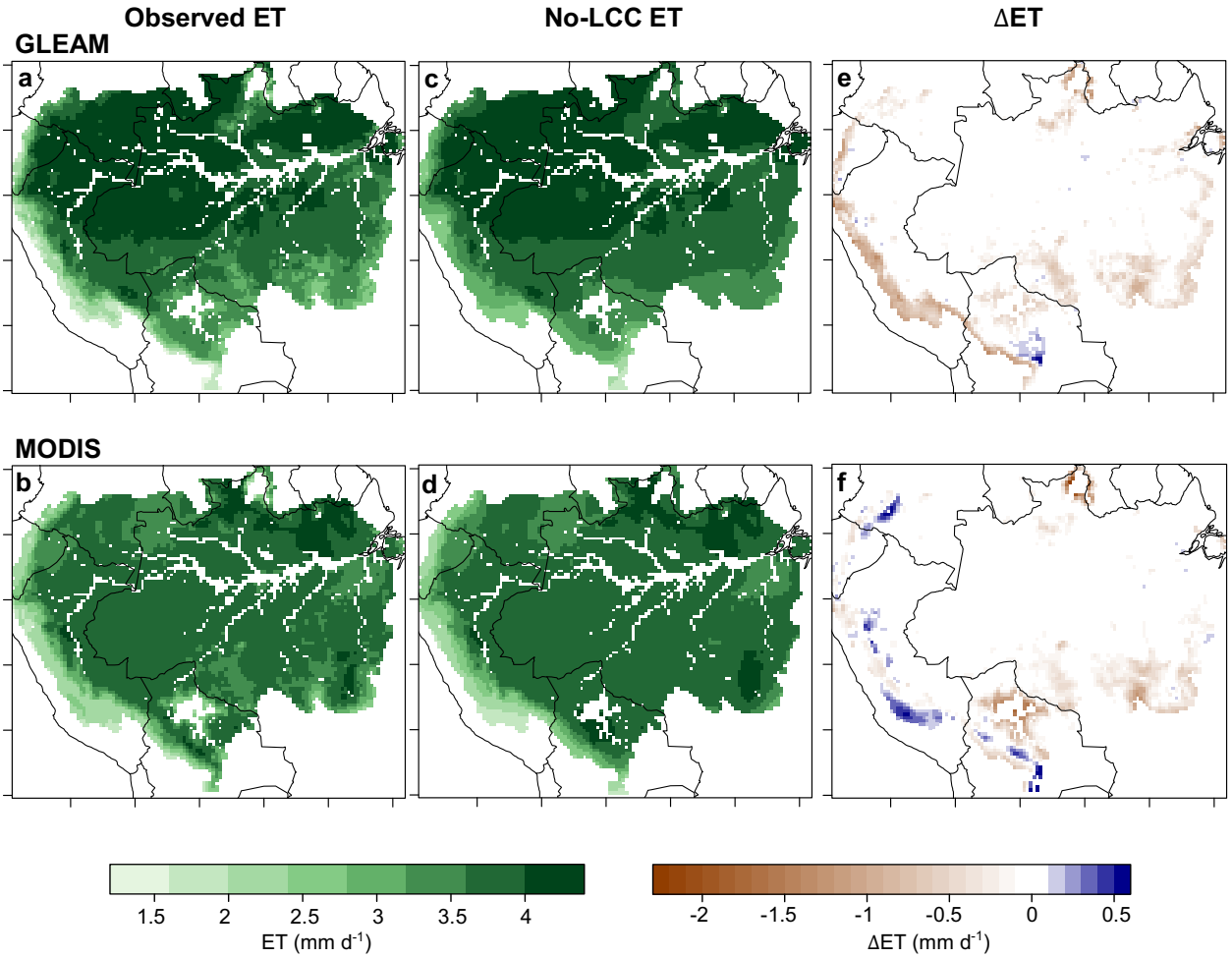

Fig. 4.2. Mean observed ET (mm d^{-1}) from GLEAM (a) and MODIS (b), and mean ET in the no-LCC scenario from GLEAM (c) and MODIS (d) for the period 2000-2018 in the Amazon basin. Mean change in ET (mm d^{-1}) as the difference between observed and no-LCC mean ET (ΔET) from GLEAM (e) and MODIS (f).

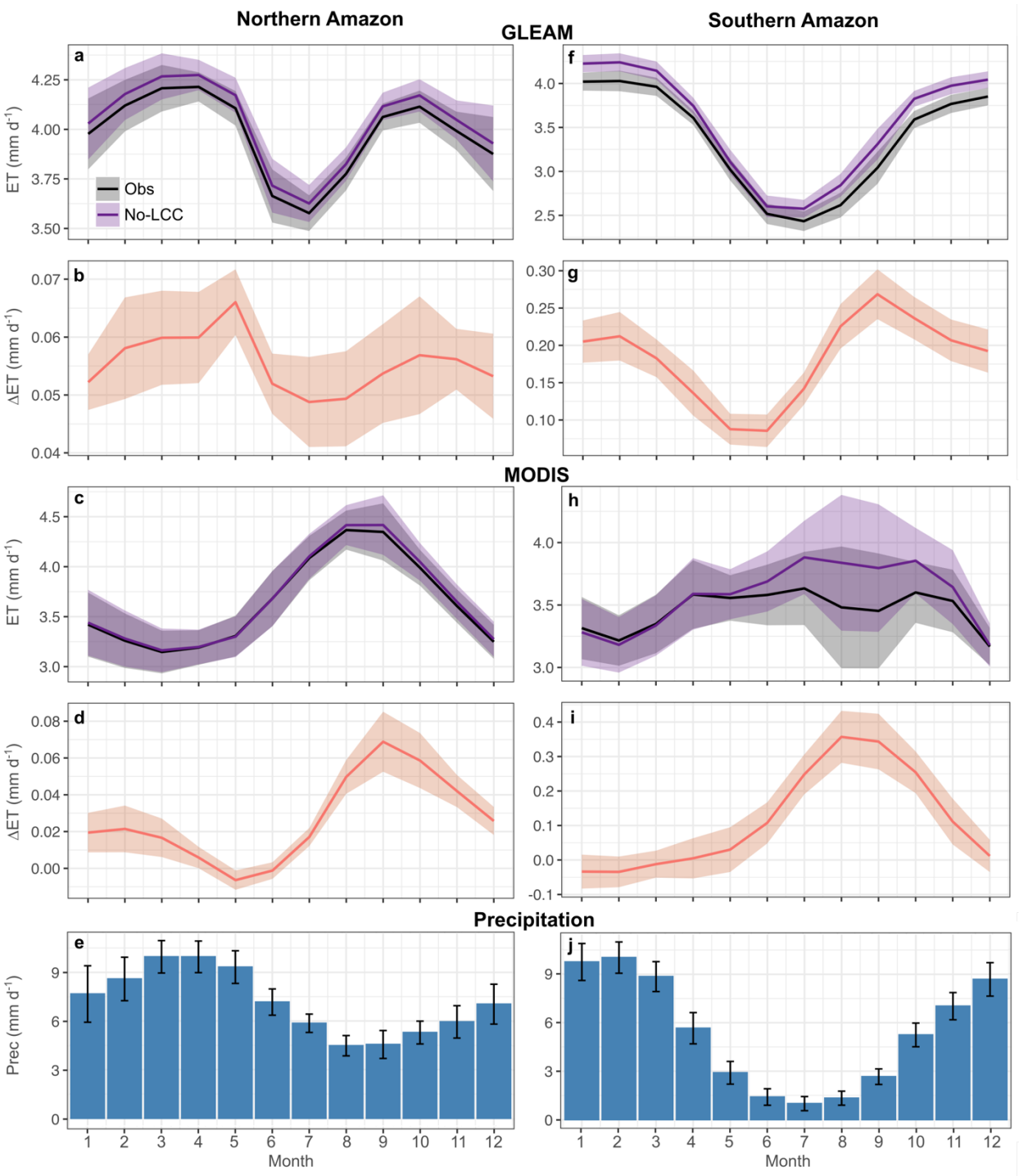

Fig. 4.3. Seasonal variation in observed and no-LCC ET from GLEAM (a,f) and MODIS (c,h). Seasonal variation in the difference between observed and no-LCC ET (ΔET) from GLEAM (b,g) and MODIS (d,i). Precipitation seasonality (e,j). All data are shown separately for the northern (a-e) and southern (f-j) regions of the Amazon. Shaded area and error bars show the standard deviation.

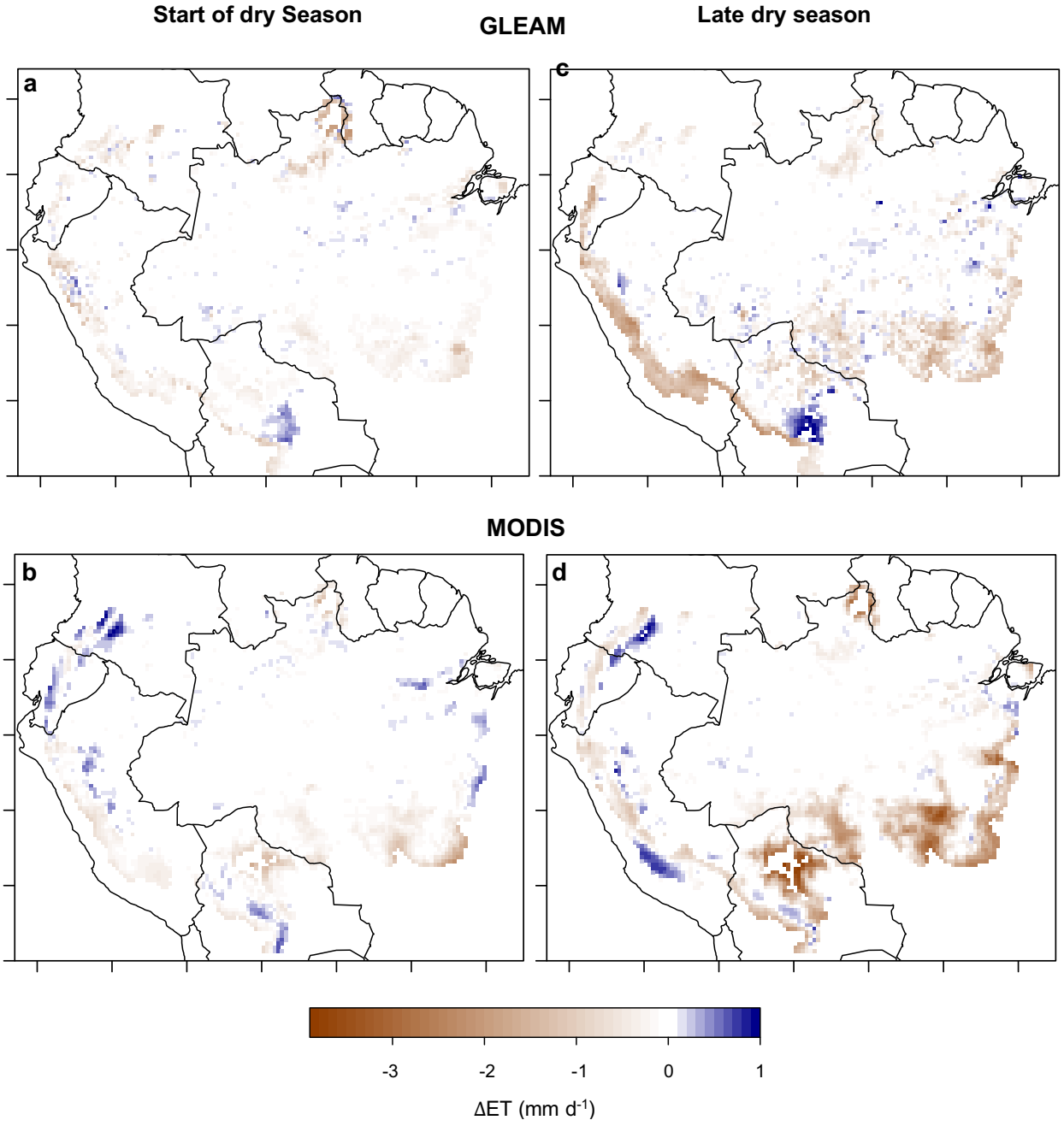

Fig. 4.4. Difference between observed and no-LCC mean annual ET (ΔET) from GLEAM (a,c) and MODIS (b,d) ET in the early dry (a-b) and late dry (c-d) season. Data correspond to June (early dry season) and September 2011 (late dry season).

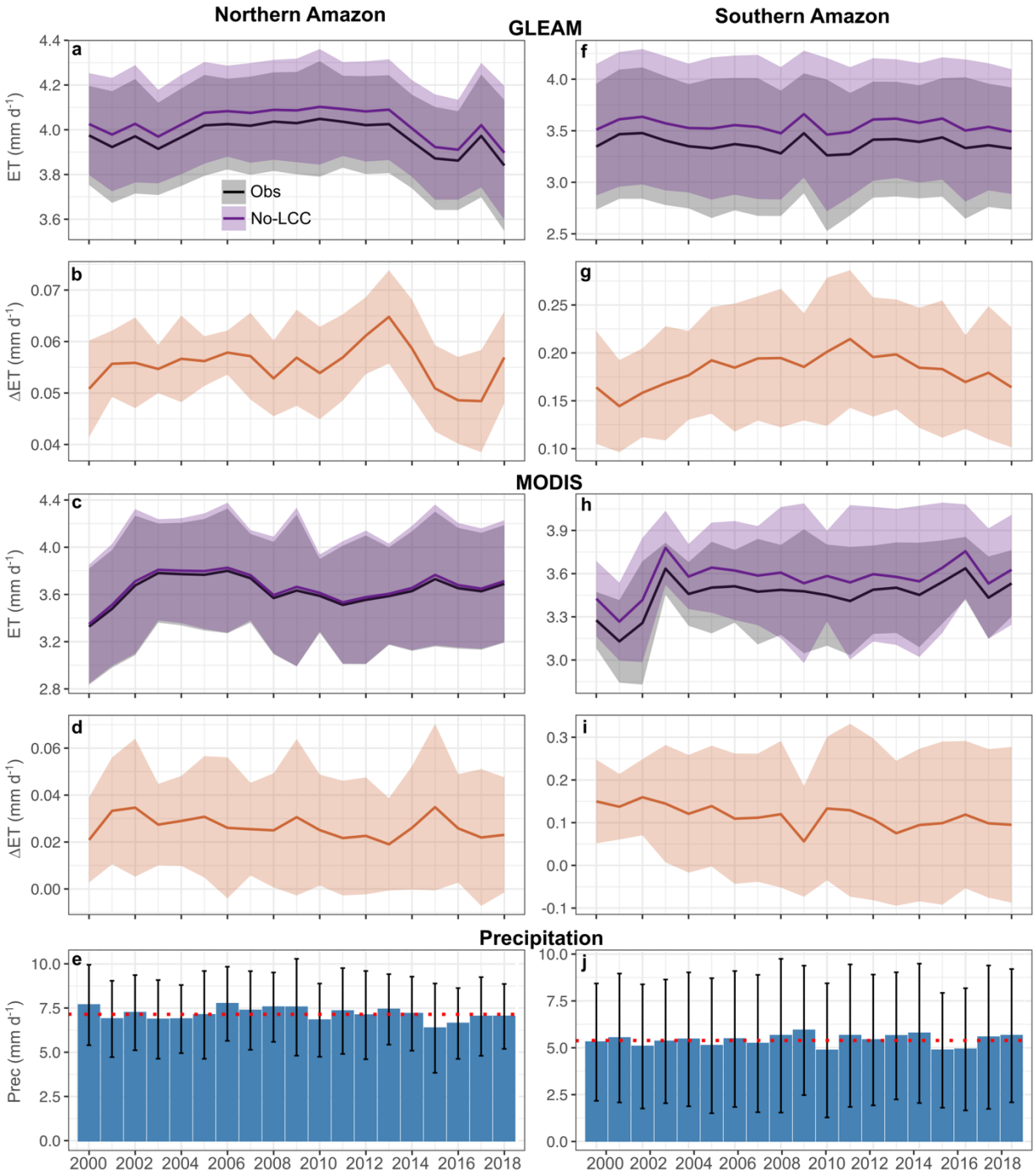

Fig. 4.5. Interannual variation in observed and no-LCC ET from GLEAM (a,f) and MODIS (c,h) for the period 2000-2018. Interannual variation in the difference between observed and no-LCC ET (ΔET) from GLEAM (b,g) and MODIS (d,i). Precipitation seasonality (e,j). All data are shown separately for the northern (a-e) and southern (f-j) regions of the Amazon. Shaded area and error bars show the standard deviation.

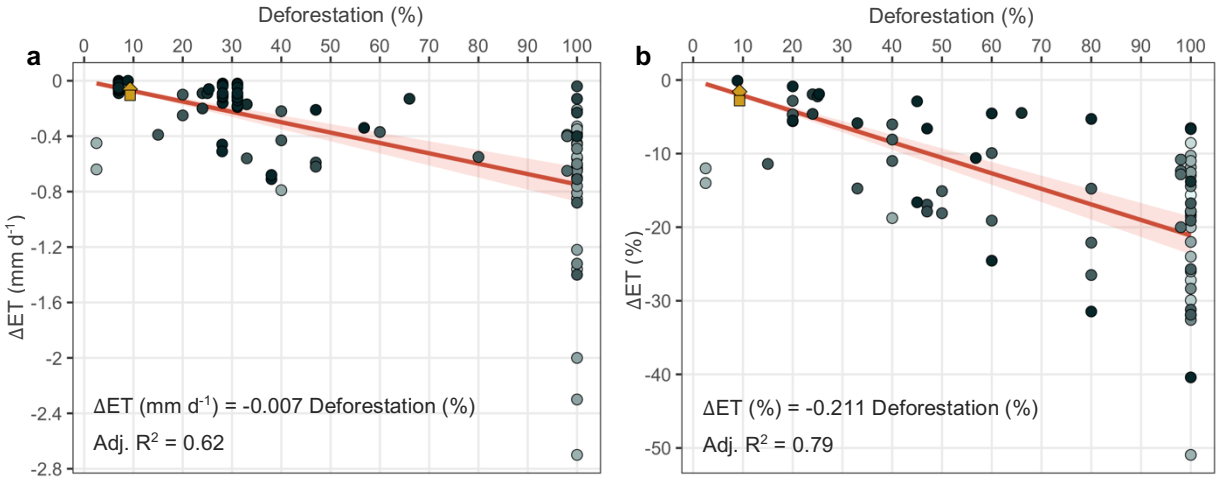

Fig. 4.6. Estimates of absolute (a) and relative (b) change in ET as a function of deforestation in the Amazon basin. The circular shapes correspond to estimates from modeling studies published between 1984 and 2017; older to newer publications are represented by lighter to darker shades. The ET change estimates from our study are represented by the golden square (GLEAM) and diamond (MODIS). The red line shows the linear regression between deforestation and change in ET. The regression intercept is set to zero. The shaded area around the line corresponds to the standard error of predicted means. The regression equation, adjusted R-squared (Adj. R^2), and sample size for each regression is displayed in each figure.

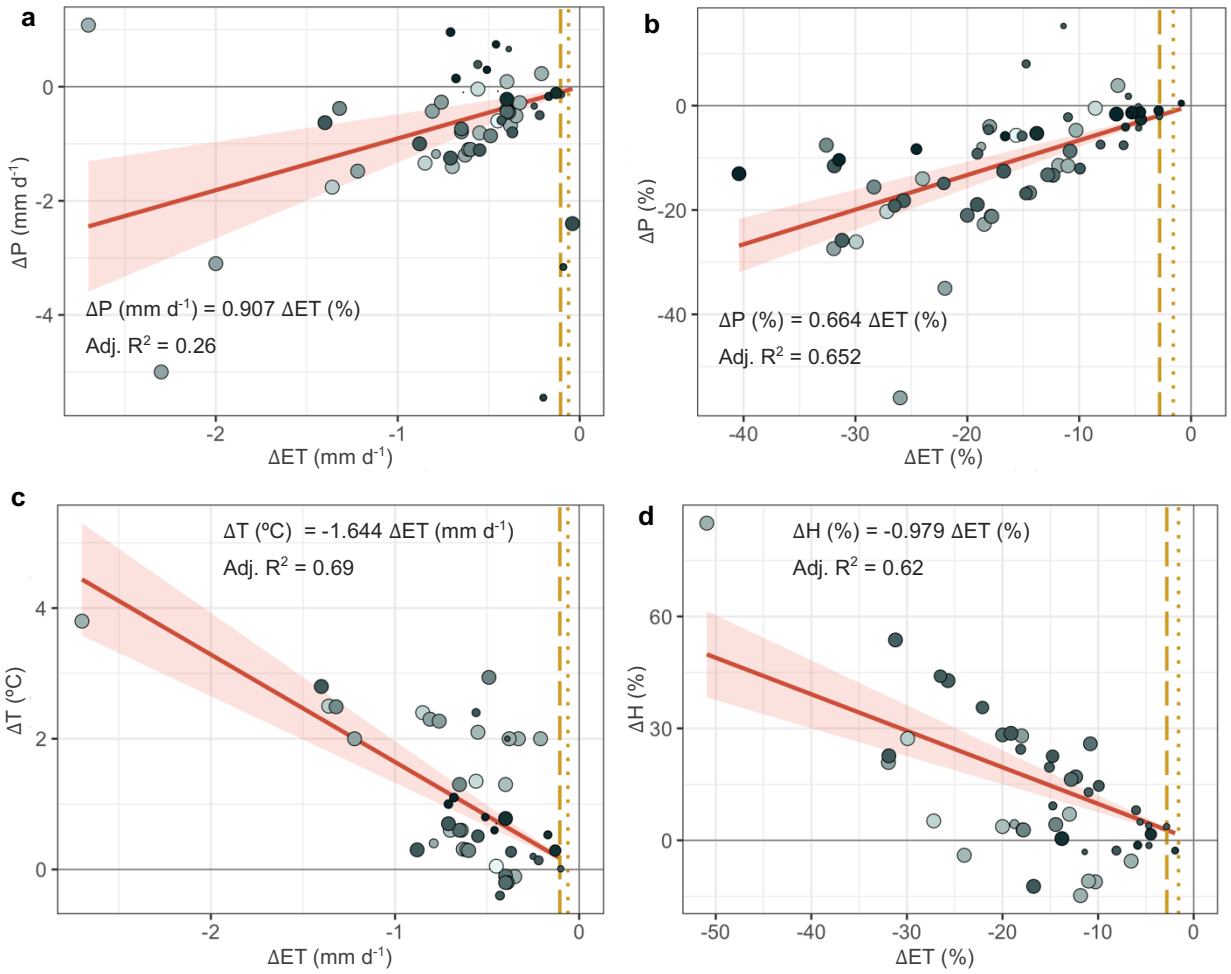

Fig. 4.7. Relationship between changes in ET and, (a-b) precipitation, (c) temperature and (d) sensible heat flux from modeling studies. Older to newer publications are represented by lighter to darker shades. The size of the circle indicates the deforestation scenario (% deforestation) used in each simulation. The estimated change in GLEAM and MODIS ET from this study are represented by the long dashed and dotted lines, respectively. The red line shows the linear regression between change in ET and change in each of the corresponding climate factors. The regression intercept is set to zero. The shaded area around the line corresponds to the standard error. The regression equation, adjusted R-squared (Adj. R^2), and sample size for each regression is displayed in each figure.

4.6 References

Alkama, Ramdane, and Alessandro Cescatti. 2016. "Biophysical Climate Impacts of Recent Changes in Global Forest Cover." *Science* 351(6273):600–604.

Alves, Lincoln Muniz, Jose A. Marengo, Rong Fu, and Rodrigo J. Bombardi. 2017. "Sensitivity of Amazon Regional Climate to Deforestation." *American Journal of Climate Change* 6(1):75–98.

Bonan, Gordon B. 2008. "Forests and Climate Change: Forcings, Feedbacks, and the Climate Benefits of Forests." *Science* 320(5882):1444–49.

Butt, Nathalie, Paula Afonso de Oliveira, and Marcos Heil Costa. 2011. "Evidence That Deforestation Affects the Onset of the Rainy Season in Rondonia, Brazil." *Journal of Geophysical Research: Atmospheres* 116(D11).

Cai, Xitian, William J. Riley, Qing Zhu, Jinyun Tang, Zhenzhong Zeng, Gautam Bisht, and James T. Randerson. 2019. "Improving Representation of Deforestation Effects on Evapotranspiration in the E3SM Land Model." *Journal of Advances in Modeling Earth Systems* 11(8):2412–27.

Cohn, Avery S., Nishan Bhattarai, Jake Campolo, Octavia Crompton, David Dralle, John Duncan, and Sally Thompson. 2019. "Forest Loss in Brazil Increases Maximum Temperatures within 50 Km." *Environmental Research Letters* 14(8):084047.

Costa, Marcos H., Márcia C. Biajoli, Luciana Sanches, Ana C. M. Malhado, Lucy R. Hutyra, Humberto R. da Rocha, Renata G. Aguiar, and Alessandro C. de Araújo. 2010. "Atmospheric versus Vegetation Controls of Amazonian Tropical Rain Forest Evapotranspiration: Are the Wet and Seasonally Dry Rain Forests Any Different?" *Journal of Geophysical Research: Biogeosciences* 115(G4).

D'Almeida, Cassiano, Charles J. Vörösmarty, George C. Hurtt, José A. Marengo, S. Lawrence Dingman, and Barry D. Keim. 2007. "The Effects of Deforestation on the Hydrological Cycle in Amazonia: A Review on Scale and Resolution." *International Journal of Climatology* 27(5):633–47.

Davidson, Eric A., Alessandro C. de Araújo, Paulo Artaxo, Jennifer K. Balch, I. Foster Brown, Mercedes M. C. Bustamante, Michael T. Coe, Ruth S. DeFries, Michael Keller, Marcos Longo, J. William Munger, Wilfrid Schroeder, Britaldo S. Soares-Filho, Carlos M. Souza, and Steven C. Wofsy. 2012. "The Amazon Basin in Transition." *Nature* 481(7381):321–28.

Dirmeyer, Paul A., and J. Shukla. 1994. "Albedo as a Modulator of Climate Response to Tropical Deforestation." *Journal of Geophysical Research: Atmospheres* 99(D10):20863–77.

ESA. 2017. *Land Cover CCI Product User Guide Version 2*. *Tech. Rep.* ESA.

Fisher, Joshua B., Forrest Melton, Elizabeth Middleton, Christopher Hain, Martha Anderson, Richard Allen, Matthew F. McCabe, Simon Hook, Dennis Baldocchi, Philip A. Townsend, Ayse Kilic, Kevin Tu, Diego D. Miralles, Johan Perret, Jean-Pierre Lagouarde, Duane Waliser, Adam J. Purdy, Andrew French, David Schimel, James S. Famiglietti, Graeme Stephens, and Eric F. Wood. 2017. "The Future of Evapotranspiration: Global Requirements for Ecosystem Functioning, Carbon and Climate Feedbacks, Agricultural Management, and Water Resources." *Water Resources Research* 53(4):2618–26.

Gräler, Benedikt, Edzer Pebesma, and Gerard Heuvelink. 2016. "Spatio-Temporal Interpolation Using Gstat." *The R Journal* 8(1):204.

Guan, Kaiyu, Ming Pan, Haibin Li, Adam Wolf, Jin Wu, David Medvigy, Kelly K. Caylor, Justin Sheffield, Eric F. Wood, Yadvinder Malhi, Miaoling Liang, John S. Kimball, Scott R. Saleska, Joe Berry, Joanna Joiner, and Alexei I. Lyapustin. 2015. "Photosynthetic Seasonality of Global Tropical Forests Constrained by Hydroclimate." *Nature Geoscience* 8(4):284–89.

Guimberteau, Matthieu, Philippe Ciais, Agnès Ducharne, Juan Pablo Boisier, Ana Paula Dutra Aguiar, Hester Biemans, Hannes de Deurwaerder, David Galbraith, Bart Kruijt, Fanny Langerwisch, German Poveda, Anja Rammig, Daniel Andres Rodriguez, Graciela Tejada, Kirsten Thonicke, Celso von Randow, Rita C. S. von Randow, Ke Zhang, and Hans Verbeeck. 2017. "Impacts of Future Deforestation and Climate Change on the Hydrology of the Amazon Basin: A Multi-Model Analysis with a New Set of Land-Cover Change Scenarios." *Hydrology and Earth System Sciences* 21(3):1455–75.

Hansen, M. C., P. V. Potapov, R. Moore, M. Hancher, S. A. Turubanova, A. Tyukavina, D. Thau, S. V. Stehman, S. J. Goetz, T. R. Loveland, A. Kommareddy, A. Egorov, L. Chini, C. O. Justice, and J. R. G. Townshend. 2013. "High-Resolution Global Maps of 21st-Century Forest Cover Change." *Science* 342(6160):850–53.

Hiemstra, Paul H., Edzer J. Pebesma, Chris J. W. Twenhöfel, and Gerard B. M. Heuvelink. 2009. "Real-Time Automatic Interpolation of Ambient Gamma Dose Rates from the Dutch Radioactivity Monitoring Network." *Computers & Geosciences* 35(8):1711–21.

Khanna, Jaya, David Medvigy, Stephan Fueglistaler, and Robert Walko. 2017. "Regional Dry-Season Climate Changes Due to Three Decades of Amazonian Deforestation." *Nature Climate Change* 7(3):200–204.

Kleidon, A., and M. Heimann. 2000. "Assessing the Role of Deep Rooted Vegetation in the Climate System with Model Simulations: Mechanism, Comparison to Observations and Implications for Amazonian Deforestation." *Climate Dynamics* 16(2–3):183–99.

Koren, Gerbrand, Erik van Schaik, Alessandro C. Araújo, K. Folkert Boersma, Antje Gärtner, Lars Killaars, Maurits L. Kooreman, Bart Kruijt, Ingrid T. van der Laan-Luijkx, Celso von Randow, Naomi E. Smith, and Wouter Peters. 2018. "Widespread Reduction in Sun-Induced Fluorescence from the Amazon during the 2015/2016 El Niño." *Philosophical Transactions of the Royal Society B: Biological Sciences* 373(1760):20170408.

Lawrence, Deborah, and Karen Vandecar. 2015. "Effects of Tropical Deforestation on Climate and Agriculture." *Nature Climate Change* 5(1):27–36.

Lean, J., and P. R. Rowntree. 1993. "A GCM Simulation of the Impact of Amazonian Deforestation on Climate Using an Improved Canopy Representation." *Quarterly Journal of the Royal Meteorological Society* 119(511):509–30.

Leite-Filho, Argemiro T., Marcos H. Costa, and Rong Fu. 2020. "The Southern Amazon Rainy Season: The Role of Deforestation and Its Interactions with Large-Scale Mechanisms." *International Journal of Climatology* 40(4):2328–41.

Li, Jin, and Andrew D. Heap. 2014. "Spatial Interpolation Methods Applied in the Environmental Sciences: A Review." *Environmental Modelling & Software* 53:173–89.

Lovejoy, Thomas E., and Carlos Nobre. 2019. "Amazon Tipping Point: Last Chance for Action." *Science Advances* 5(12):eaba2949.

Maeda, Eduardo Eiji, Xuanlong Ma, Fabien Hubert Wagner, Hyungjun Kim, Taikan Oki, Derek Eamus, and Alfredo Huete. 2017. "Evapotranspiration Seasonality across the Amazon Basin." *Earth System Dynamics* 8(2):439–54.

Malhi, Yadvinder, J. Timmons Roberts, Richard A. Betts, Timothy J. Killeen, Wenhong Li, and Carlos A. Nobre. 2008. "Climate Change, Deforestation, and the Fate of the Amazon." *Science* 319(5860):169–72.

Martens, Brecht, Diego G. Miralles, Hans Lievens, Robin van der Schalie, Richard A. M. de Jeu, Diego Fernández-Prieto, Hylke E. Beck, Wouter A. Dorigo, and Niko E. C. Verhoest. 2017. "GLEAM v3: Satellite-Based Land Evaporation and Root-Zone Soil Moisture." *Geoscientific Model Development* 10(5):1903–25.

Mayorga, E., M. G. Logsdon, M. V. R. Ballester, and J. E. Richey. 2012. "LBA-ECO CD-06 Amazon River Basin Land and Stream Drainage Direction Maps." 318.801127 MB.

Mayorga, Emilio, Miles G. Logsdon, Maria Victoria R. Ballester, and Jeffrey E. Richey. 2005. "Estimating Cell-to-Cell Land Surface Drainage Paths from Digital Channel Networks, with an Application to the Amazon Basin." *Journal of Hydrology* 315(1–4):167–82.

Miralles, D. G., T. R. H. Holmes, R. A. M. De Jeu, J. H. Gash, A. G. C. A. Meesters, and A. J. Dolman. 2011. "Global Land-Surface Evaporation Estimated from Satellite-Based Observations." *Hydrology and Earth System Sciences* 15(2):453–69.

Miralles, D. G., C. Jiménez, M. Jung, D. Michel, A. Ershadi, M. F. McCabe, M. Hirschi, B. Martens, A. J. Dolman, J. B. Fisher, Q. Mu, S. I. Seneviratne, E. F. Wood, and D. Fernández-Prieto. 2016. "The WACMOS-ET Project – Part 2: Evaluation of Global Terrestrial Evaporation Data Sets." *Hydrology and Earth System Sciences* 20(2):823–42.

Nepstad, D. C., C. R. de Carvalho, E. A. Davidson, P. H. Jipp, P. A. Lefebvre, G. H. Negreiros, E. D. da Silva, T. A. Stone, S. E. Trumbore, and S. Vieira. 1994. "The Role of Deep Roots in the Hydrological and Carbon Cycles of Amazonian Forests and Pastures." *Nature* 372(6507):666–69.

Nobre, Carlos A., Piers J. Sellers, and Jagadish Shukla. 1991. "Amazonian Deforestation and Regional Climate Change." *Journal of Climate* 4(10):957–88.

Ochoa-Sánchez, Ana, Patricio Crespo, Galo Carrillo-Rojas, Adrián Sucozhañay, and Rolando Célleri. 2019. "Actual Evapotranspiration in the High Andean Grasslands: A Comparison of Measurement and Estimation Methods." *Frontiers in Earth Science* 7.

Olson, David M., Eric Dinerstein, Eric D. Wikramanayake, Neil D. Burgess, George V. N. Powell, Emma C. Underwood, Jennifer A. D'amico, Illanga Itoua, Holly E. Strand, John C. Morrison, Colby J. Loucks, Thomas F. Allnutt, Taylor H. Ricketts, Yumiko Kura, John F. Lamoreux, Wesley W. Wettengel, Prashant Hedao, and Kenneth R. Kassem. 2001. "Terrestrial Ecoregions of the World: A New Map of Life on EarthA New Global Map of

Terrestrial Ecoregions Provides an Innovative Tool for Conserving Biodiversity." *BioScience* 51(11):933–38.

Paca, Victor Hugo da Motta, Gonzalo E. Espinoza-Dávalos, Tim M. Hessels, Daniel Medeiros Moreira, Georges F. Comair, and Wim G. M. Bastiaanssen. 2019. "The Spatial Variability of Actual Evapotranspiration across the Amazon River Basin Based on Remote Sensing Products Validated with Flux Towers." *Ecological Processes* 8(1):6.

Pebesma, Edzer J. 2004. "Multivariable Geostatistics in S: The Gstat Package." *Computers & Geosciences* 30(7):683–91.

Plant, Richard. 2012. *Spatial Statistics in Ecology and Agriculture Using R and Geoda*. Baton Rouge, UNITED STATES: CRC Press LLC.

Polcher, J., and K. Laval. 1994. "A Statistical Study of the Regional Impact of Deforestation on Climate in the LMD GCM." *Climate Dynamics* 10(4):205–19.

Prevedello, Jayme A., Gisele R. Winck, Marcelo M. Weber, Elizabeth Nichols, and Barry Sinervo. 2019. "Impacts of Forestation and Deforestation on Local Temperature across the Globe." *PLOS ONE* 14(3):e0213368.

R Core Team. 2019. *R: A Language and Environment for Statistical Computing*. Vienna, Austria: R Foundation for Statistical Computing.

Ramos da Silva, Renato, David Werth, and Roni Avissar. 2008. "Regional Impacts of Future Land-Cover Changes on the Amazon Basin Wet-Season Climate." *Journal of Climate* 21(6):1153–70.

Restrepo-Coupe, Natalia, Naomi M. Levine, Bradley O. Christoffersen, Loren P. Albert, Jin Wu, Marcos H. Costa, David Galbraith, Hewlley Imbuzeiro, Giordane Martins, Alessandro C. da Araujo, Yadvinder S. Malhi, Xubin Zeng, Paul Moorcroft, and Scott R. Saleska. 2017. "Do Dynamic Global Vegetation Models Capture the Seasonality of Carbon Fluxes in the Amazon Basin? A Data-Model Intercomparison." *Global Change Biology* 23(1):191–208.

Running, S., Q. Mu, M. Zhao, and A. Moreno. 2019. *MOD16A2GF MODIS/Terra Net Evapotranspiration Gap-Filled 8-Day L4 Global 500 m SIN Grid V006 [Data Set]*. NASA EOSDIS Land Processes DAAC.

Running, S. W., Q. Mu, M. Zhao, and A. Moreno. 2019. "User's Guide MODIS Global Terrestrial Evapotranspiration (ET) Product (MOD16A2/A3 and Year-End Gap-Filled MOD16A2GF/A3GF) NASA Earth Observing System MODIS Land Algorithm (For Collection 6) Version 2.2."

Saleska, Scott R., Scott D. Miller, Daniel M. Matross, Michael L. Goulden, Steven C. Wofsy, Humberto R. da Rocha, Plinio B. de Camargo, Patrick Crill, Bruce C. Daube, Helber C. de Freitas, Lucy Hutyra, Michael Keller, Volker Kirchhoff, Mary Menton, J. William Munger, Elizabeth Hammond Pyle, Amy H. Rice, and Hudson Silva. 2003. "Carbon in Amazon Forests: Unexpected Seasonal Fluxes and Disturbance-Induced Losses." *Science* 302(5650):1554–57.

Singh, Prafull, and Pradipika Verma. 2019. "Chapter 5 - A Comparative Study of Spatial Interpolation Technique (IDW and Kriging) for Determining Groundwater Quality." Pp. 43–56 in *GIS and Geostatistical Techniques for Groundwater Science*, edited by S. Venkatramanan, M. V. Prasanna, and S. Y. Chung. Elsevier.

Soares-Filho, Britaldo Silveira, Daniel Curtis Nepstad, Lisa M. Curran, Gustavo Coutinho Cerqueira, Ricardo Alexandrino Garcia, Claudia Azevedo Ramos, Eliane Voll, Alice McDonald, Paul Lefebvre, and Peter Schlesinger. 2006. "Modelling Conservation in the Amazon Basin." *Nature* 440(7083):520–23.

Spracklen, D. V., and L. Garcia-Carreras. 2015. "The Impact of Amazonian Deforestation on Amazon Basin Rainfall." *Geophysical Research Letters* 42(21):9546–52.

Staal, Arie, Obbe A. Tuinenburg, Joyce H. C. Bosmans, Milena Holmgren, Egbert H. van Nes, Marten Scheffer, Delphine Clara Zemp, and Stefan C. Dekker. 2018. "Forest-Rainfall Cascades Buffer against Drought across the Amazon." *Nature Climate Change* 8(6):539.

Swann, Abigail L. S., Marcos Longo, Ryan G. Knox, Eunjee Lee, and Paul R. Moorcroft. 2015. "Future Deforestation in the Amazon and Consequences for South American Climate." *Agricultural and Forest Meteorology* 214–215:12–24.

Vergopolan, Noemi, and Joshua B. Fisher. 2016. "The Impact of Deforestation on the Hydrological Cycle in Amazonia as Observed from Remote Sensing." *International Journal of Remote Sensing* 37(22):5412–30.

Voldoire, A., and J. F. Royer. 2004. "Tropical Deforestation and Climate Variability." *Climate Dynamics* 22(8):857–74.

Wright, Jonathon S., Rong Fu, John R. Worden, Sudip Chakraborty, Nicholas E. Clinton, Camille Risi, Ying Sun, and Lei Yin. 2017. "Rainforest-Initiated Wet Season Onset over the Southern Amazon." *Proceedings of the National Academy of Sciences* 114(32):8481–86.

Xu, Donghui, Elizabeth Agee, Jingfeng Wang, and Valeriy Y. Ivanov. 2019. "Estimation of Evapotranspiration of Amazon Rainforest Using the Maximum Entropy Production Method." *Geophysical Research Letters* 46(3):1402–12.

Zemp, D. C., C. F. Schleussner, H. M. J. Barbosa, and A. Rammig. 2017. "Deforestation Effects on Amazon Forest Resilience." *Geophysical Research Letters* 44(12):6182–90.

CHAPTER 5. CONCLUSIONS

The first year within my PhD I realized how, despite much advance in our knowledge about tropical ecosystems, we still had so much to learn about them. I realized, from my own experience with models and from literature, that most of our state-of-the-art land surface models misrepresent broad patterns of vegetation seasonality in these regions. This discrepancy is particularly significant as tropical ecosystems constitute the largest part of global terrestrial photosynthesis. The goal of my research was to grow our knowledge about tropical ecosystems' photosynthetic activity seasonality, its relationship with climate and with land cover change.

In the first study, I characterize the relationship of photosynthetic activity with the two main climate drivers in the tropics at the seasonal scale; precipitation and radiation. I found that most regions in the tropics have a positive correlation with both climate drivers, or a positive correlation with one of the drivers and negative with the other one. Each of these types of relationships are characterized by specific climate properties. For instance, light-driven photosynthetic activity (i.e., positive correlation with radiation and negative with precipitation) is found in regions with high mean annual precipitation and a short dry season. The correlation between precipitation and radiation itself also contributes to explain these relationships. Regions where precipitation and radiation are uncorrelated or positively correlated tend to have positive correlation with both climate drivers. Regions where the two drivers are negatively correlated tend to have a positive correlation with one driver and negative with the other one. Based on our classification, ecosystem models tend to overestimate positive correlations with precipitation and underestimate positive correlations with radiation.

In the second chapter, I show the distinct seasonal effects of land cover change on photosynthetic activity and transpiration in two ecosystems of the southern Amazon. I demonstrate decreases in photosynthetic activity and transpiration of forested regions with land cover change. However, this decrease occurs specifically during the dry season. During the wet season, forested regions with high land cover change increase photosynthetic activity. In shrubland regions, land cover change increases photosynthetic activity during the wet season. No other significant effects are found during the wet season or in transpiration in shrubland areas. In general, the annual and seasonal range of variation in photosynthetic activity and transpiration increases under high land cover change.

In the last study, I estimated the amount of evapotranspiration that is inhibited by deforestation in the tropical forests of the Amazon basin. I compared this result with estimates from previous modeling studies. According to my estimates, ET decreased on average between 1.58 and 2.81% in the entire the Amazon basin in the period of 2000-2018. Overall, I found close agreement between this estimated change in ET with those from modeling studies. I also found that these changes are mostly focused in the southern Amazon, where most of the deforestation occurs, and during the dry season. I did not find evident interannual variation in the effects of deforestation, not during extremely wet or dry years. Findings from this study are particularly concerning given (1) our agreement in the decrease in ET with models' simulations, and (2) models' prediction of decrease in precipitation and temperature associated with decrease in ET.

The studies presented in this dissertation cover a wide range of tropical regions, with relatively long-term datasets of photosynthetic activity and evapotranspiration. These projects provide new insights, demonstrations and techniques to study tropical forests. Remote sensing of the Earth and our ecosystems will keep growing and improving. Studies like this should be increasingly used to evaluate and monitor changes in vegetation activity in the tropics. This information can be used not only to improve our understanding of tropical ecosystems, but also in policy making and model benchmarking. I hope I can use what I learned throughout these years to keep making use of technology and data analysis techniques to learn new things about tropical ecosystems.

APPENDIX A. CHAPTER 2 SUPPLEMENTARY INFORMATION

Table A. 1. Spatial resolutions of the datasets analyzed.

DATASET	ORIGINAL SPATIAL RESOLUTION (DEGREES)
MAIAC EVI	0.05 x 0.05
SIF	0.5 x 0.5
CLM 4.5	1.25 x 0.94
JULES	1.875 x 1.25
LPJ-GUESS	1 x 1
FLUXCOM	0.5 x 0.5
VPM	0.5 x 0.5
GOSIF	0.05 x 0.05

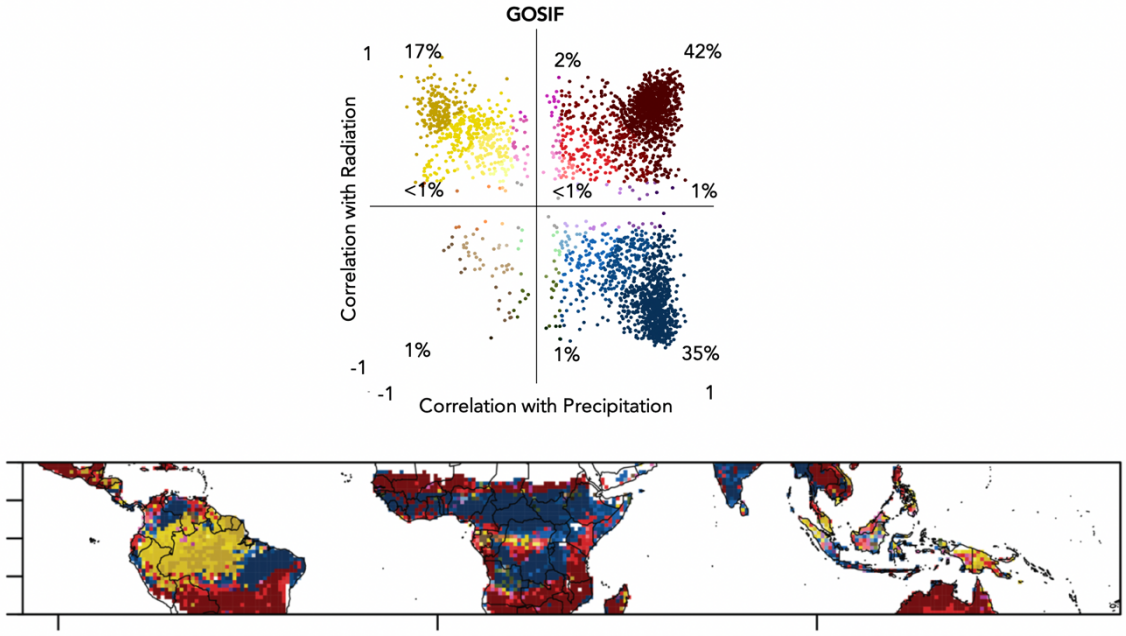

Fig. A. 1. Scatterplot (upper panel) and map (lower panel) for GOSIF data, showing the maximum correlation coefficient from the CCF analysis for vegetation productivity from GOSIF with precipitation (x axis) and radiation (y axis). The numbers in the scatterplot indicate the percentage of pixels corresponding to the type of relationship where the number is located.

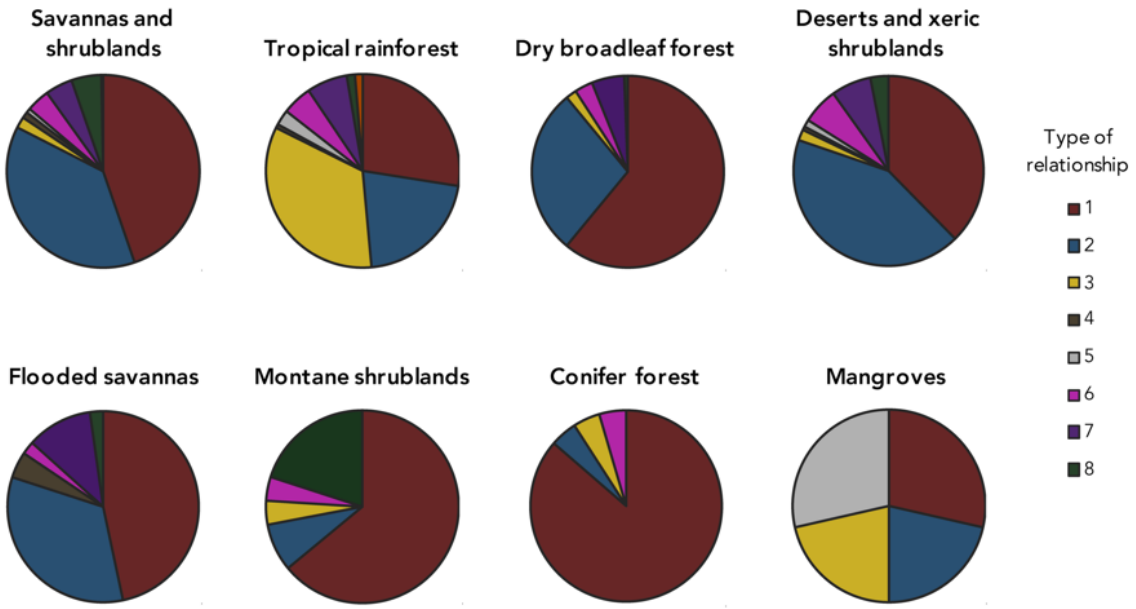

Fig. A. 2. Types of relationships by biome (based on SIF results). The pie charts show the proportion of pixels with each type of relationship in each biome. Colors and numbers of the types of relationships (legend) correspond to the colors and numbers in the reference panel in Fig. A1.

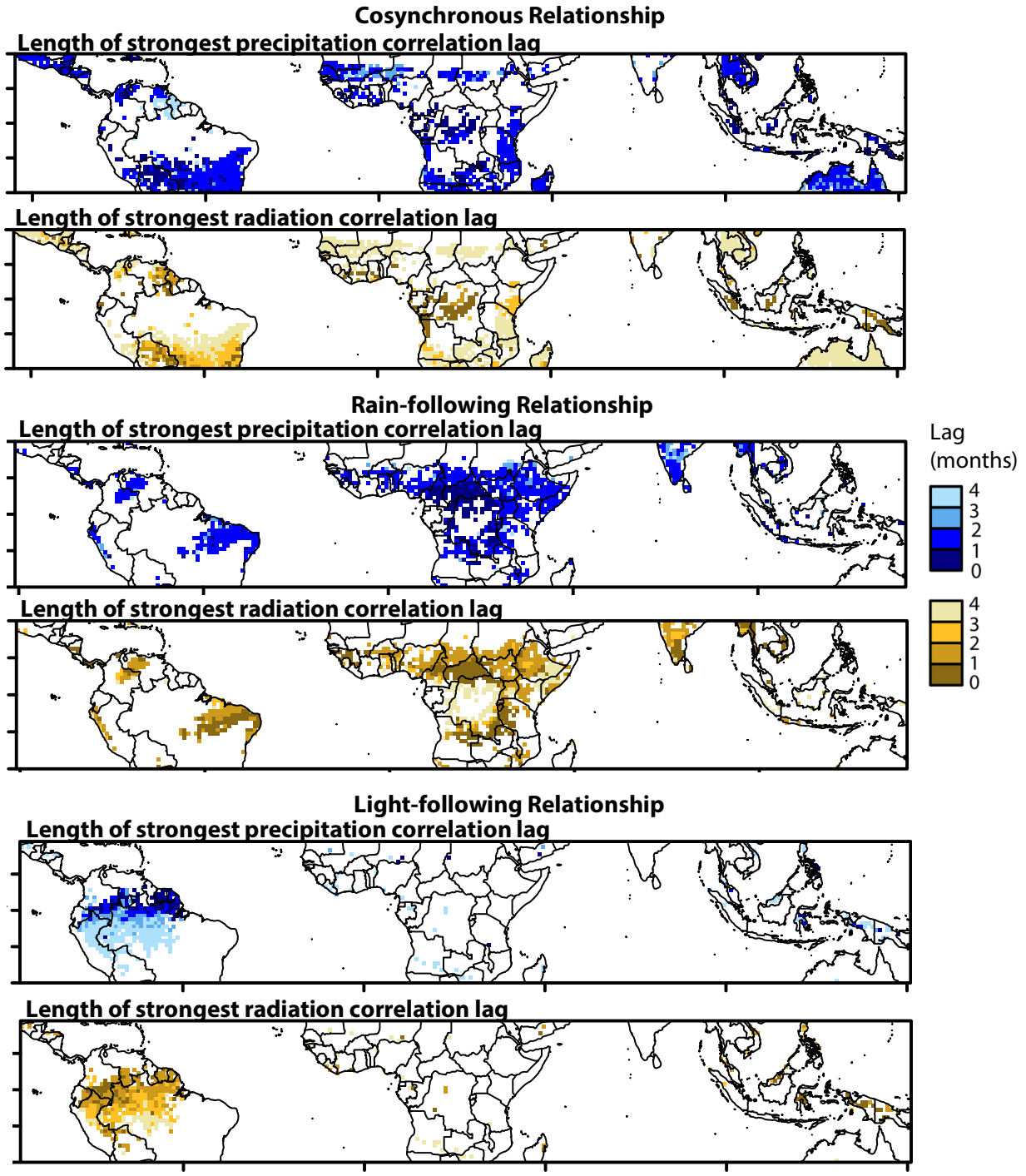

Fig. A. 3. Spatial distribution of the most strongly and significant correlated length of lag between SIF and precipitation and radiation, shown for the three most common types of relationships (cosynchronous, rain-following and light-following). Only lags are shown; that is, lags in which peaks in SIF follow peaks or troughs in the climate variable by 0-4 months. Precipitation and radiation lags are plotted separately for each type of relationship

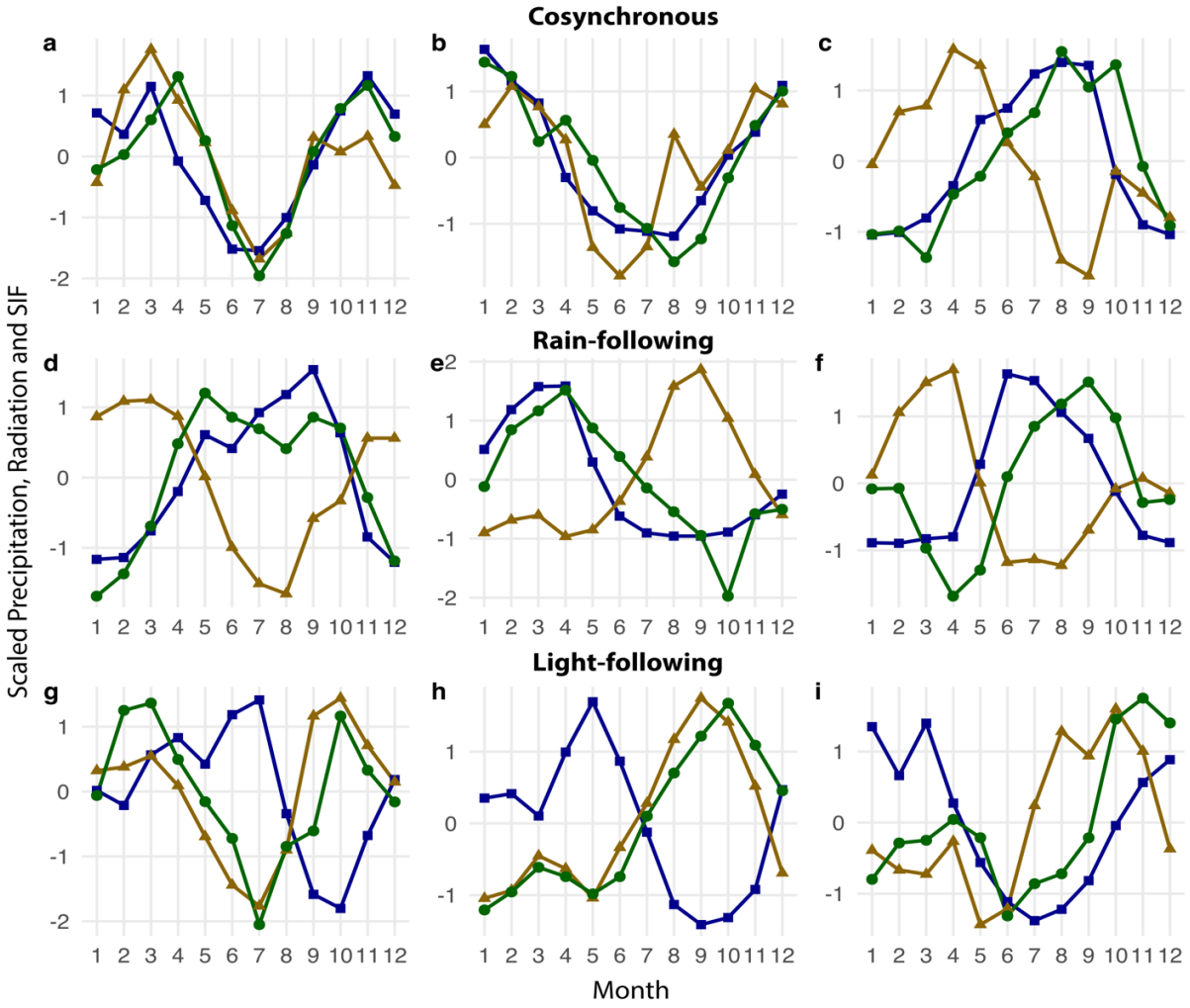

Relationship type	Plot	Lon	Lat	Biome	Location	Precipitation		Radiation	
						r	Lag	r	Lag
Cosynchronous	a	25.5	-2.5	Rainforest	Africa	0.59	0	0.55	0
	b	-54.5	-16.5	Savanna	S. America	0.58	1	0.48	2
	c	104.5	15.5	Dry Forest	Asia	0.72	1	0.58	4
Rain-following	d	21.5	7.5	Savanna	Africa	0.78	0	-0.66	0
	e	-45.5	-4.5	Xeric shrubland	S. America	0.47	1	-0.53	1
	f	95.5	17.5	Rainforest	Asia	0.66	1	-0.22	2
Light-following	g	121.5	-1.5	Rainforest	Asia	-0.29	1	0.54	0
	h	-52.5	4.5	Rainforest	S. America	-0.57	1	0.57	1
	i	-70.5	-8.5	Rainforest	S. America	-0.56	4	0.49	2

Fig. A. 4. Seasonality profiles of Precipitation, Radiation and SIF for the three main types of relationships. All data are scaled to fit and be comparable in the same plot. Relevant information of each site is provided in the accompanying table.

Table A. 2. Biome specific Kappa coefficients (κ) and overall difference (D, %) between SIF and each of the other photosynthetic activity datasets (Fig. 2). Larger numbers indicate closer agreement between the results of two datasets. Larger D values indicate larger differences between the results of two datasets.

	MAIAC EVI	CLM4.5	JULES	LPJ-GUESS	FLUXCOM	VPM
Rainforest	κ = 0.45	0.19	0.24	0.30	0.28	0.34
	D = 41.72	62.78	58.56	52.62	53.78	45.36
Dry forest	0.53	0.26	0.23	0.33	0.48	0.50
	41.72	45.68	46.63	39.76	22.89	24.26
Grasslands and savannas	0.45	0.35	0.33	0.40	0.46	0.46
	31.64	40.29	41.75	34.91	32.85	30.7
Flooded grasslands and savannas	0.44	0.38	0.52	0.43	0.46	0.44
	28.57	34.15	26.19	30.61	28.57	30.61
Montane grasslands and shrublands	0.53	0.57	0.53	0.48	0.41	0.46
	18.0	23.08	22.45	22.64	25.0	20.75
Deserts and xeric shrublands	0.31	0.33	0.30	0.12	0.29	0.27
	33.75	34.38	41.48	35.63	39.24	31.48
Mangroves	0.31	-0.17	-0.08	0.00	0.28	0.15
	40.0	72.73	70.0	69.57	52.17	60.87

APPENDIX B. CHAPTER 3 SUPPLEMENTARY INFORMATION

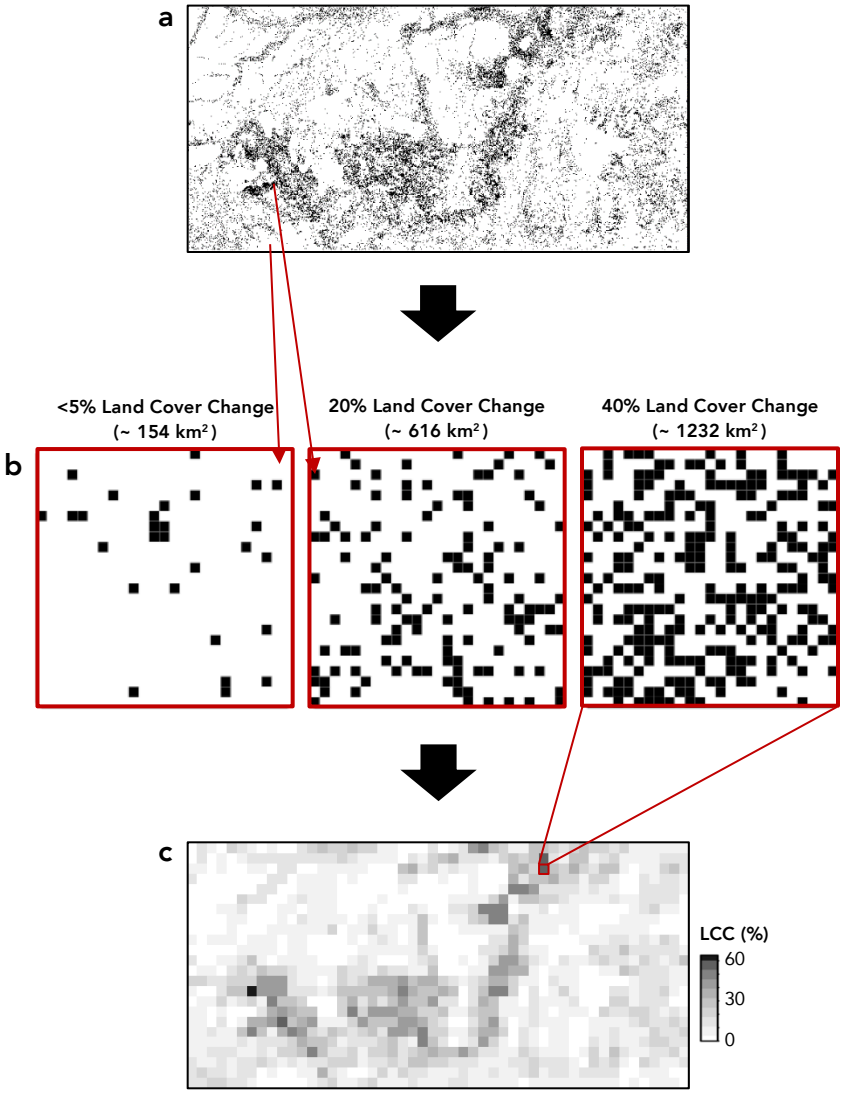

Fig. B. 1 Representation of LCC definitions in this study. The upper panel (a) is the map of land cover change at the original 300m x 300m resolution. Each black dot is a pixel with land cover change from 1992 to 2015. White pixels had the same land cover type in 1992 and 2015. The middle panel (b) is the representation of land cover change calculations from 300m to 0.5º resolution. Each large square represents a 0.5º x 0.5º pixel (SIF and transpiration resolution) with a total area of 3000 km^2. The smaller black and white pixels contained in the large pixel represent the 300m x 300m pixels (LCC resolution). Each black dot is a pixel with land cover change from 1992 to 2015. White pixels had the same land cover type in 1992 and 2015. Land cover change (%) at 0.5º x 0.5º resolution is calculated based on the number of 300m-resolution pixels that changed land cover type between 1992 and 2015 (black pixels). Examples of the <5%, 20% and 40% LCC thresholds selected for this study are shown in (b). The bottom panel (c) is the final map of land cover change at 0.5º x 0.5º resolution.

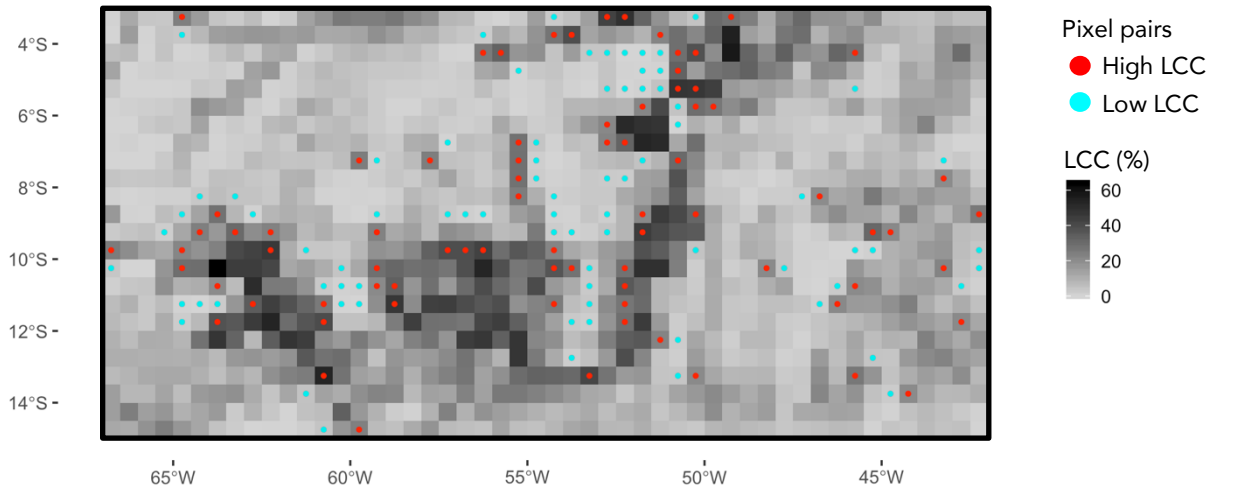

Fig. B. 2. High and low land cover change pixels selected for SIF and transpiration comparison. The percentage LCC calculation is explained in Fig. S1.

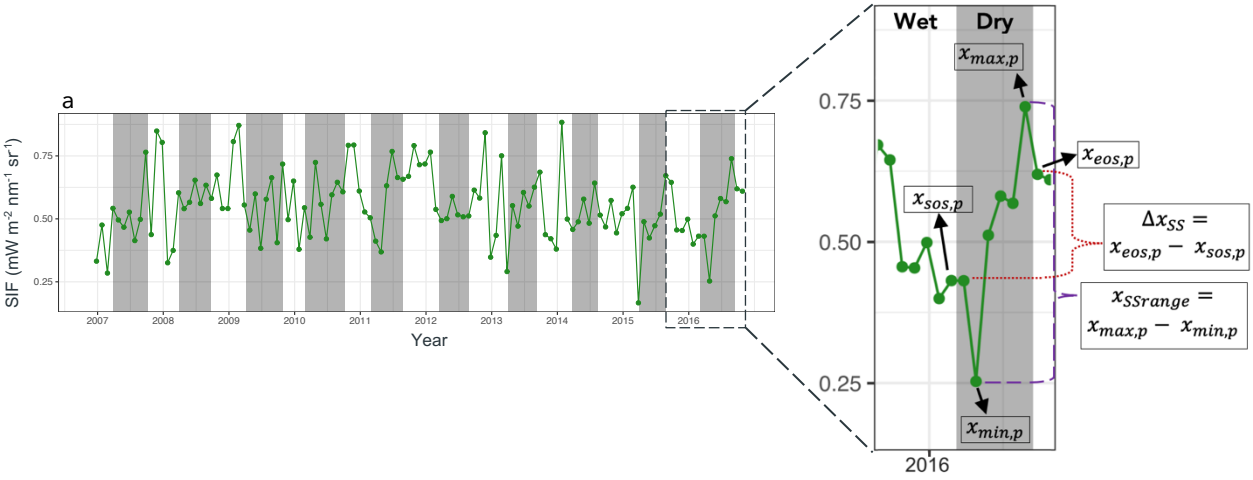

Fig. B. 3. (a) Monthly SIF 2007-2017 for one of the selected pixels. The shaded areas correspond to the dry season. (b) Close-up of the dry season in 2016 to graphically show some of the terms used to calculate the annual and seasonal metrics. Each of the terms shown above are calculated for each year and each season, and then averaged across years and seasons.

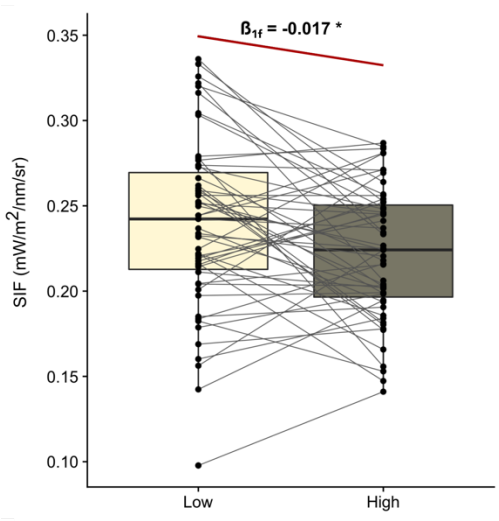

Fig. B. 4. Example of estimate of the effect of LCC in annual mean minimum SIF in forests (ß1f). Each boxplot shows the minimum, first quartile, median, third quartile, and maximum data points. The black dots in the vertical line of each boxplot represent each data point or pixel of each category. Pairs of data points or pixels are connected by the gray lines. The ß1f estimate shown in the red line is the average of all the slopes of the lines between each pair of points. In the linear mixed model used to calculate the ß1f estimate, the effects of elevation and spatial autocorrelation are accounted for. The asterisk (*) indicates a statistically significant effect of LCC ($p < 0.05$)

Table B. 1. Number of pixels selected for SIF and transpiration (TR) analysis by threshold and ecosystem type. Number of pairs in parentheses.

LCC Threshold	**Total**		**Forests**		**Shrublands**	
	SIF	**TR**	**SIF**	**TR**	**SIF**	**TR**
10	348 (174)	376 (188)	240 (120)	262 (131)	108 (54)	108 (54)
20	134 (67)	146 (73)	110 (55)	122 (61)	24 (12)	24 (12)
30	58 (29)	68 (34)	56 (28)	66 (33)	2 (1)	2 (1)
40	26 (13)	32 (16)	26 (13)	32 (16)	0	0

Table B. 2. Linear mixed model estimates and p-values for comparisons of precipitation seasonality between low and high land cover change pixels.

ECOSYSTEM	SEASON	METRIC	ESTIMATE	P-VALUE
ALL LC	Annual	Total P	-0.002	0.271
	Wet	Length	1.318	0.357
	Dry	Length	-1.288	0.372
	Wet	Total P	-6.724	0.702
	Dry	Total P	-12.395	0.126
FORESTS	Annual	Total P	-0.002	0.357
	Wet	Length	2.023	0.230
	Dry	Length	-1.978	0.247
	Wet	Total P	-5.390	0.790
	Dry	TotalP	-9.945	0.290
SHRUBLANDS	Annual	Total P	-0.001	0.796
	Wet	Length	-3.625	0.180
	Dry	Length	3.383	0.173
	Wet	Total P	-17.485	0.702
	Dry	Total P	2.615	0.768

Dry and wet season in the area of study

The median durations of the wet and dry seasons in the region range from 110 to 222 and from 149 to 245 days, respectively, as estimated in RADS. In general terms, the length of the dry season increases from west to east. The median total precipitation of the wet season ranged from 476 to 2507 mm across the study region, while the median for the dry season was between 29 and 1189 mm. The wet season most commonly started in the second half of the year, between September and January. The date of end of the wet season or start of the dry season varied more widely, ranging from March through June. The wet-to-dry transition occurred earlier in the year in the south and later in the north. Within pixels, these dates varied by between 3-90 days for the start of the wet season, and between 3-75 days for the start of the dry season, from 2007-2015.

APPENDIX C. CHAPTER 4 SUPPLEMENTARY INFORMATION

Table C. 1. Cross-validation results for Universal Kriging.

	Mean MSE	Mean RMSE
GLEAM	-0.000799	0.119569
MODIS	-0.000375	0.107965

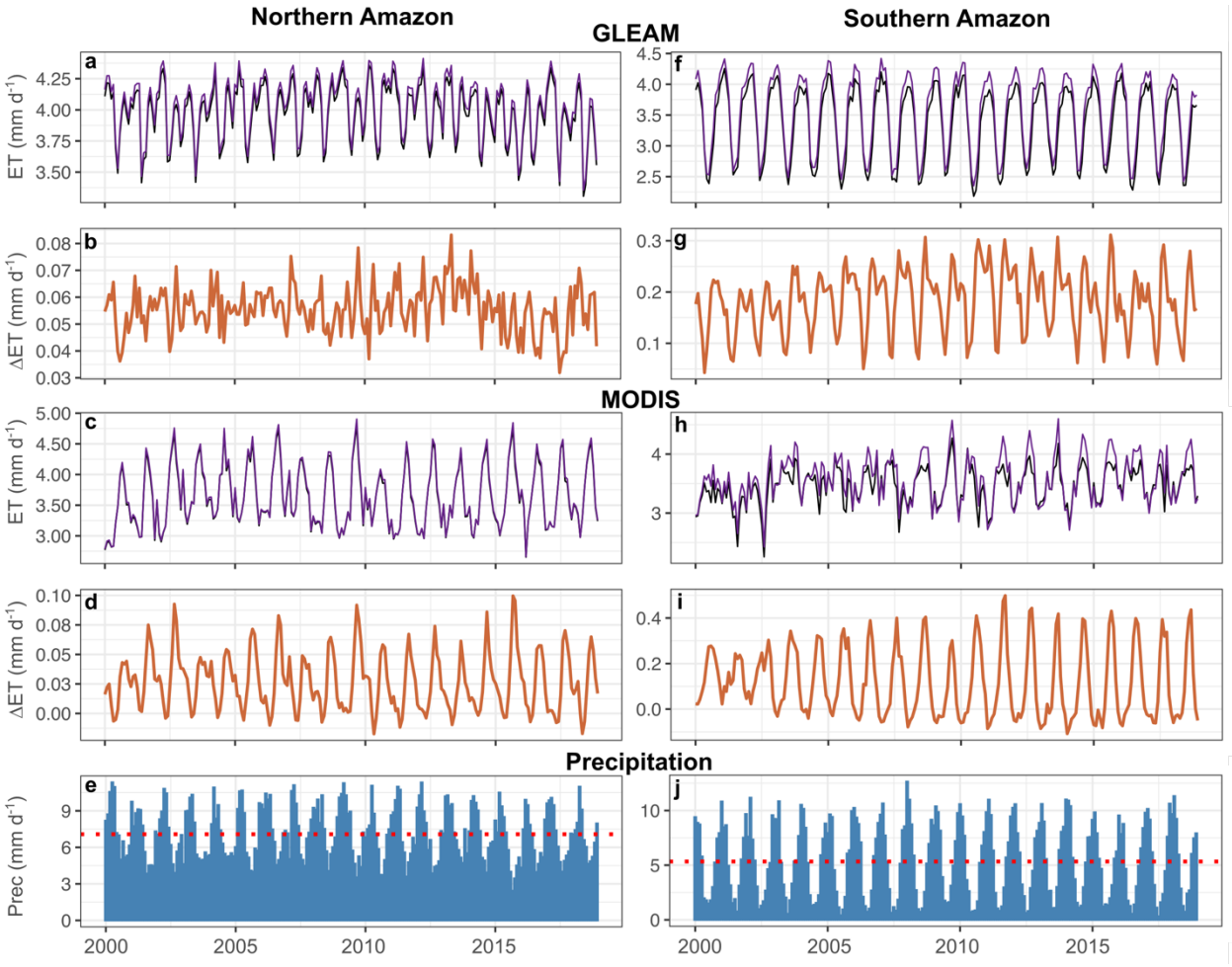

Fig. C. 1. Time series of the monthly observed and no-LCC ET from GLEAM (a,f) and MODIS (c,h) for the period 2000-2018. Time series of the difference between observed and no-LCC ET from GLEAM (b,g) and (d,i) MODIS. Time series of precipitation (e,j). All data are shown separately for the northern (a-e) and southern (f-j) regions of the Amazon

Table C. 2 List of modeling studies of the effects of deforestation on ET included in our analyses.

Study	ID	Year of Publica-tion	Region	Time	Model type	Model Name
(Alves et al. 2017)	1	2017	Southern and Northeastern Amazon	51 years integration (1960 to 2010) + present day simulation + perturbed simulations	RCM	PRECIS-HadRM3P
(Bagley et al. 2013)	2	2013	Amazon rain forest	2003-2010 (April-June and July-September)	Meso+LSM	WRF+NoahLSM
(Correia, Alvalá, and Manzi 2008)	3	2008	Amazon basin	1999-2001 (1 month of spinup)	RCM+LSM	ETA+SSiB
(Costa et al. 2007)	4	2007	Amazon basin	20 years (10 years of spinup)	GCM+LSM	CCM3+IBIS
(Costa and Foley 1997)	5	1997	Amazon basin	10 years (5 years of spinup)	LSM	LSX
(Costa and Pires 2010)	6	2010	Amazon basin	20 years (10 years of spinup)	GCM+LSM	CCM3+ IBIS
(Dickinson and Henderson-Sellers 1988)	7	1988	Amazon basin	13 months	GCM+LSM	CCM+ BATS
(Dickinson and Kennedy 1992)	8	1992	Amazon basin	7 years for control + 3 years for deforestation scenario	GCM+LSM	CCM1+ BATS1e
(Dirmeyer et al. 1992, in Zeng, Dickinson, and Zeng 1996)	9	1992	Amazon basin	NA	NA	NA
(Dirmeyer and Shukla 1994)	10	1994	Amazon basin	4 years (3 months of spinup)	AGCM	COLA
(Dos Santos et al. 2018)	11	2018	Iriri basin	17 years (1998-2015)	Hydrological	SWAT
(Eltahir and Bras 1994)	12	1994	Amazon basin sub-region (256 x 10^4 km^2)	Two months (January and July)	Meso+LSM	MM4+ BATS
(Gedney and Valdes 2000)	13	2000	Amazon basin	11-12 years for control and deforestation scenarios (1 year of spinup)	GCM	European Centre's Integrated Forecast System

(Guimberteau et al. 2017)	14	2017	Amazon basin	1970-2100 (1970-2008 represents current climate conditions and 2009-2100 represents future climate projections)	GCM+LSM	LSMs: ORCHIDEE, INLAND-DGVM, LPJmL-DGVM GCMs: CCSM3, UKMO-HadCM3, PCM
(Henderson-Sellers and Gornitz 1984)	15	1984	Amazon basin	20 years for control and 10 years for deforestation simulations (5 last years used for analysis)	GCM	GISS
(Henderson-Sellers et al. 1993)	16	1993	Amazon basin	6 years	GCM+Ocean	CCM1-Oz+ BATS
(Kleidon and Heimann 2000)	17	2000	Amazon basin	20 years (5 years of spinup)	GCM	ECHAM 4
(Lean and Warrilow 1989)	18	1989	Amazon basin	3 years	GCM	UKMO
(Lean and Rowntree 1993)	19	1993	Amazon basin	3 years	GCM	UKMO
(Lean and Rowntree 1997)	20	1997	Amazon basin	10 years	GCM	UKMO
(Lean et al. 1996, in Zeng et al. 1996)	21	1996	Amazon basin	11 years	GCM	UKMO
(Lejeune et al. 2015)	22	2015	Amazon basin	1979-2010 (8 years of spinup)	RCM+ LSM	COSMO+ CLM3.5
(McGuffie et al. 1995)	23	1995	Amazon basin	6 years	GCM+ Ocean	CCM1-Oz+ BATS
(Medvigy, Walko, and Avissar 2010)	24	2010	Amazon basin	1998-2005	Variable-resolution GCM	OLAM
(Moraes, Franchito, and Rao 2012)	25	2012	Amazon basin (results reported for 5ºN and 5ºS)	1 year (6 months of spinup)	Coupled biosphere–atmosphere statistical–dynamical model	SDM
(Panday et al. 2015)	26	2015	Xingu basin	2001-2010	Water budget approach + LSM	IBIS

(Polcher and Laval 1994b)	27	1994	Amazon basin	1.1 years	GCM+ LSM	LMD+ SECHIBA
(Polcher and Laval 1994a)	28	1994	Amazon basin	11 years	GCM+ LSM	LMD+ SECHIBA
(Ramos da Silva, Werth, and Avissar 2008)	29	2008	Amazon basin	60-day period (January-February)	RCM	RAMS
(Shukla, Nobre, and Sellers 1990)	30	1990	Amazon basin	1 year	GCM	NMC + SiB
(Silva, Pereira, and da Rocha 2016)	31	2016	Amazon basin	1999-2007 (2 years of spinup)	RCM+ LSM	RegCM3+ BATS
(Sud et al. 1996)	32	1996	Amazon basin	1979-1982 (2 months of spinup)	GCM+ LSM	GLA+ SSiB
(Swann et al. 2015)	33	2015	Amazon basin	2005-2007	RCM+ LSM	BRAMS+ ED2
(Voldoire and Royer 2004)	34	2004	Amazon basin	1970-1999	GCM+ LSM	ARPEGE-Climat+ ISBA
(Voldoire and Royer 2005)	35	2005	Amazon basin	25 years (5 years of spinup)	GCM+ LSM	ARPEGE-Climat+ ISBA
(Walker, Sud, and Atlas 1995)	36	1995	Amazon basin	5-day period (February and March 1979)	GCM+ LSM	GLA+ SSiB
(Zemp et al. 2017)	37	2017	Amazon basin	1989-1995	Empirical approach	NA
(Zeng et al. 1996)	38	1996	Amazon basin	NA	Intermediate-level model	NA
(Zhang, Henderson-Sellers, and McGuffie 1996)	39	1996	Amazon basin	36 years (25 + 11 years for the control and deforestation experiment)	GCM+ LSM	CCM1+ BATS1e
(Sampaio et al. 2007)	40	2007	Eastern Amazon	87 months (27 months of spinup)	GCM+ LSM	CPTEC-INPE+ SSiB

AGCM: Atmospheric general circulation model; GCM: Global circulation model; LSM: Land surface model; Meso: Mesoscale model; RCM: Regional circulation model; + indicates coupled models

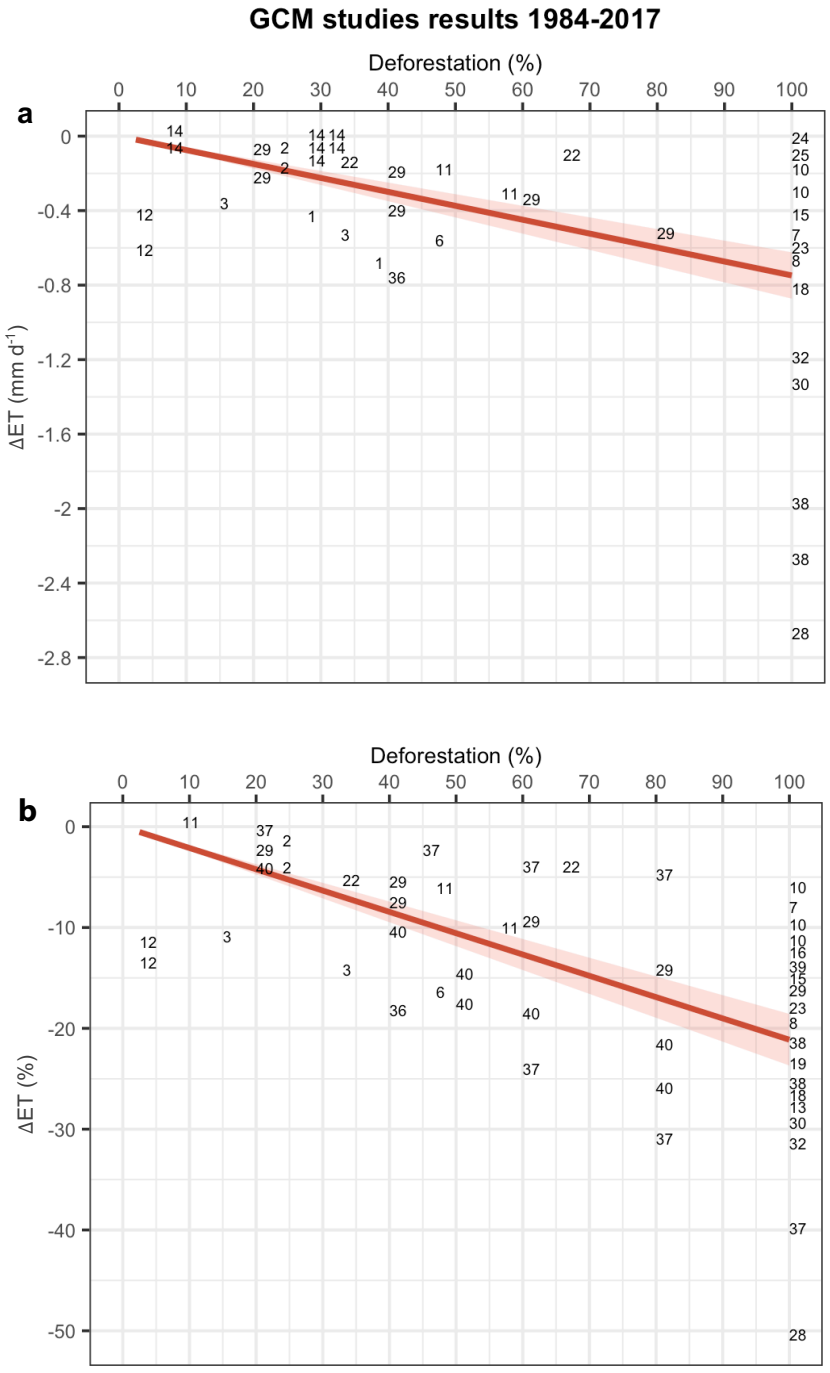

Fig. C. 2. Estimates of absolute (a) and relative (b) change in ET due to deforestation in the Amazon basin. ET change estimates are marked with numbers. Each number corresponds to the publication in which the estimate was reported. See the full record of publications with their corresponding numbers in table S2. The red line shows the linear regression between deforestation and change in ET. The regression intercept is set to zero. The shaded area around the line corresponds to the standard error of predicted means.

References

Alves, Lincoln Muniz, Jose A. Marengo, Rong Fu, and Rodrigo J. Bombardi. 2017. "Sensitivity of Amazon Regional Climate to Deforestation." *American Journal of Climate Change* 6(1):75–98.

Bagley, Justin E., Ankur R. Desai, Keith J. Harding, Peter K. Snyder, and Jonathan A. Foley. 2013. "Drought and Deforestation: Has Land Cover Change Influenced Recent Precipitation Extremes in the Amazon?" *Journal of Climate* 27(1):345–61.

Correia, F. W. S., R. C. S. Alvalá, and A. O. Manzi. 2008. "Modeling the Impacts of Land Cover Change in Amazonia: A Regional Climate Model (RCM) Simulation Study." *Theoretical and Applied Climatology* 93(3):225–44.

Costa, Marcos H., Silvia N. M. Yanagi, Paulo J. O. P. Souza, Aristides Ribeiro, and Edson J. P. Rocha. 2007. "Climate Change in Amazonia Caused by Soybean Cropland Expansion, as Compared to Caused by Pastureland Expansion." *Geophysical Research Letters* 34(7).

Costa, Marcos Heil, and Jonathan A. Foley. 1997. "Water Balance of the Amazon Basin: Dependence on Vegetation Cover and Canopy Conductance." *Journal of Geophysical Research: Atmospheres* 102(D20):23973–89.

Costa, Marcos Heil, and Gabrielle Ferreira Pires. 2010. "Effects of Amazon and Central Brazil Deforestation Scenarios on the Duration of the Dry Season in the Arc of Deforestation." *International Journal of Climatology* 30(13):1970–79.

Dickinson, Robert E., and Ann Henderson-Sellers. 1988. "Modelling Tropical Deforestation: A Study of GCM Land-Surface Parametrizations." *Quarterly Journal of the Royal Meteorological Society* 114(480):439–62.

Dickinson, Robert E., and Patrick Kennedy. 1992. "Impacts on Regional Climate of Amazon Deforestation." *Geophysical Research Letters* 19(19):1947–50.

Dirmeyer, Paul A., and J. Shukla. 1994. "Albedo as a Modulator of Climate Response to Tropical Deforestation." *Journal of Geophysical Research: Atmospheres* 99(D10):20863–77.

Dos Santos, Vanessa, François Laurent, Camila Abe, and François Messner. 2018. "Hydrologic Response to Land Use Change in a Large Basin in Eastern Amazon." *Water* 10(4):429.

Eltahir, E. a. B., and R. L. Bras. 1994. "Precipitation Recycling in the Amazon Basin." *Quarterly Journal of the Royal Meteorological Society* 120(518):861–80.

Gedney, Nicola, and Paul J. Valdes. 2000. “The Effect of Amazonian Deforestation on the Northern Hemisphere Circulation and Climate.” *Geophysical Research Letters* 27(19):3053–56.

Guimberteau, Matthieu, Philippe Ciais, Agnès Ducharne, Juan Pablo Boisier, Ana Paula Dutra Aguiar, Hester Biemans, Hannes de Deurwaerder, David Galbraith, Bart Kruijt, Fanny Langerwisch, German Poveda, Anja Rammig, Daniel Andres Rodriguez, Graciela Tejada, Kirsten Thonicke, Celso von Randow, Rita C. S. von Randow, Ke Zhang, and Hans Verbeeck. 2017. “Impacts of Future Deforestation and Climate Change on the Hydrology of the Amazon Basin: A Multi-Model Analysis with a New Set of Land-Cover Change Scenarios.” *Hydrology and Earth System Sciences* 21(3):1455–75.

Henderson-Sellers, A., R. E. Dickinson, T. B. Durbidge, P. J. Kennedy, K. McGuffie, and A. J. Pitman. 1993. “Tropical Deforestation: Modeling Local- to Regional-Scale Climate Change.” *Journal of Geophysical Research: Atmospheres* 98(D4):7289–7315.

Henderson-Sellers, A., and V. Gornitz. 1984. “Possible Climatic Impacts of Land Cover Transformations, with Particular Emphasis on Tropical Deforestation.” *Climatic Change* 6(3):231–57.

Kleidon, A., and M. Heimann. 2000. “Assessing the Role of Deep Rooted Vegetation in the Climate System with Model Simulations: Mechanism, Comparison to Observations and Implications for Amazonian Deforestation.” *Climate Dynamics* 16(2–3):183–99.

Lean, J., and P. R. Rowntree. 1993. “A GCM Simulation of the Impact of Amazonian Deforestation on Climate Using an Improved Canopy Representation.” *Quarterly Journal of the Royal Meteorological Society* 119(511):509–30.

Lean, J., and P. R. Rowntree. 1997. “Understanding the Sensitivity of a GCM Simulation of Amazonian Deforestation to the Specification of Vegetation and Soil Characteristics.” *Journal of Climate* 10(6):1216–35.

Lean, J., and D. A. Warrilow. 1989. “Simulation of the Regional Climatic Impact of Amazon Deforestation.” *Nature* 342(6248):411–13.

Lejeune, Quentin, Edouard L. Davin, Benoit P. Guillod, and Sonia I. Seneviratne. 2015. “Influence of Amazonian Deforestation on the Future Evolution of Regional Surface Fluxes, Circulation, Surface Temperature and Precipitation.” *Climate Dynamics* 44(9):2769–86.

McGuffie, K., A. Henderson-Sellers, H. Zhang, T. B. Durbidge, and A. J. Pitman. 1995. "Global Climate Sensitivity to Tropical Deforestation." *Global and Planetary Change* 10(1):97–128.

Medvigy, David, Robert L. Walko, and Roni Avissar. 2010. "Effects of Deforestation on Spatiotemporal Distributions of Precipitation in South America." *Journal of Climate* 24(8):2147–63.

Moraes, E. C., Sergio H. Franchito, and V. Brahmananda Rao. 2012. "Amazonian Deforestation: Impact of Global Warming on the Energy Balance and Climate." *Journal of Applied Meteorology and Climatology* 52(3):521–30.

Panday, Prajjwal K., Michael T. Coe, Marcia N. Macedo, Paul Lefebvre, and Andrea D. de Almeida Castanho. 2015. "Deforestation Offsets Water Balance Changes Due to Climate Variability in the Xingu River in Eastern Amazonia." *Journal of Hydrology* 523:822–29.

Polcher, J., and K. Laval. 1994a. "A Statistical Study of the Regional Impact of Deforestation on Climate in the LMD GCM." *Climate Dynamics* 10(4):205–19.

Polcher, J., and K. Laval. 1994b. "The Impact of African and Amazonian Deforestation on Tropical Climate." *Journal of Hydrology* 155(3):389–405.

Ramos da Silva, Renato, David Werth, and Roni Avissar. 2008. "Regional Impacts of Future Land-Cover Changes on the Amazon Basin Wet-Season Climate." *Journal of Climate* 21(6):1153–70.

Sampaio, Gilvan, Carlos Nobre, Marcos Heil Costa, Prakki Satyamurty, Britaldo Silveira Soares-Filho, and Manoel Cardoso. 2007. "Regional Climate Change over Eastern Amazonia Caused by Pasture and Soybean Cropland Expansion." *Geophysical Research Letters* 34(17).

Shukla, J., C. Nobre, and P. Sellers. 1990. "Amazon Deforestation and Climate Change." *Science* 247(4948):1322–25.

Silva, Maria Elisa Siqueira, Gabriel Pereira, and Rosmeri Porfírio da Rocha. 2016. "Local and Remote Climatic Impacts Due to Land Use Degradation in the Amazon 'Arc of Deforestation.'" *Theoretical and Applied Climatology* 125(3):609–23.

Sud, Y. C., W. K. M. Lau, G. K. Walker, J. H. Kim, G. E. Liston, and P. J. Sellers. 1996. "Biogeophysical Consequences of a Tropical Deforestation Scenario: A GCM Simulation Study." *Journal of Climate* 9(12):3225–47.

Swann, Abigail L. S., Marcos Longo, Ryan G. Knox, Eunjee Lee, and Paul R. Moorcroft. 2015. "Future Deforestation in the Amazon and Consequences for South American Climate." *Agricultural and Forest Meteorology* 214–215:12–24.

Voldoire, A., and J. F. Royer. 2004. "Tropical Deforestation and Climate Variability." *Climate Dynamics* 22(8):857–74.

Voldoire, Aurore, and Jean-François Royer. 2005. "Climate Sensitivity to Tropical Land Surface Changes with Coupled versus Prescribed SSTs." *Climate Dynamics* 24(7):843–62.

Walker, G. K., Y. C. Sud, and R. Atlas. 1995. "Impact of the Ongoing Amazonian Deforestation on Local Precipitation: A GCM Simulation Study." *Bulletin of the American Meteorological Society* 76(3):346–62.

Zemp, D. C., C. F. Schleussner, H. M. J. Barbosa, and A. Rammig. 2017. "Deforestation Effects on Amazon Forest Resilience." *Geophysical Research Letters* 44(12):6182–90.

Zeng, Ning, Robert E. Dickinson, and Xubin Zeng. 1996. "Climatic Impact of Amazon Deforestation—A Mechanistic Model Study." *Journal of Climate* 9(4):859–83.

Zhang, H., A. Henderson-Sellers, and K. McGuffie. 1996. "Impacts of Tropical Deforestation. Part I: Process Analysis of Local Climatic Change." *Journal of Climate* 9(7):1497–1517..